

AD-A190 253

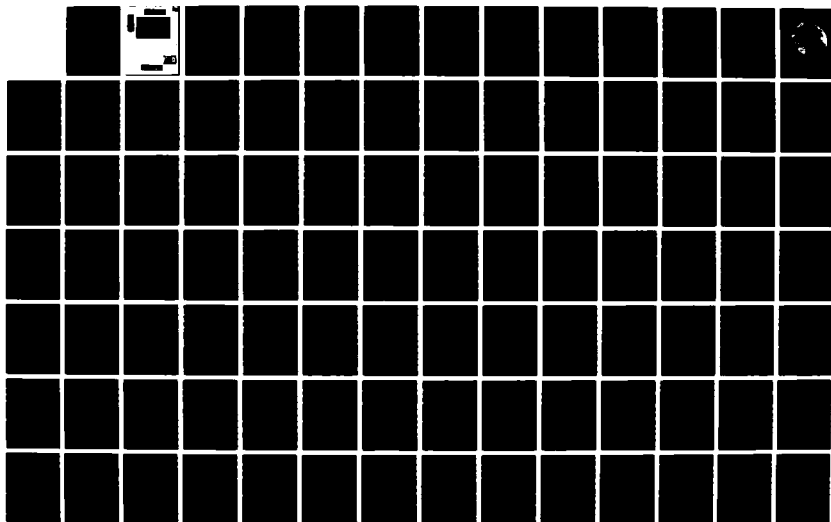
ANALYSIS OF CENTRAL ARCTIC NOISE EVENTS(U)
MASSACHUSETTS INST OF TECH CAMBRIDGE DEPT OF OCEAN
ENGINEERING N TOWNSEND-MANNING JUN 87 N00220-85-0-1262

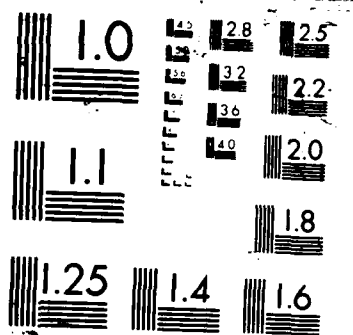
1/2

UNCLASSIFIED

F/B 28/1

ML





DEPARTMENT OF OCEAN ENGINEERING

MASSACHUSETTS INSTITUTE OF TECHNOLOGY

CAMBRIDGE, MASSACHUSETTS 02139

ANALYSIS OF CENTRAL ARCTIC
NOISE EVENTS

by

MARY TOWNSEND-MANNING
Ocean Engineering - Course XIIIA

NAVAL ENG. & SM(ME)
June 1987



ANALYSIS OF CENTRAL ARCTIC
NOISE EVENTS

by

MARY TOWNSEND-MANNING
B.S., San Diego State University
(1975)

SUBMITTED TO THE DEPARTMENT OF
OCEAN ENGINEERING
IN PARTIAL FULFILLMENT OF THE REQUIREMENTS
FOR THE DEGREES OF
NAVAL ENGINEER

and

MASTER OF SCIENCE IN MECHANICAL ENGINEERING
at the

MASSACHUSETTS INSTITUTE OF TECHNOLOGY
June, 1987

N00228-85-G-3262

© Massachusetts Institute of Technology 1987

Signature of Author *Mary Townsend-Manning*
Department of Ocean Engineering
May, 1987

Certified by *Ira Dyer*
Ira Dyer
Professor, Ocean Engineering
Thesis Supervisor

Accepted by *A. Douglas Carmichael*
A. Douglas Carmichael, Chairman
Departmental Graduate Committee
Department of Ocean Engineering

The author hereby grants to the U.S. Government and its agencies permission
to reproduce and to distribute copies of this thesis in whole or in part.

This document has been approved
for public release and sale; its
distribution is unlimited.

88 1 15 044

Accession For	
NTIS GRA&I	<input checked="" type="checkbox"/>
DTIC TAB	<input type="checkbox"/>
Unannounced	<input type="checkbox"/>
Justification	<i>form 50 PL</i>
By	
Distribution/	
Availability Codes	
Dist	Avail and/or Special
<i>A-1</i>	

ANALYSIS OF CENTRAL ARCTIC

NOISE EVENTS

by

MARY TOWNSEND-MANNING

Submitted to the Department of Ocean Engineering
on May 8, 1987 in partial fulfillment of the
requirements for the Degrees of Naval Engineer and
Master of Science in Mechanical Engineering

ABSTRACT

An analysis was done of central Arctic Ocean acoustic data to determine the temporal and spatial characteristics of transient noise events. Digital ambient noise data from the FRAM IV experiment of April 1982 were searched for ambient noise transients using a detection program. The time series of the resulting detections were examined visually to categorize each detection as a transient, artifact or false alarm. The transient events were located in space using time delays between signal arrival at different hydrophones. The cross shape of the FRAM IV horizontal array permitted location in both bearing and range. The source strength of each event was calculated using a simple dipole source model. Refraction and scattering of the acoustic path in the Arctic Ocean was taken into account.

The overall number of events detected, and hence their interarrival times and spatial density, were all affected by the background ambient noise level. The detection program used the same threshold signal-to-noise level for all data tapes, so when ambient noise levels were low more detections occurred. The mean interarrival time between events was 100 seconds. The interarrival time fit a J shaped gamma probability distribution. The number of events detected per area decreased with range from the array center. Half of the events occurred within 3000 meters of the array. In this area there were 0.3 events per square kilometer per hour. The event population showed no predominant angular dependence. The strengths calculated using the simple dipole model had a mean of 430 kN overall and 260 kN during quiet times. Stronger events occurred during times with high ambient noise levels.

Thesis Supervisor: Dr. Ira Dyer

Title: Professor of Ocean Engineering

TABLE OF CONTENTS

Abstract	2
Table of Contents	3
List of Figures	4
List of Tables	7
Chapter 1 - Introduction	8
Thesis Motivation	8
Thesis Contents	12
Chapter 2 - Detection of Noise Events	13
Data Collection	13
Event Detector Program	16
Visual Confirmation	28
Chapter 3 - Location of Noise Events	35
Event Location Program	35
Effects of Refraction on Location	47
Chapter 4 - Strength of Noise Events	55
Acoustic Source Model	56
Effects of Refraction on Transmission Loss	57
Strength of Background Noise	71
Chapter 5 - Analysis of Noise Events	76
Detection Analysis	76
Temporal Analysis	79
Spatial Analysis	91
Strength Analysis	98
Chapter 6 - Summary and Thoughts	108
References	110
Acknowledgements	112
Appendix A - Event Detector Program	114
Appendix B - Location Program	123
Appendix C - Event Summary	144
Appendix D - Refraction Path Calculations	164

LIST OF FIGURES

Figure 1-1: Location of the FRAM IV Arctic experiment conducted in the spring of 1982.	11
Figure 2-1: FRAM IV horizontal hydrophone array.	14
Figure 2-2: Schematic of the recording system used for FRAM IV data collection.	15
Figure 2-3: Block diagram of major modules of the detection program.	18
Figure 2-4: Frequency response of the Parks-McClellan digital bandpass filter used in detection.	19
Figure 2-5: Diagram of event detection module flow and decision making.	21
Figure 2-6: Sketch showing point of measurement for event time delays. The event is timed at its zero crossing between the largest pair of positive and negative peaks. (The measurement/analysis system has a polarity of negative voltage for positive pressure.)	33
Figure 3-1: Coordinate system used for calculation of event location.	36
Figure 3-2: Least squares fit of time delays and test location slant range.	37
Figure 3-3: Least squares fit to a false location 180° away.	41
Figure 3-4: Areas covered by <i>location</i> , <i>farlocate</i> and <i>finelocate</i> .	42
Figure 3-5: Noise events located within a 2 km square surrounding the array origin.	45
Figure 3-6: Position of all noise events located.	46
Figure 3-7: Sound velocity profile used in predicting refractive paths.	48

Figure 3-8: Scheme used to compute refractive propagation paths. Source is located at $z = 0\text{m}$ and hydrophone at $z = 93\text{m}$. Sound speed gradients change at 80m, 254m and 362m.	49
Figure 3-9: Time difference between the slant range acoustic path and the refractive path as a function of horizontal range.	52
Figure 3-10: Scatter plot of standard deviation and range for all located noise events.	53
Figure 4-1: Assumed dipole source orientation and definition of launch angle, θ .	57
Figure 4-2: Spherical spreading.	60
Figure 4-3: Spreading loss in refraction.	62
Figure 4-4: Specular and non-specular reflections from the ice/water interface.	65
Figure 4-5: Probability of a ray bundle crossing a certain depth at a given horizontal range.	67
Figure 4-6: Spherical (heavy line) and refractive spreading loss, $G(r)$, as a function of horizontal range.	70
Figure 4-7: Composite central Arctic ambient noise spectrum observed during the FRAM IV experiment.	72
Figure 5-1: Normalized ambient noise pressure, number of unique events per tape, and number of false alarms per tape for each data tape examined.	77
Figure 5-2: Average number of false alarms and unique events per data tape for four ranges of ambient noise pressure.	78
Figure 5-3: Number of events per interarrival time bin.	80
Figure 5-4: Half-gaussian distribution compared with experimental values.	84
Figure 5-5: Exponential distribution compared with experimental values.	85

Figure 5-6: Semi log plot of exponential distribution and experimental values against bin number.	86
Figure 5-7: J shaped distribution compared with experimental values.	88
Figure 5-8: Semi log plot of J shaped distribution and experimental values against bin number.	89
Figure 5-9: Scheme for annuli each of area equal to 30 km^2 .	92
Figure 5-10: Number of events per radius annulus.	93
Figure 5-11: Number of events per 30° sector. Angles are measured from the northern leg of the hydrophone array.	96
Figure 5-12: Number of events per 30° sector. Radius gives the number of events, while angle indicates the sector measured from the northern leg of the array. Each ring represents 10 events.	97
Figure 5-13: Number of events per 10° sector. Radius gives the number of events, while angle indicates the sector measured from the northern leg of the array.	99
Figure 5-14: Mean hydrophone peak pressure measured for events between 100 m and 20,000 m, plotted against horizontal range from the FRAM IV array origin.	100
Figure 5-15: Distribution of strength for a population of noise events.	103
Figure 5-16: Dipole strength for events between 300 m and 20,000 m, plotted against horizontal range from the array origin.	104
Figure 5-17: 10 log of Dipole strength (dB re 1 N) versus 10 log of horizontal range from the array origin (dB re 1 m) for events occurring during an ambient noise level of 0.01 to 0.02 Pa.	106
Figure A-1: Flow chart of the <i>hdetect</i> program.	118

LIST OF TABLES

Table 2-1: Determination of the Best RATIO	25
Table 2-2: Detection Statistics for Two Visual Confirmation Methods	31
Table 3-1: Results of <i>location</i> Program Accuracy Test	55
Table 4-1: 20 to 80 Hz Band Ambient Noise rms Pressure	75
Table 5-1: Number of Events per Interarrival Time Bin	91
Table 5-2: Comparison of Distribution Functions	90
Table 5-3: Background Noise Level Dependence of Interarrival Time	91
Table 5-4: Number of Events per Annulus	94
Table 5-5: Average Number of Events per Annulus for 4 Ambient Noise Levels	95
Table 5-6: Mean Hydrophone Peak Pressure for 4 Ambient Noise Levels	101
Table 5-7: Strength Distribution for a Population of Events	100
Table 5-8: Dipole Strength versus Ambient Noise Levels	102
Table C-1: Event Location Summary	145
Table C-2: Tape Summary	152
Table C-3: Event Interarrival Time Summary	153
Table C-4: Event Strength Summary	159
Table D-1: Angles, Ranges and Times for Reflective Propagation Paths	165
Table D-2: Spreading Loss Function, $G(r)$	160

CHAPTER 1

INTRODUCTION

Thesis Motivation

This thesis investigates the spatial distribution, strength and rate of occurrence of low frequency central Arctic noise events. During the last 30 years there has been a growing commercial, military and academic interest in the Arctic region.

In this relatively unexplored area there is increasing evidence of rich mineral and petroleum resources. Research into methods of locating these assets and constructing facilities to exploit them have received much attention. These facilities must be able to withstand the harsh Arctic surroundings. The study of Arctic acoustics helps in understanding the Arctic environment and climate. It has been shown that there is a direct correlation between 10 to 20 Hz ambient sound pressure and environmental stresses and moments[10]. The ability to use acoustic noise levels as an environmental predictor would be a useful tool in the protection of commercial Arctic facilities.

The Arctic ocean serves as a military arena for several submarine fleets. The underice environment makes detection difficult, increasing the strategic role of those fleets. Because of the sound velocity profile of the central Arctic there is a surface duct which channels sound for long distances. But, the underice profile scatters

sound energy, effectively filtering out high frequencies[11]. The result is that only low frequency signals travel far in the Arctic, and therefore the low frequency range is the best for detecting adversary submarines. The importance of understanding the low frequency ambient noise field becomes apparent. The actual central Arctic ambient noise level is at times much quieter than the open ocean, but it contains unpredictable transient noise events which interfere with conventional detection schemes. It has been hypothesized that the background ambient noise is the summation of these transients from throughout the Arctic basin[7]. Analysis of the spatial and temporal distribution of these transients is a logical next step in understanding low frequency noise, and improving our submarine detection capability.

The academic challenge of the Arctic lies in the sparseness of field data. The Arctic cannot be casually sampled. Even simple experiments require expensive expeditions. The harsh environment takes its toll on researchers and equipment, and reduces the amount of usable data. Hence, the study of the Arctic is like a jigsaw puzzle with few pieces present. The total picture remains a stimulating mystery.

This study analyzes data collected during the FRAM IV experiment by Massachusetts Institute of Technology and

Woods Hole Oceanographic Institute personnel. The FRAM IV ice camp was located in the Barents (Nansen) Abyssal Plain at approximately 84° N by 15° E, as shown in Figure 1-1. The ice was 3 meter thick multi-year pack ice. The ice activity was low; there was no ice ridging or lead formation around the camp during the experiment.

The FRAM IV ice camp was set up from 25 March to 11 May 1982. This study analyzes data taken between March 27th and April 22nd. The weather was mild, with temperature ranged from -35° to -4° C, and wind speed from 1 to 23 knots.

The ambient noise was sensed with a large horizontal hydrophone array which consisted of two non-uniformly spaced line arrays, crossing at right angles. The data were digitally recorded on a multichannel system.

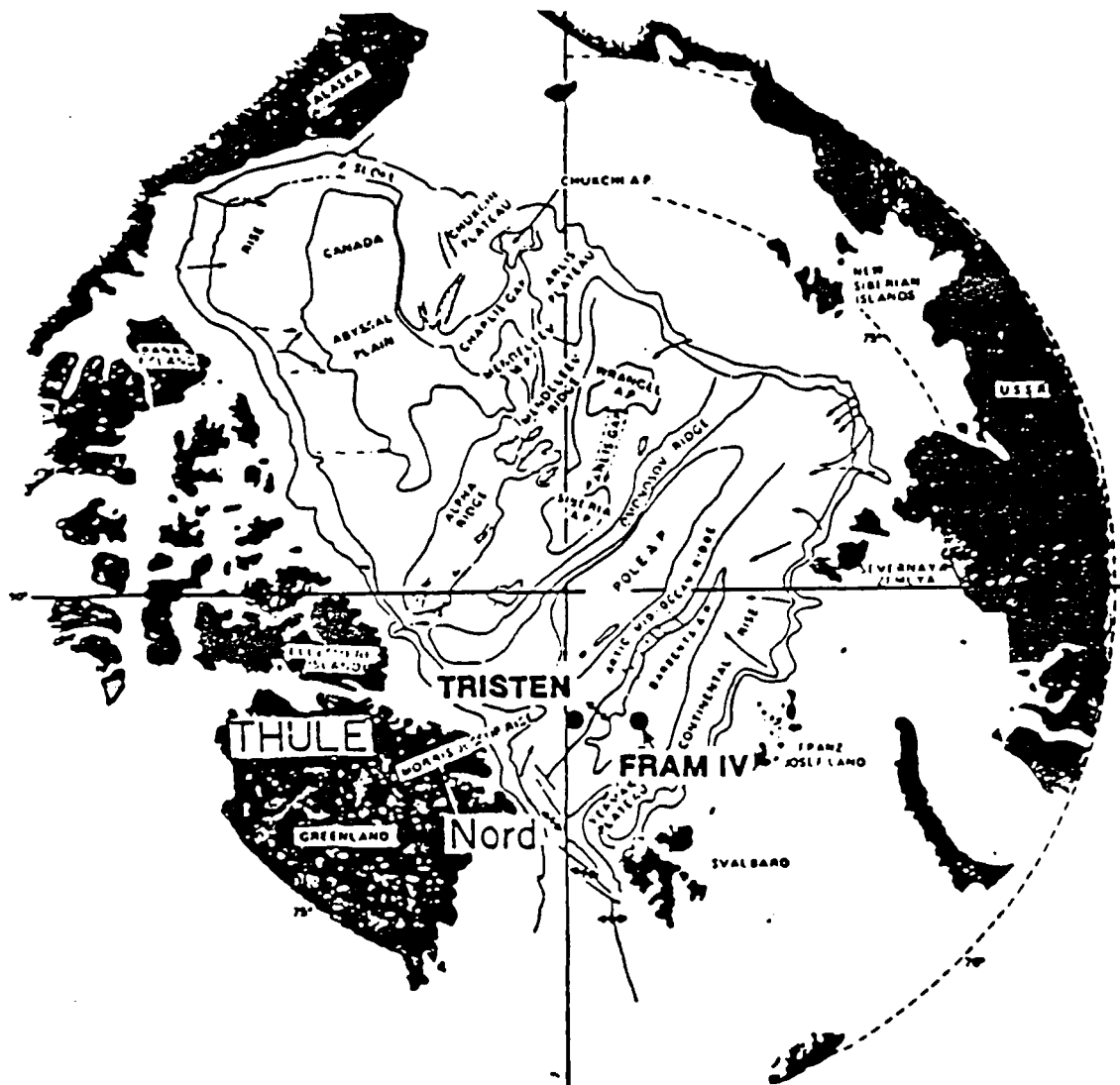


Figure 1-1 Location of the FRAM IV Arctic experiment conducted in the spring of 1982. [11]

Thesis Contents

My work in this area began long after the FRAM IV ambient noise data were collected. The first step was finding the events in the raw data. The data consisted of magnetic tapes each containing 20 minutes of digitized noise levels. A program was written which searched the ambient noise tapes for possible events. Chapter 2 describes the automated and manual techniques used to accomplish this detection.

These events were then located in space using the difference in arrival time between hydrophones. This was also done with a computer program. The program plotted the arrival time delays against range to a trial location, did a least squares fit, and chose the location with the best fit. This is covered in Chapter 3.

The peak voltages for each event were used with the dipole source model to predict peak source strength. The background ambient noise strength was also determined. These strength calculations are found in Chapter 4.

In Chapter 5 the distribution of event interarrival time was determined. The event locations and strengths were analyzed, and a spatial density found.

Chapter 6 summarizes the key results of this study.

CHAPTER 2

DETECTION OF NOISE EVENTS

Data Collection

Twenty nine FRAM IV ambient noise tapes were searched in order to find a population of noise events for this study. The specific tapes were chosen from the possible 67 in order to cover the entire range of days of the FRAM IV experiment. However, there were several days when no ambient noise tapes were recorded. To help fill these gaps five reverberation tapes were also searched. These tapes were recorded prior to the reverberation shot being fired, or they were recorded so late in the experiment (80 minutes after the shot) that reverberations were no longer present.

The FRAM IV experiemnt used the horizontal array of omnidirectional hydrophones pictured in Figure 2-1. The hydrophones were suspended from the ice into the water to a depth of 93 meters below the air/ice interface. The two crossed lines of the array allowed the possibility of localizing events in space. Although 26 hydrophones are shown in Figure 2-1, only 24 at a time could be used to record data. In most cases a few of the recording channels were used for other sensors (geophones or hydrophones used in a vertical array). Most of the time 19 to 21 horizontal array hydrophone data were recorded.

The FRAM IV ambient noise tapes were recorded digitally. Figure 2-2 shows a schematic of the system used

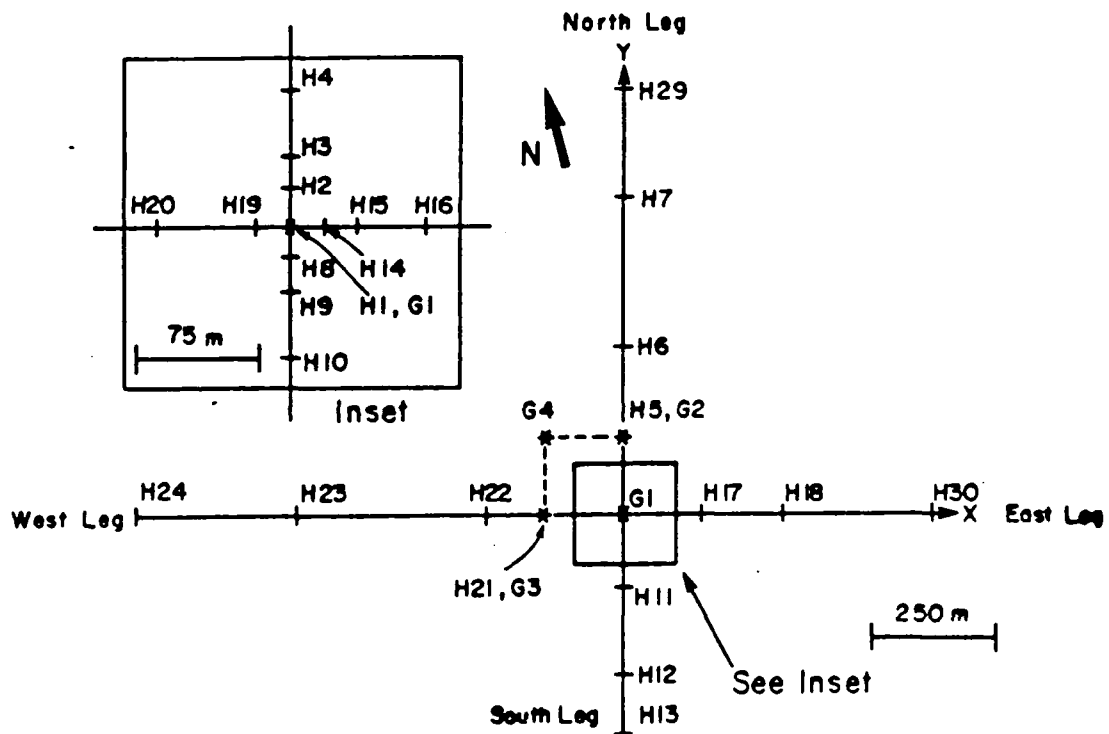


Figure 2-1 FRAM IV horizontal hydrophone array. [13]

FRAM IV DATA ACQUISITION

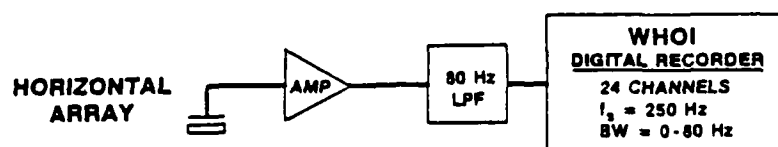


Figure 2-2 Schematic of the recording system used for FRAM IV data collection. [4]

for collecting the data. The input from each hydrophone was put through a gain ranging amplifier and a low pass 80 Hz filter. It was sampled at 250 Hz and recorded on 20 minute magnetic tape[4]. The 24 channel recorder had a 120 dB dynamic range[12].

Event Detector Program

The event detector program was written to take digital data from a FRAM IV tape and determine where in that tape noise events occurred. The program was originally written to take data directly from a tape drive, but subsequently modified to take the data from a file. The *framread* program, with a *-head* switch is used to read the tape into the file. This will eliminate any headers and then read the digital data straight into a file. A FRAM II tape may be read into a similar file using *framread* and the switches *-head* and *-fram2*. The *framread* program was written by G. Duckworth, and is available to the Arctic Acoustics Program at MIT.

The event detection programs source codes, flow chart, and a short users guide are found in Appendix A. The event detection program which reads from a file is called *hdetect*. The *detection* program reads from a tape drive. Both programs are written in the c programming language for a UNIX operating system.

The event detection program follows the block diagram

of Figure 2-3. The program initialization portion defines variables and constants, zeros flags, and requests user input such as tape number, date, time and channels(hydrophones) to be used, as well as, the name of input and output files. After this information is requested from the user, the program no longer requires attention.

The event detection program then reads in a file of data, filters the data, squares each data point, and takes the square root. The filter was a Parks-McClellan digital 20 to 80 Hz bandpass filter. Its frequency response is shown in Figure 2-4. The range of this filter was chosen to avoid the Nyquist frequency (125 Hz) and hydrophone cable strum (1-20 Hz), and to be compatible with the analog 80 Hz low pass filter the data went through before being recorded. The data were squared and then rooted to ensure positive peak values for all data points.

The next portion of the program used a threshold detection scheme to check each channel for possible noise events. For a particular channel a short average of the four most recent data points was compared to a long average of 64 recent data points. If the ratio of short average to long average was over a certain value that channel would be flagged for a possible event. The time of the flag and the value of the short average were also recorded. All other channels averages were taken similarly. If at least 50% of

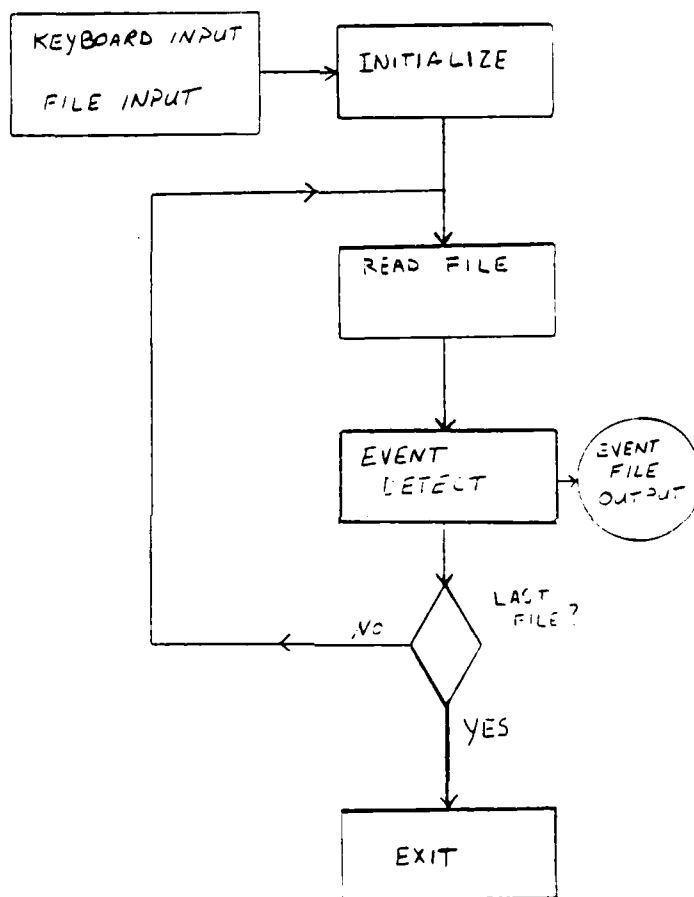


Figure 2-3 Block diagram of major modules of the detection program.

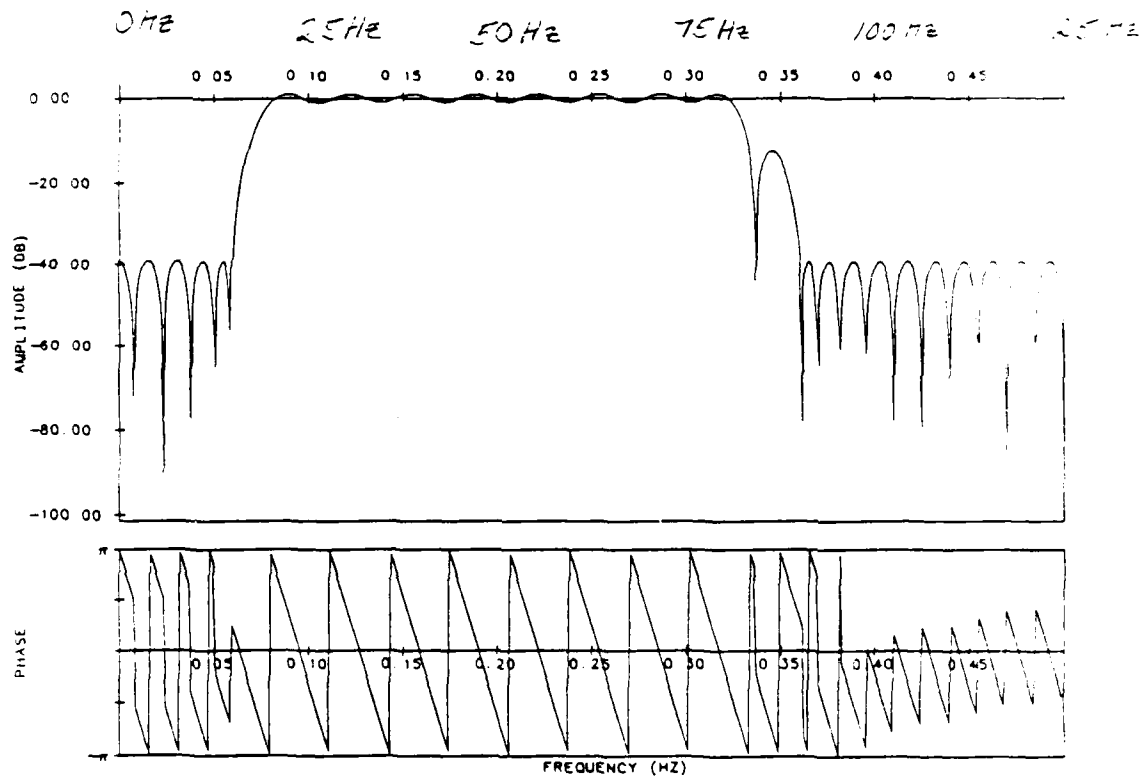


Figure 2-4 Frequency response of the Parks-McClellan digital bandpass filter used in detection.

the channels were flagged, an event would be declared. Then the program would shift to the next time increment of data and the process would be repeated.

A more detailed diagram of the event detection module is seen in Figure 2-5. There are four submodules: reset flag, set flag, new event, and deactivate old event modules. The reset and set flag modules deal with the channel flags which trip when a particular channel experiences a large signal-to-noise ratio (i.e. the RATIO of short average to long average exceeds a certain level). The new event and deactivate old event modules deal with an active event matrix which identifies active events, and stores channel flag time and amplitude for each declared event.

The reset flag module resets the channel flag if it has been more than 0.3 seconds since the channel tripped. Spurious peaks on a channel might flag a channel prematurely. This reset module prevents a number of channels with spurious peaks over a long time period from being falsely declared an event. The value of this RESET DELAY was determined by examining known events and noting that about half the channels tripped within a 0.3 second period.

The set flag module determines if the short average to long average RATIO has been exceeded and, if it has, the module 1) checks to see if the channel flag is already

FROM READ FILE MODULE

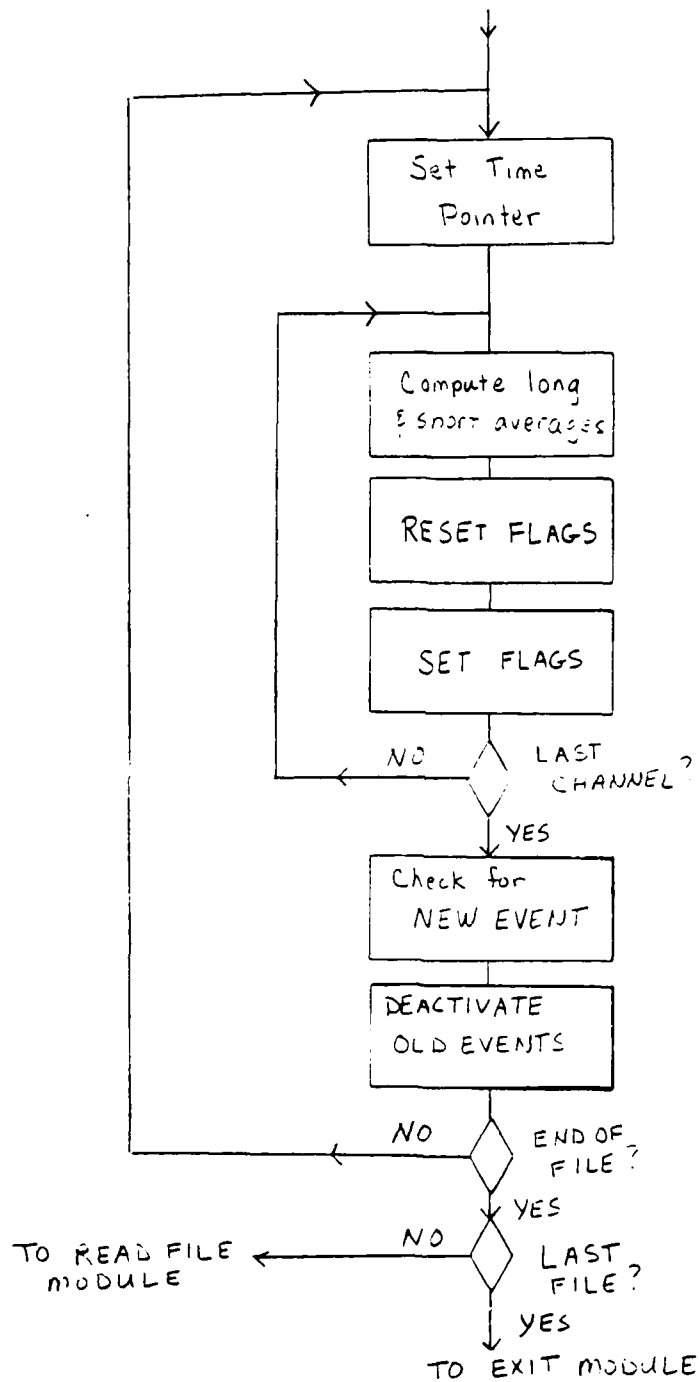


Figure 2-5 . Diagram of event detection module flow and decision making.

tripped, 2) checks to see if this detection is part of a recently declared event, and 3) adds its detection information to the active event or the channel flag, or discards the information depending on the circumstances. The short average length of 4 (= 0.016 sec) was chosen so that it matched the length of the signal (0.02 sec). This provides the maximum signal level since this is long enough to get all of the signal and short enough not to average it with the lower surrounding background noise level. The long average length of 64 was chosen because a length ratio of 15 to 1 had been suggested by Kelly[9] for the Large Aperture Seismic Array (LASA). The detection and localization schemes used by this large horizontal array were directly applicable to the FRAM IV hydrophone array data. The choice of detection RATIO was done through a series of tests, and the selection was made by balancing detection rate and false alarm rate.

When an event is declared the information in the channel flags is transferred to the active event matrix, and the channel flags are cleared. So if a channel has a detection and its channel flag is not already tripped, the set flag module must first see if the detection belongs to a recently declared event. If the active event already has that channel flagged, the information is replaced by the new detection only if their times differ by less than 0.02 seconds and the new detection amplitude is greater. This

means that the existing data can only be replaced by a detection of the same signal having a higher peak value. If the active event does not have that channel flagged, the detection information is entered in the active event matrix, and the channel flag is not tripped. The oldest active events are checked first, and the detection information entered in only one event. If all of the active events already have input for this channel, and it has been more than 0.02 sec since the most recent input, the detection is considered potentially part of an undeclared event, and its channel flag is tripped.

If a detection is made on a channel and its channel flag is already tripped, the information in the channel flag will be replaced with the new detection only if the new detection amplitude is greater.

The new event module checks to see if at least 50% of the channel flags have been tripped, and if so, declares a new event. The 50% mutual occurrence criterion was used in the LASA program with good results[9]. All the channel flag information is transferred to the active event matrix, and the channel flags are reset.

The deactivate old event module was used to remove events which were past. A set EVENT DELAY time after an event is declared, it is written to the output file and erased from the active event matrix. This prevents spurious peaks from being added to a event long past. The

EVENT DELAY time of 0.5 second was chosen because inspection of the known events revealed that most channels tripped within a 0.8 second period. The RESET DELAY (0.03 sec) plus the EVENT DELAY result in this 0.8 second look for each event.

The output of the event detection program is an output file which contains the time each event was declared, which channels were flagged and the time delay and peak amplitude for each channel. The time delays are relative to the earliest channel flag time, so one of the channels always has a zero time delay.

The first version of the *detection* program was written to take a new short average and long average at every data point (every 0.004 seconds). This program took 4 to 8 hours to search a 20 minute data tape. A concession to speed was made and the program changed to compute averages at every fourth sample point (every 0.016 seconds). This reduced the accuracy of the time delays and the ability of the program to pick up events. The *RATIO* had to be lowered in order to get the same detections which were obtained previously.

Studies to find the best signal-to-noise *RATIO* were conducted several times. Development of the LASA detection system had revealed that a 7 dB signal-to-noise ratio was needed for 75% detection[8]. This equates to a 5 to 1 ratio of signal power to noise power. Since I was working

with pressure vice power I used 2.2 as my starting RATIO. This RATIO engulfed me in false alarms. A quick study was done around the 2.4 level. The first 10 minutes of tape 4013 were run at RATIOS of 2.4, 2.45 and 2.48. This tape had been visually examined in detail previously, so the events were known. The results are shown in Table 2-1. Also shown in Table 2-1 are the results of a second study, done after the program had been changed to average less often.

Table 2-1 Determination of the Best RATIO

Average taken at every data point

RATIO	detection rate	false alarm rate
2.4	94%	25%
2.45	75%	18%
2.48	71%	8%

Average taken at every fourth data point

RATIO	detection rate	false alarm rate
2.3	76%	46%
2.38	71%	29%
2.4	59%	33%
2.5	59%	33%

detection rate = # event detections / # of known events
FA rate = # non-event detections / total detections

Notice how the detection rate has decreased and the false alarm rate increased as a result of only averaging at every fourth data point. Averaging less frequently means there is a smaller probability that the data points to be averaged will all lie near the peak amplitude of the signal. The signal level is generally lower than that detected when averaging every data point, and a lower signal-to-noise RATIO must be used to detect the same events. But when the signal-to-noise RATIO is lowered the false alarm rate increases.

The RATIO of 2.38 was settled on. This is a compromise which gives a detection rate which finds most high and medium strength events, and which has a tolerable false alarm rate. Because the detection rate is less than 100% (71%) there were events present which could be seen visually, but were not picked up by the detection program. The RATIO could have been adjusted to detect all events seen visually, but at the cost of a multitude of false alarms. The RATIO was kept at 2.38 and used for the detection of all data tapes.

The final version of the *hdetect* program read digital data from a framread file, detected possible events using the less frequent averaging scheme, and supplied the event time and channel time delays and amplitudes to an output file. Once the RATIO had been satisfactorily set the program was used to search the FRAM IV ambient noise tapes

for events, and no further program development was done. Weaknesses in the program were subsequently discovered, but have not been corrected.

The biggest problem is the accuracy of the event time (the time when 50% of the channels have been flagged). An event time reported by the event detection program will not exactly match that found by plotting the time series. The times are usually within 3 seconds of each other, but have been off by as much as 13 seconds in one case. The time difference between the two methods is greater at the end of a tape, and is likely to occur after a particularly strong event has taken place (though there were times when time discrepancies developed without strong events present, and also many strong events existed which did not induce discrepancies). Typically, there might be no time difference at the first part of the tape, then after a strong event a three second discrepancy would be seen and this would be consistent until the end of the tape. Because the errors did not appear randomly throughout the tape, and because they developed impulsively, I believe that the problem lies in the time counter of the event detection program becoming offset from the time of the raw data, perhaps because of short records in the raw data. The event detection program was not written to correct the time keeper in the event of a short record. Correcting this may eliminate the time discrepancy problem.

It has already been mentioned that the accuracy of the time delays deteriorated when the program was changed to run more quickly. This also made the detection of the event peak amplitude less likely. As a result, in order to get accurate locations and source strengths, both time delays and peak voltages had to be taken manually from time series plots of each event.

The other major problem of the event detector program is that it does not discriminate between an Arctic noise transient and an artifact such as an air gun blast or a reverberation shot. Short, strong signals are reported as possible events. Adding this discrimination to the program is the next step in improving its usefulness.

Visual Confirmation

Visual confirmation was required for all possible noise events in order to eliminate artifacts, false alarms and multiple detections of the same event. In addition, in a few cases visual confirmation revealed two events where there had only been one detection.

The event detection program was designed to preclude the need for plotting a time series of each event. The output of the program contains time delay and voltage amplitude information which can be used directly in the location program. However, because of the decreased accuracy of the time delay and amplitude information, and

because of the event time discrepancy mentioned previously, it was necessary to plot the time series of each event.

The first step of the visual confirmation is to review the tape log for any artifacts that may have occurred during the recording. The times are noted, and these are compared to the event times given by the detection program. Then a time series of the artifact was plotted to determine which detections were associated with it. In general, an artifact such as an air gun blast did not affect detections for over 20 seconds.

The visual confirmation portion of the procedure evolved from a very limited look only at events which could not be located with the detection program generated time delays, to a three step plotting procedure for each event. During the early period of this work the *hdetect* program output was used directly as the input to the location program. The location program used the time delays to determine the event's location in space. Those events which could not be located needed a closer look, and so their time series were plotted. The plots were made of a 2 second period including the event time given by the *hdetect* program. Often there was no apparent event in this time series plot, and the detection was declared a false alarm. When an event did plot, manual time delays were taken and used to locate the event. These manual delays located these events with better accuracy than the *hdetect*

generated time delays. It soon became apparent that the best answers would be obtained by taking manual time delays of all events. Trying to localize the events with the program generated time delays was dropped from the procedure, and the first step after getting the *hdetect* program output became doing a 2 second time series plot of each event.

After a dozen tapes had been analyzed in this manner the discovery of the event time discrepancy was made. After plotting a dozen events right at the time shown by the program, the final two dozen event of tape 4009 all appeared to be false alarms. The quality of the tape was good (low background noise), so this seemed highly suspicious. A broader search of the time around each event showed that the final two dozen events were not false alarms, but were events with times 5 seconds different than those indicated by the program, so that none of those events had shown up on the 2 second time series plots. The method of visually confirming events was changed so that a waterfall plot was made around the time of each event. This showed the exact time of the event, and helped discern the pattern of time discrepancy between time series and the *hdetect* program. Once the pattern was found events were easy to find and false alarms could be noted. The confirmed events were then plotted with 2 second time series.

The final step of visual confirmation was simply plotting and replotting the events to the proper gain so that the higher voltage amplitudes would not be cut off. These peak voltages were manually taken from the time series plots and used to determine source strength.

The final method used for visual confirmation was:

- 1) Check tape log for artifacts, and eliminate those from further analysis.
- 2) Plot a waterfall time series around each possible event, separate real events from false alarms, and find true event times.
- 3) Plot 2 second time series of each real event, adjusting gain to keep from clipping higher voltages.

Using this technique certainly reduced the false alarm rate. A breakdown of the detection statistics for tapes that had been examined by both methods is found in Table 2-2.

Table 2-2 Detection Statistics for Two Visual Confirmation Methods

	Artifacts	Events	False Alarms
Original Method w/ 2 sec plots	16.9%	37.5%	45.6%
Ultimate Method w/ waterfall plot 2 sec plot	16.2%	65.4%	18.4%

(Percentages of detections classed in each category)

The human interpreter was a necessary tool in this scheme. There was not necessarily a one-to-one correspondence between events and detections. There were cases where a strong event would cause multiple detections, and cases where two events occurred at the same time and caused only a single detection. In some cases a series of detections seemed to be an event and an echo, or perhaps straf. This would be counted as a single event.

The method of determining whether a detection was a false alarm or a weak event was sometimes difficult. In general, if the detection program indicated a possible event, "something" could be seen on the waterfall plot. The detection was dismissed as a false alarm if no pattern for taking time delays could be seen. (Because of the shape of the hydrophone array there were consistent patterns of time delays depending upon the direction to the event.) Presumably the false alarm rate depends upon the training and attention of the human interpreter.

Manual time delays were taken from an arbitrary reference to the crossing of the largest peak to peak amplitudes, as shown in Figure 2-6. For most events this was clear, but for weak or complex events some intuition was needed.

Voltage amplitudes were taken as the maximum peak voltage in the event signal. All were taken as magnitudes regardless of sign.

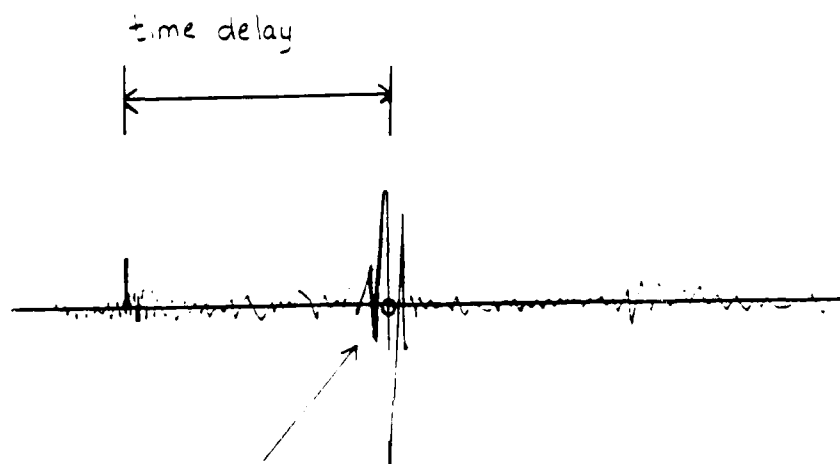


Figure 2-6 Sketch showing point of measurement for event time delays. The event is timed at its zero crossing between the largest pair of positive and negative peaks. (The measurement/analysis system has a polarity of negative voltage for positive pressure.)

All types of noise event signatures previously observed by Dyer[7] were seen in the ambient noise tapes I evaluated. The majority of events were pops and extended pops. There were also a few whines and straf events. While signature types were noted in general, the signature type of each individual event was not recorded.

CHAPTER 3

LOCATION OF NOISE EVENTS

Event Location Program

The program used for localization was based on the program *FQUAK* by Peter Stein [13]. This program places the event at different trial locations and computes the slant range to each hydrophone. Figure 3-1 shows the coordinate system used for these calculations. These are plotted against the time delays and a least square fit is done to determine slope as shown in Figure 3-2.

$$\text{slope} = \frac{(N \sum \Delta t R - \sum \Delta t \sum R)}{N \sum R^2 - (\sum R)^2} = A \quad (3-1)$$

$$\text{y intercept} = \frac{\sum \Delta t - (A \sum R)}{N} = B \quad (3-2)$$

The standard deviation of the time delays from the slope line is figured.

$$\text{sigma} = \sqrt{\frac{(\Delta t - AR - B)^2}{N}} = \sigma \quad (3-3)$$

The location having the lowest standard deviation is the location of the event. The inverse of the slope is the group speed of the signal. The y intercept of the plot is added to the reference time of the manual time delays to get the time the event actually occurred (as opposed to when it reached the hydrophone array).

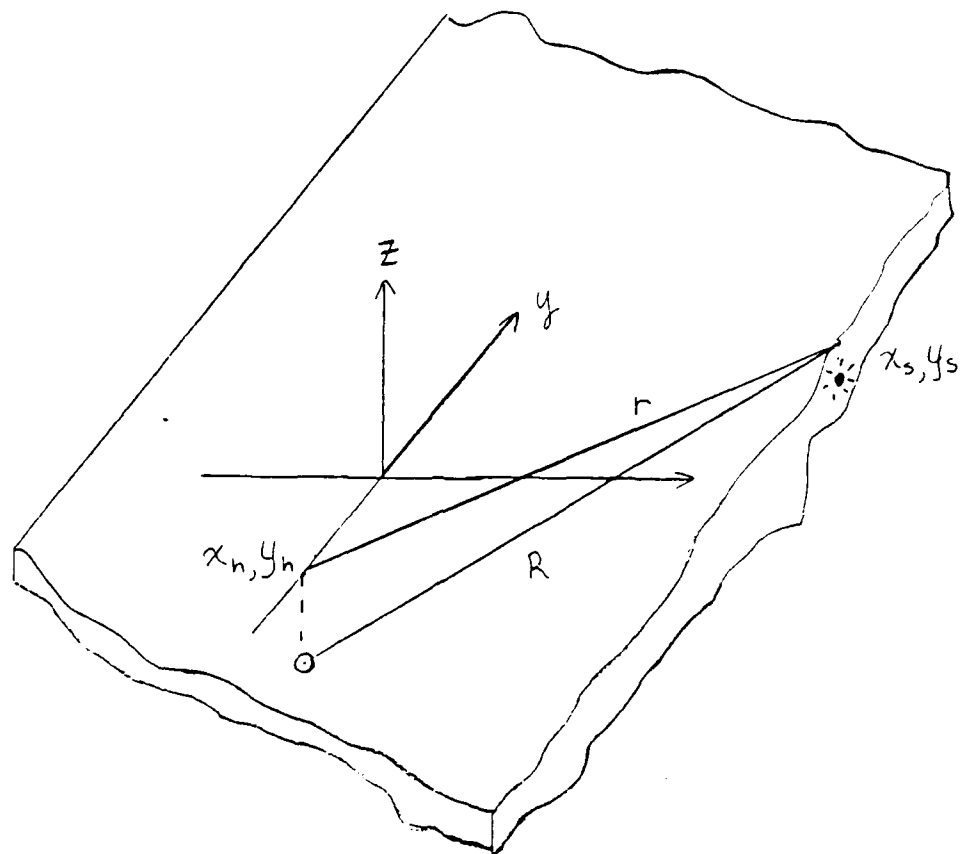


Figure 3-1 Coordinate system used for calculation of event location.

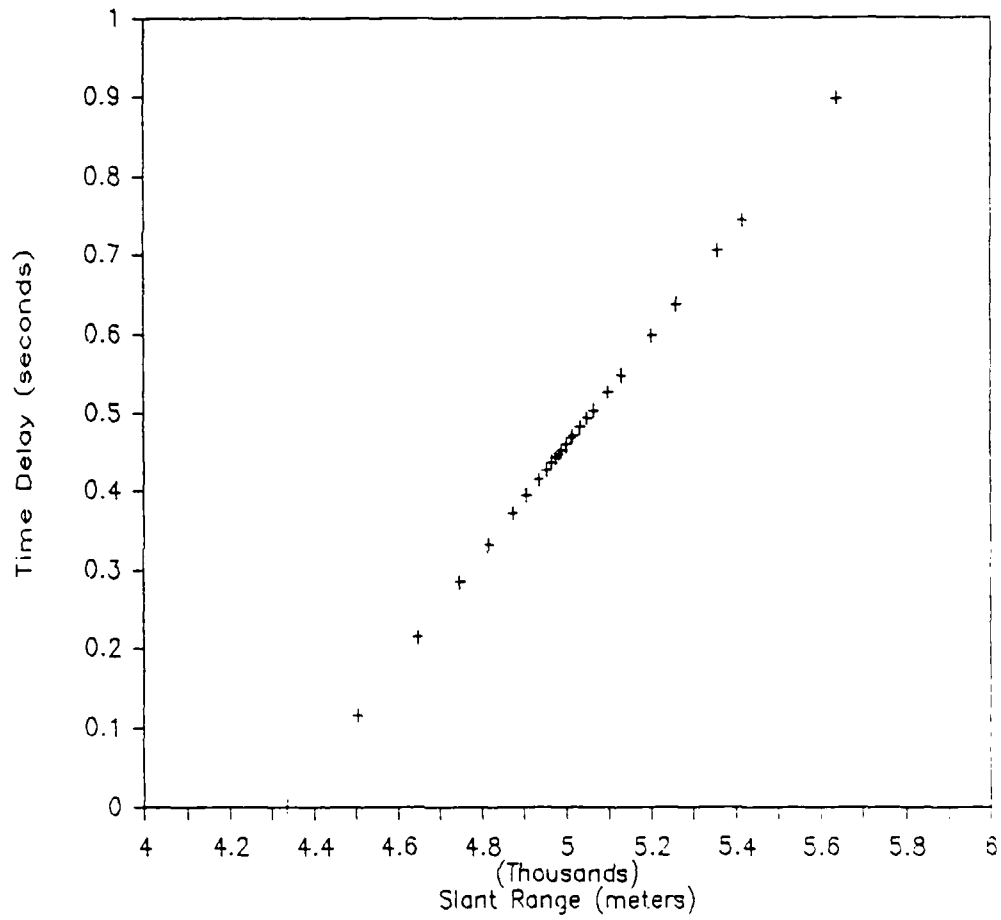


Figure 3-2 Least squares fit of time delays and test location slant range.

I have assumed that the strongest peak pressure sensed at the hydrophone is due to a waterborne acoustic propagation path from a source located in the ice sheet. The signal enters the water near the source and propagates directly toward the hydrophone.

I have assumed that the signal does not bounce off the ocean bottom or the ice canopy before reaching the hydrophone. Paths bouncing off the bottom would produce signals with much lower energy than the direct path signal, and can be ignored. Signals bouncing off the ice canopy are too energetic to ignore but, as I show subsequently, they do not affect the time delay computations significantly.

The location program is based on arrival times being related to slant range, R , and does not take the upward refraction of the acoustic path into account. The impact this has on the results is discussed in the next section.

The location program takes as input a file of time delays and voltage amplitudes, and outputs a file containing the best event location, sound speed, and standard deviation. It also computes source strength based on the voltage amplitude inputs, the event location and a spherical spreading loss. This feature was originally included so that the source strength could be computed directly from the event detection program outputs. Since the peak voltages recorded by the detection program are not as accurate as those done by hand, and since the

transmission loss does not follow simple spherical spreading, these computed source strengths were not used for any part of this study.

The *FQUAK* program set up a grid of points around a specified center position. The grid consisted of a point every 100 meters from -5000 to +5000 meters in both the x and y directions. This resulted in 100 x 100 test locations. When the best test location was found the interval spacing was reduced to every 10 meters, and another 10,000 test locations were generated using the best location of the first round as the new center. The process was repeated with a 1 meter interval to get the final answer. The scheme evaluated a total of 30,000 test locations, covered a range out to 5000 meters, and took about 20 minutes to run.

I noted that a significant number of events found with *FQUAK* were at the range limit of 5000 meters. The program location was written to search a larger area faster. The fineness of the grid was decreased to 20 x 20 vice 100 x 100. A 1000 meter interval was added to enable the program to search out to 10,000 meters. This reduced the total number of test locations to 1600 (20 x 20 x 4), and the time to one minute. location gave answers which were very consistent with *FQUAK*, except in one particular situation.

The wider grid size led to one problem. The location program sometimes found the lowest standard deviation for a

point in the quadrant directly opposite the true location. This was suggested by the sound speed being reported as approximately -1440 m/sec, as illustrated in Figure 3-3. This problem was solved by modifying *location* to make the program *finelocate*. This program used the grid size and spacing of *FQUAK*, and centered the search so that the user could designate which of the quadrants would be searched. A casual look at the manual time delays of an event easily reveals the appropriate quadrant. This program works well, but is as slow as the original *FQUAK*. It was used rarely.

As with the original *FQUAK*, I began to notice that some events were located at the range limit of the *location* program. This led to the modification of the *location* program to form the program *farlocate*. This program uses the *location* grid size and fineness, but allows the center point to be any of the far corners of the original *location* grid, or at the limit range at each of the cardinal points. This is shown in Figure 3-4. This allowed events to be located out to 20,000 meters.

The *location* program source code and a brief user's manual are found in Appendix B. This program was written in the c programming language for the UNIX operating system. This program was developed to the point of usefulness, and then used to locate events. No further program development was done (except the very minor changes to produce *finelocate* and *farlocate*), so there are surely

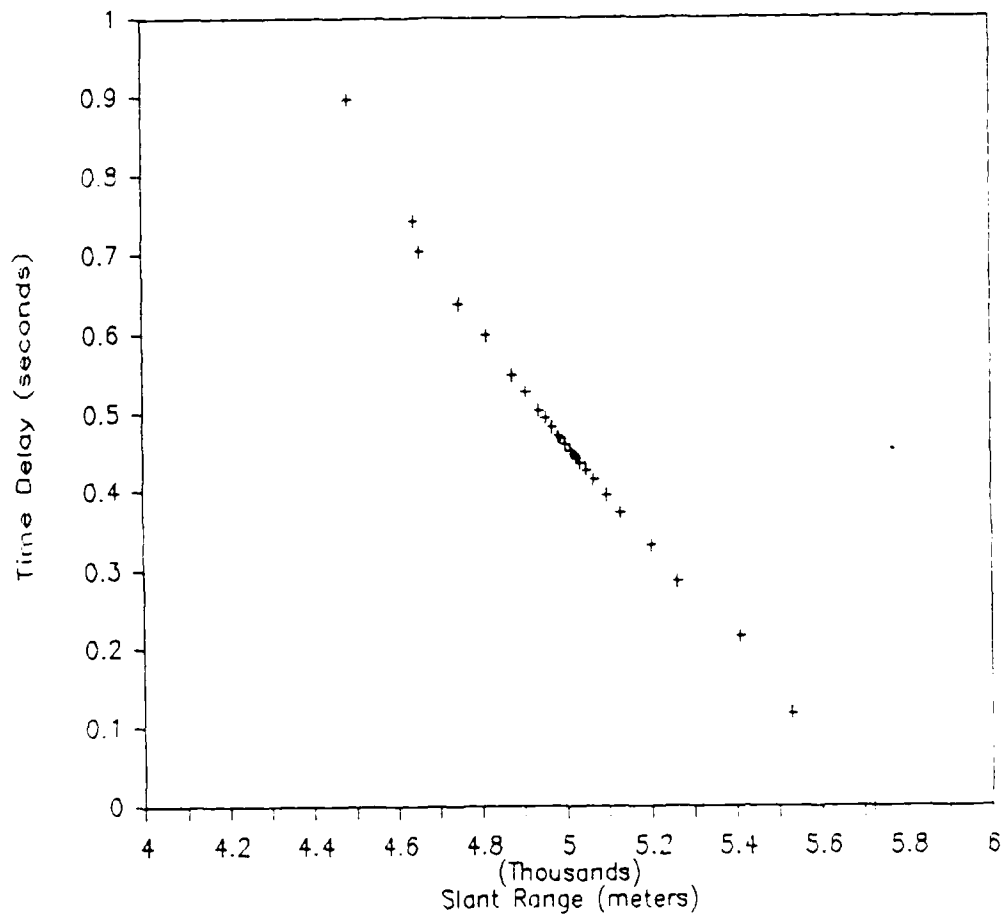
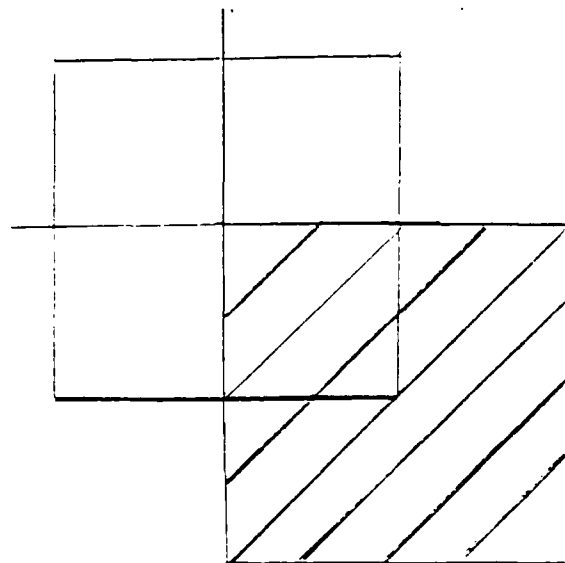
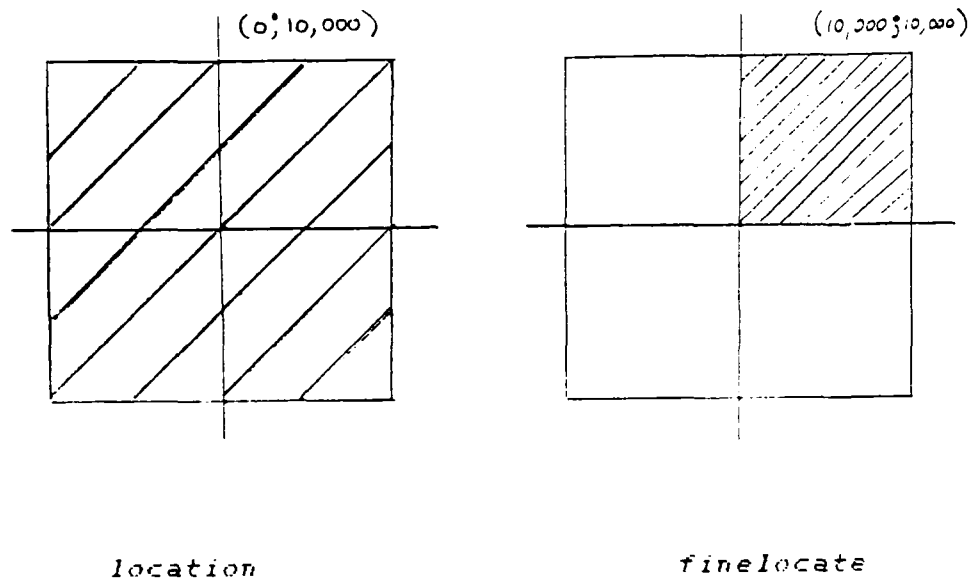


Figure 3-3 Least squares fit to a false location 180° away.



farlocate

Figure 3-4 Areas covered by *location*, *farlocate* and *finelocate*.

improvements to be made.

The location program is quite interactive. One hydrophone with a bad time delay can change the slope and location a great deal. An event is located by eliminating bad time delays and checking the sound speed and standard deviation of the location. In some cases no hydrophones needed to be removed, but in most cases at least one hydrophone was removed before an event was considered located. The sound speed was the major indicator of whether an event had been located. If the sound speed was between 1380 and 1500 m/s the event was considered located. Of course an attempt was made to get close to 1440 m/sec. This had to be balanced with reducing the standard deviation. A standard deviation below 0.01 seconds was considered good.

A table summarizing all of the events and their location parameters is found in Appendix C. The standard deviations (σ) are given in two sets of units. The first is the σ calculated by the *location* program, and it is in seconds. The second σ is a translation of that standard deviation to meters using the sound speed calculated for each particular event. The standard deviations ranged from 0.0010 to 0.0327 sec, with 0.0077 sec being the average. The significance of this standard deviation will be discussed in the next section.

In some cases just removing suspect time delays did

not lead to a localization. A reexamination of the event time series was done to see if any of the manual time delays was incorrect. Often a reexamination of the time series produced a change of 1 to 4 of the time delays. These corrected values plus values from the other channels would then be used to locate the event. About 15% of the events required reexamination. Most of those were subsequently located.

Despite the above efforts, there were a few events that could not be located within the 1380 to 1500 m/sec sound speed limits. These events may be from propagation paths other than the assumed direct acoustic path. Events arriving primarily through the ice longitudinal wave or the ice flexural wave would have phase speeds above and below my sound speed limits. These non-locatable events are indicated in the event location summary of Appendix C, and they were not used for any analysis which required accurate location.

Figure 3-5 shows the position of the events located within a 2 km square centered on the array origin. Figure 3-6 shows the position of all events located.

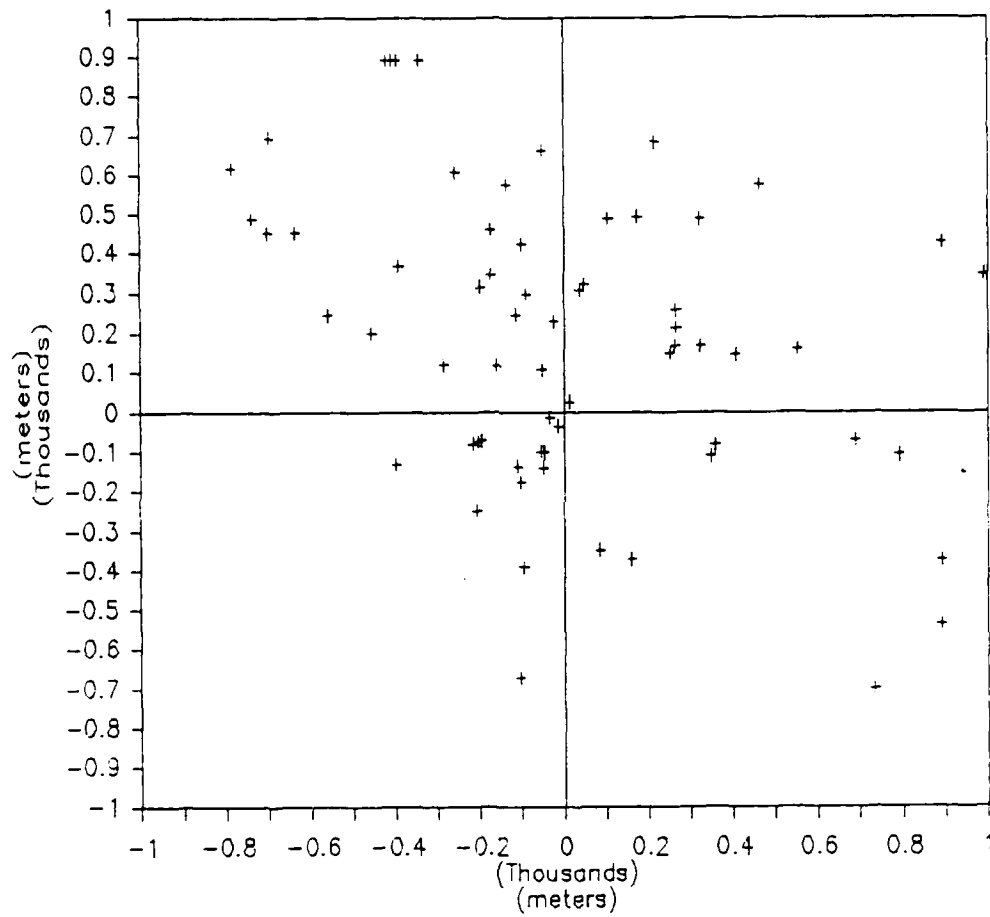


Figure 3-5 Noise events located within a 2 km square surrounding the array origin.

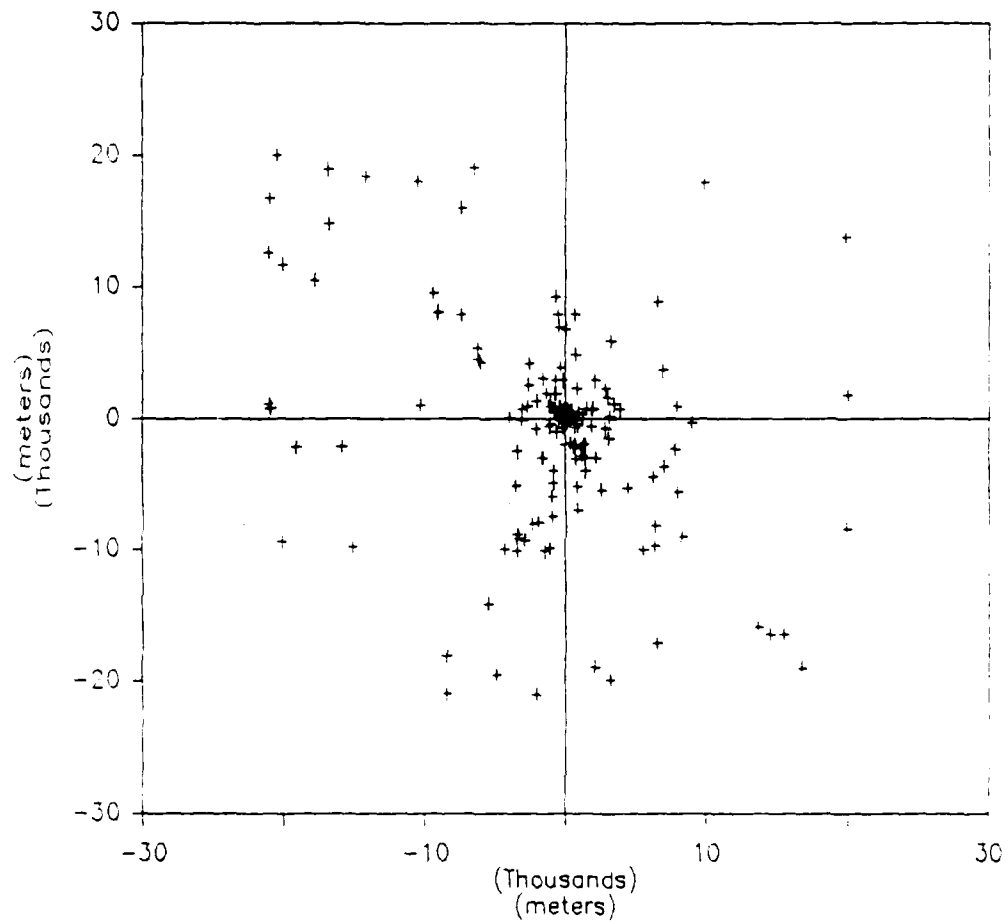


Figure 3-6 Position of all noise events located.

Effects of Refraction on Location

A sound speed profile was used to get the refractive paths for various ranges. This was simplified by the fact that all the hydrophones were at a depth of 93 meters. Assuming that only the "direct" path is involved means that each horizontal range has to have a unique launch angle in order to reach the hydrophone at its specific depth. Rays were launched into the layers of the sound velocity profile and the horizontal range to the hydrophone was calculated. The time required to travel the refractive path can be calculated and compared to that of the slant range. This time error can then be related to the error of the location program.

Figure 3-7 shows the linearized sound velocity profile that was used. It is based on the sound velocity profile reported for the eastern Arctic ocean by Chen[11]. Figure 3-8 helps to illustrate the scheme used to calculate the ray paths. Equations 3.4, 3.5 and 3.6 were used to calculate angles, ranges, depths, and propagation time.

$$z = \frac{V_0}{g \cos \theta_0} \left| \cos \theta_0 - \cos \theta_1 \right| \quad (3-4)$$

$$r = \frac{V_0}{g \cos \theta_0} \left| \sin \theta_0 - \sin \theta_1 \right| \quad (3-5)$$

$$t = \frac{1}{2g} \left| \ln \frac{(1 + \sin \theta_1)(1 - \sin \theta_0)}{(1 - \sin \theta_1)(1 + \sin \theta_0)} \right| \quad (3-6)$$

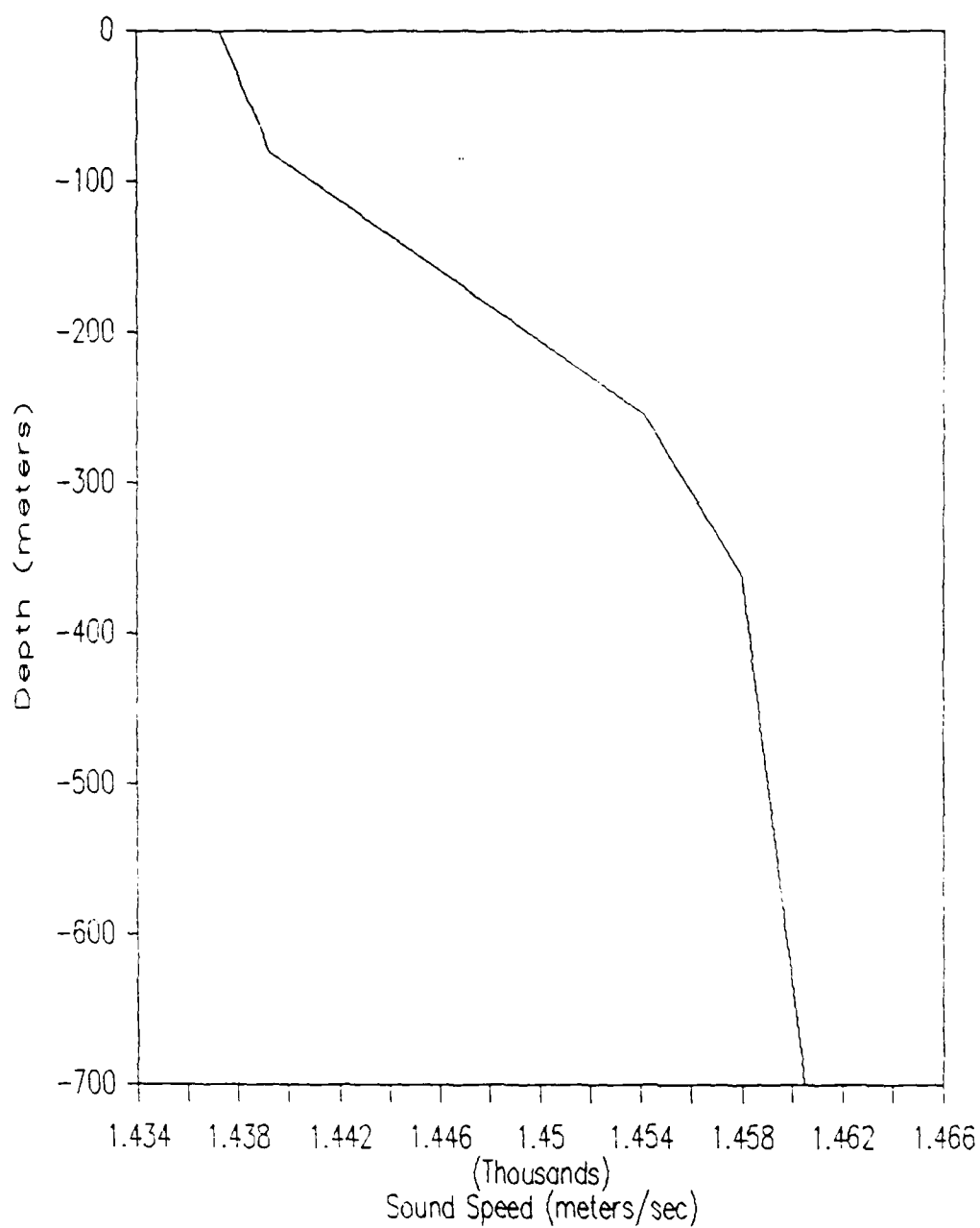


Figure 3-7 Sound velocity profile used in predicting refractive paths.

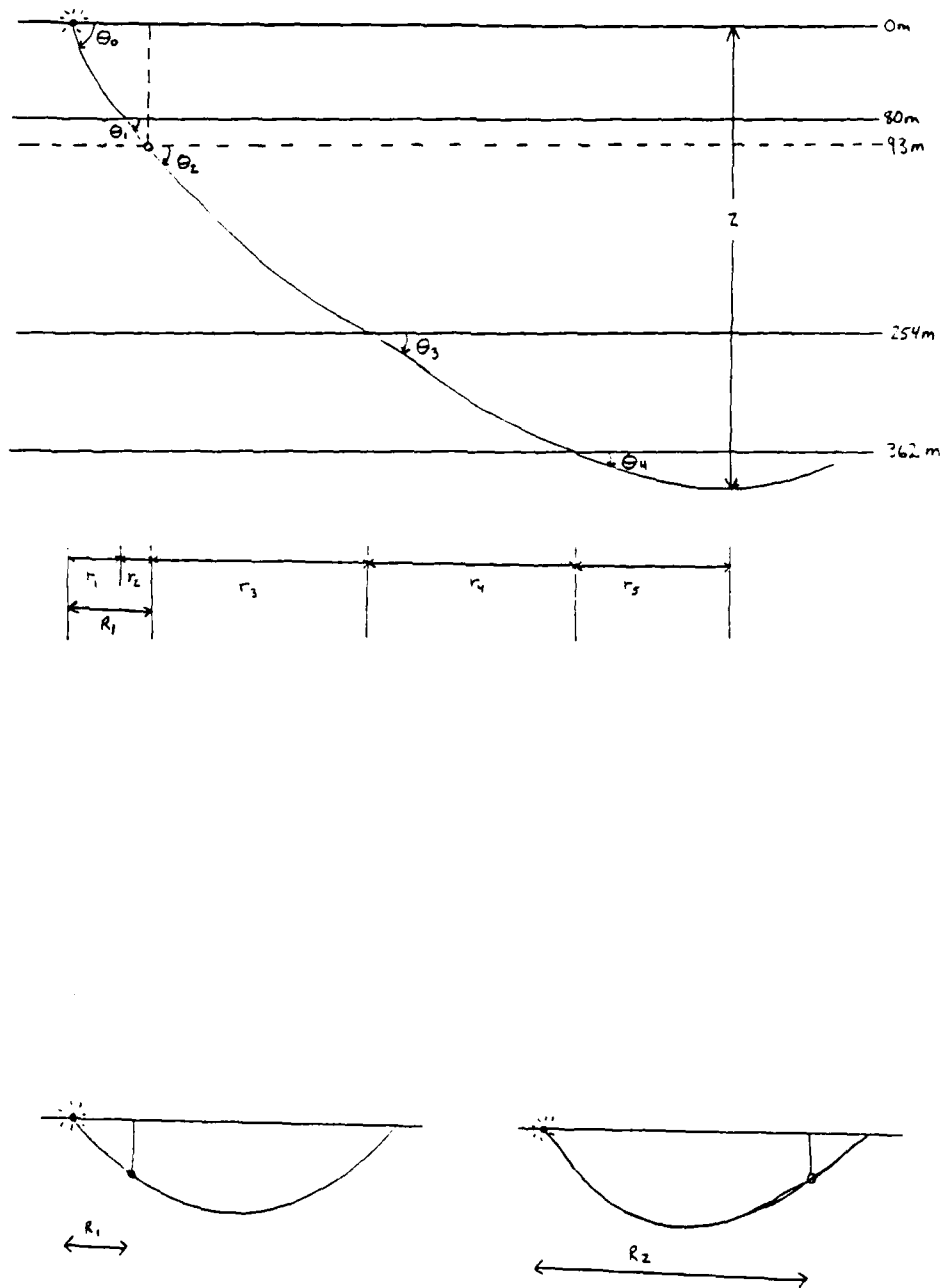


Figure 3-8 Scheme used to compute refractive propagation paths. Source is located at $z = 0\text{m}$ and hydrophone at $z = 93\text{m}$. Sound speed gradients change at 80m, 254m and 362m.

Using the known depths (z) and estimated speed gradients (g) of Figure 3-7, and choosing a particular launch angle (θ_0), all of the subsequent angles of intersection of the layer interfaces ($\theta_1, \theta_3, \theta_4$) can be found from Equation 3-4. The angle which intercepts the hydrophone at its depth (θ_2) can also be found. With the angles known, the horizontal range and propagation time for each layer can be determined with Equations 3-5 and 3-6. These are combined to get the total horizontal range and propagation time. It should be noted that there are two ranges and times for each launch angle. The first path is that which intercepts the hydrophone on the way down, while the other intercepts the hydrophone as it is refracted back toward the surface. The maximum depth reached by the propagation path was also found, and those paths that went below 754 meters, resulting in a range greater than 30600 meters were not reported. A tabular summary was made of launch angle, horizontal range from the hydrophone, maximum depth and propagation time, and this may be found in Appendix D, along with more detailed tables listing θ_{1-4} , r_{1-5} and t_{1-4} .

Rays connecting source and hydrophone with one or more bounces from the ice were not considered here. The effect of those rays will be taken into account in Chapter 4.

The refractive propagation time was less than the slant range propagation time because the refracted path

travels through faster water. The slant range propagation time was calculated by dividing the slant range by 1438.46 m/sec, the average sound speed between 0 and 93 meters depth. The time difference between the slant range path and the refracted path are shown in Figure 3-9 as a function of horizontal range.

This time difference is greater than the average standard deviation of the location program only after 13,000 meters, and the time difference at 20,000 meters is only about twice that average. The standard deviation does not reflect the time difference due to refraction because all of the hydrophone time delays are adjusted in the same manner and direction. Figure 3-10 shows that sigma does not grow with horizontal range. Refraction effects do not influence the standard deviation greatly. Closer than 13,000 meters the range error caused by other factors masks any error from ignoring refraction.

There is a better point of focus for examining the effect of refraction, and that is the change in time delay, not the change in the propagation time itself. A point was chosen at approximately 5 km from the origin of the hydrophone array, and another chosen at approximately 6 km. The slant range propagation times and refractive propagation times were calculated for each point. The time delay between these two points was 0.6857 sec for the refractive path and 0.6930 sec for the slant range path.

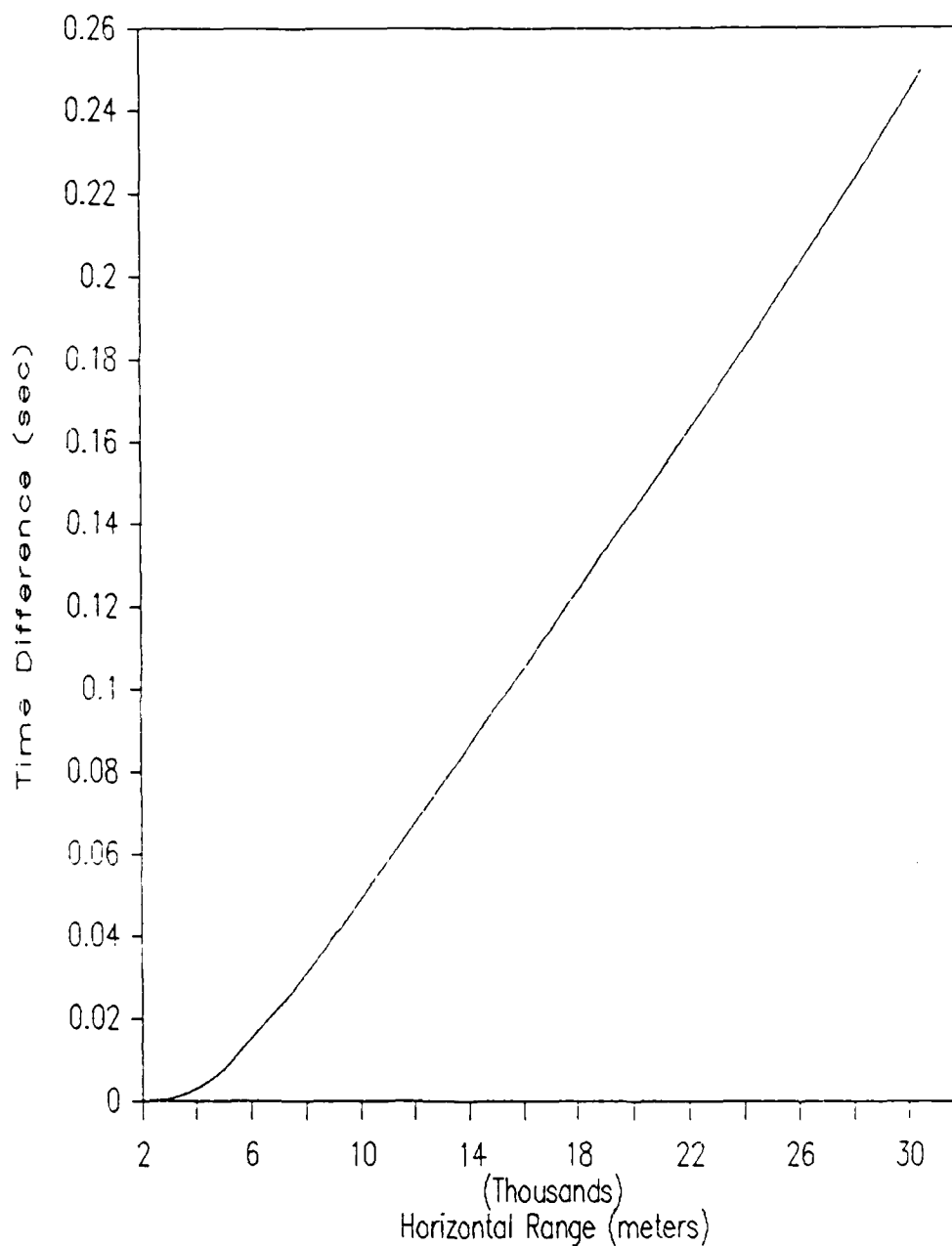


Figure 3-9 Time difference between the slant range acoustic path and the refractive path as a function of horizontal range.

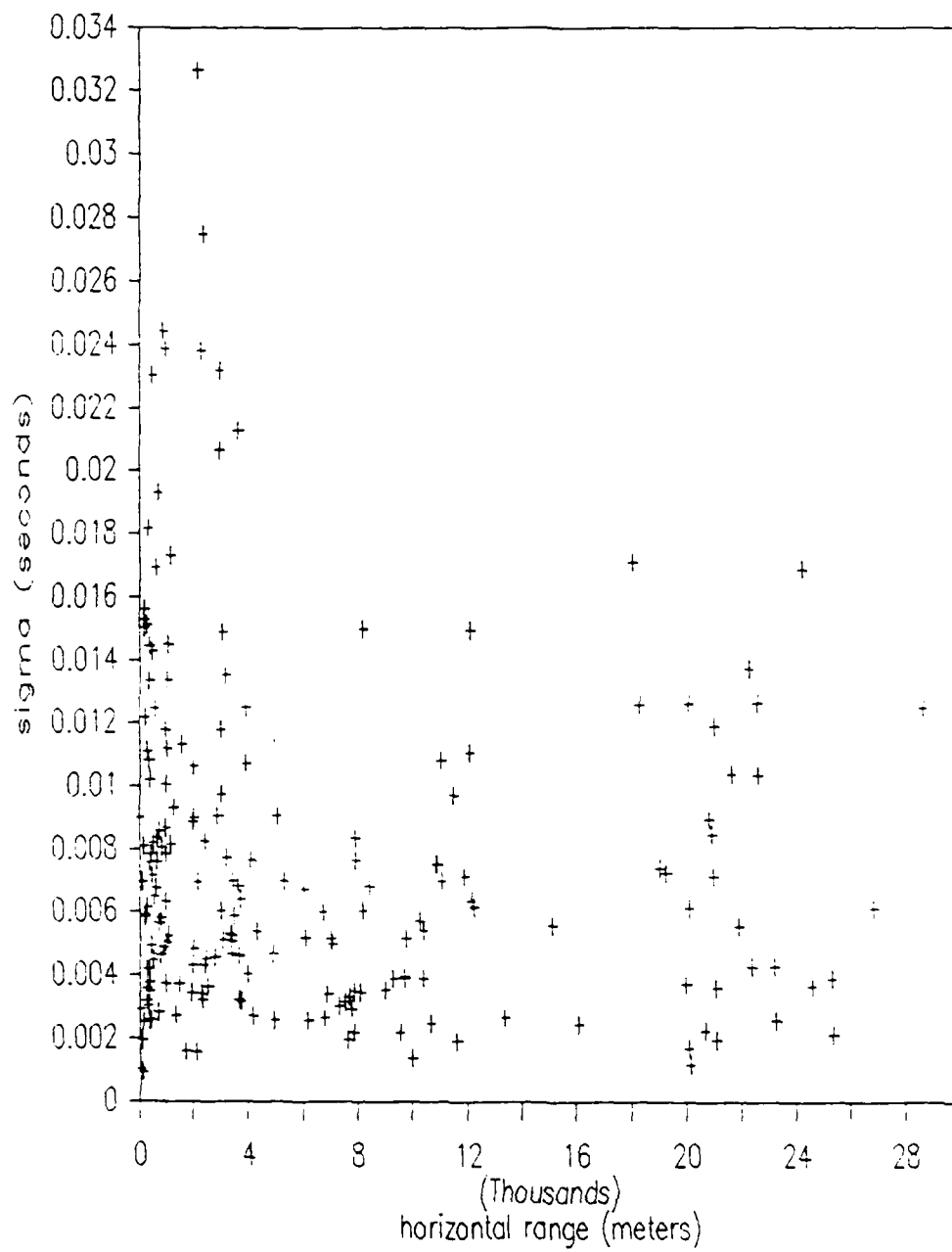


Figure 3-10 Scatter plot of standard deviation and range for all located noise events.

The difference was 0.0073 (about 1%), or a deviation of 0.0037 sec for each hydrophone. Two points at approximately 18 and 20 km were also evaluated. The difference between their time delays was 0.0182 sec (about 0.2%), or 0.0091 sec per hydrophone. These numbers are the same order as the total error of the location program.

The location program may compensate for some of this error by raising the sound speed. If just the points above were used, the sound speed would go from 1438.5 to 1453.8 at 5 km and to 1458.6 at 20 km. With 24 time delays being used in the location program the effect may not be as great.

The main source of error in the location program is the quality of the manual time delays. When the signal-to-noise ratio was low, picking the correct peak was often difficult. The standard deviation will reflect the judgement of the person picking off the time delays. The time delays were only measured to the closest 0.003 sec. It is interesting to note that 0.006 seconds equates to the width of a pencil tip on the time series plot scale.

The final question to be answered is "How do the standard deviation and refraction errors equate to the range and bearing accuracy of the location program." Two hypothetical noise events were investigated, one at 5000 meters (2845, 4136) and the other at 20,000 meters (-8253, 18896). The time delays for slant range propagation

and refractive propagation were calculated. The *location* program was run for each set of time delays, and for each set partially contaminated with 0.016 sec errors. (Zero, +0.016 and -0.016 were each added to one-third of the time delays.) The results are summarized in Table 3-1.

Table 3-1 Results of *location* Program Accuracy Test

	R (m)	ΔR (m)	θ (deg)	$\Delta \phi$ (deg)	σ (sec)	c (m/s)
slant range						
5 km	4725	-295	55.6	+0.1	0.0003	1440
20 km	18477	-2143	113.7	+0.1	0.0002	1437
refraction						
5 km	4724	-296	55.6	+0.1	0.0003	1454
20 km	18477	-2143	113.7	+0.1	0.0002	1458
slant range w/						
5 km	4191	-829	55.8	+0.3	0.0127	1453
20 km	20526	-94	113.9	+0.3	0.0130	1443
refraction w/						
5 km	4209	-811	55.8	+0.3	0.0130	1466
20 km	20526	-94	113.9	+0.3	0.0130	1463

The refraction contaminated by errors case is closest to what was input into the *location* program for the field events. This table gives an estimate of the accuracy of the *location* program as 800 m at 5 km, and 2000 m at 20 km. The bearing accuracy is excellent.

CHAPTER 4

STRENGTH OF NOISE EVENTS

Acoustic Source Model

The dipole is considered a possible source model. Peak values for the source parameter of force, F , are used.

The acoustic pressure due to a non-convecting compact dipole source, in a nonrefracting infinite medium, is[5]:

$$p = \frac{\sin \theta}{4\pi R} \left[\frac{1}{c} \frac{\partial F}{\partial t} + \frac{F}{R} \right], \quad (4-1)$$

where R = slant range.

Figure 4-1 shows the orientation of the presumed dipole.

The angle θ is the launch angle from the horizontal plane down into the water.

Assuming that F may be expressed as a harmonic,

$|\partial F / \partial t| = \omega F = 2\pi f F$. the pressure may then be expressed as

$$|p| = \frac{\sin \theta}{4\pi R} \left[\frac{2\pi f F}{c} + \frac{F}{R} \right]. \quad (4-2)$$

Solving for F gives

$$F_0 = \frac{p_0 4\pi R^2 c}{\sin \theta [2\pi f R + c]}. \quad (4-3)$$

In the far field the $2\pi f R$ term dominates the sum in

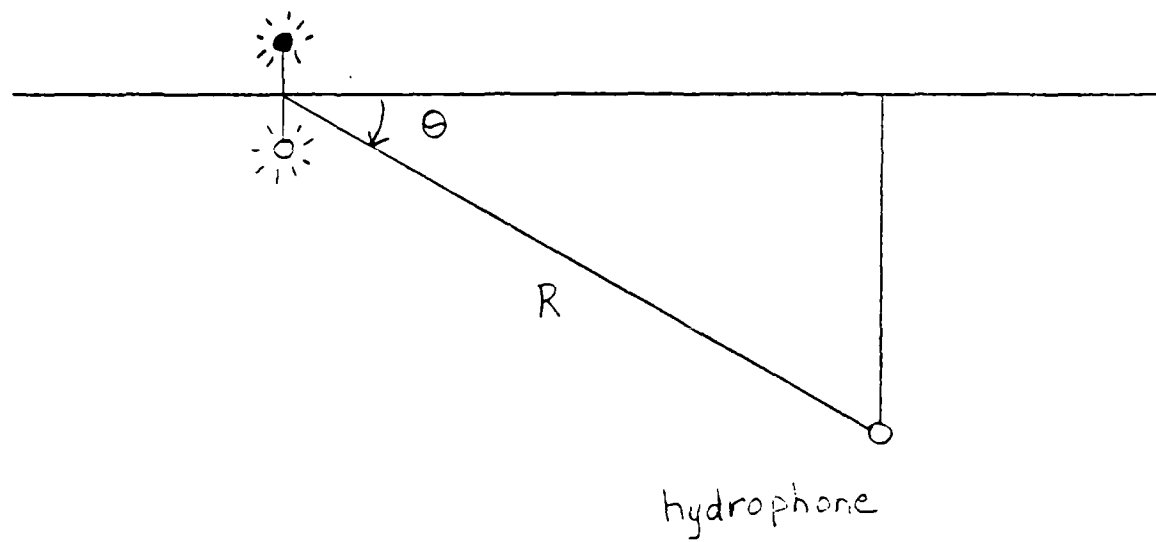


Figure 4-1 Assumed dipole source orientation and definition of launch angle, θ .

the denominator. For the lowest frequency considered in this study (20 Hz), c (1440 m/sec) is 10% of $2\pi fR$ at 115 meters and only 1.1% of $2\pi fR$ at 1000 meters. When the c in the denominator is neglected the force can be written as:

$$F_0 = \frac{2p_0 R \lambda}{\sin \theta} , \quad (4-4)$$

where λ is the wavelength.

The peak pressure, p_0 , should lead to the peak force, F_0 . This definition of force was used as the parameter for dipole strength. Event signatures that were recorded from a source within 300 m of a hydrophone were not used to calculate dipole strength, F_0 , from peak pressure, p_0 .

For this model the peak acoustic pressure must be found. The hydrophone sensitivity of -159 dB re 1 volt per 1 μ Pa was used to convert voltage to pressure[17].

$$1 \text{ volt} \Rightarrow 89 \text{ N/m}^2 = 89 \text{ Pa} . \quad (4-5)$$

The dipole strength formula requires wavelength, λ . Frequency was taken from the time series plots for each event via axis crossing rate, and λ was determined by dividing c (1440 m/sec) by the frequency.

Launch angle needed for the dipole model can be found as in Chapter 3 by assuming a sound velocity profile and computing the refractive path. There is a unique launch

angle for each horizontal range when the path is purely refractive, but a range of launch angles when surface reflection paths are included.

The final parameter in the dipole strength formula is slant range. The answers obtained using slant range are the strengths based on spherical spreading in a non-absorptive medium, equation 4-4. Because the spherical spreading assumption is a poor one, (refractive and surface reflective propagation paths are caused by the Arctic sound velocity profile), equation 4-4 must be modified. The effect of refraction on spreading loss will be discussed in the next section.

Volumetric absorption was found by using the absorption formulas of Dyer[5]. Assuming a pH of 8.2, a salinity of 33.5 ‰, a temperature of 0° C and a pressure of 40 atmospheres, I calculated the total volumetric absorption to be 1.3×10^{-3} dB/km for an 80 Hz signal. For my maximum horizontal range of 20 km, the absorption would be 0.026 dB. This is not significant, and I therefore did not include a volumetric absorption correction in the strength calculations.

Effects of Refraction on Transmission Loss

Spherical spreading loss in a nonrefracting medium is illustrated in Figure 4-2[14]. The sound pressure is presumed to spread radially. The sound pressure squared

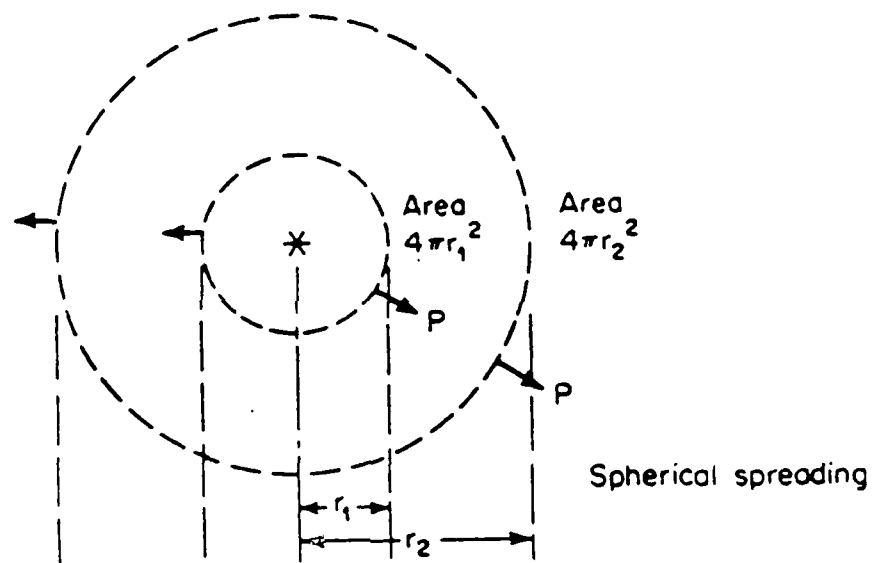


Figure 4-2 Spherical spreading. (From Urlick[14])

is proportional to intensity, and intensity is the power per unit area. Since the power from a source is constant

$$P = I_1 4\pi R_1^2 = I_2 4\pi R_2^2 \quad (4-6)$$

The intensity at the reference range of 1 meter can be related to other intensities by

$$I_R = \frac{I_{ref} 4\pi}{4\pi R^2} = \frac{I_{ref}}{R^2} \quad (4-7)$$

Since $I = p^2/\rho c$, this can be expressed in terms of transmission loss, H.

$$H = -10 \log \frac{p_R^2}{p_{ref}^2} = 10 \log R^2 = 20 \log R \quad (4-8)$$

in dB re the distance reference, taken as 1 m.

The spreading scheme for a refractive medium is shown in Figure 4-3[2]. This is based on ray theory which assumes that acoustic energy does not cross the rays, with energy contained between two rays being conserved. The intensity at the reference range between the two rays shown is:

$$I = \frac{P}{2\pi R \cos \theta_0 R \Delta \theta} = \frac{P}{2\pi \cos \theta_0 \Delta \theta} \quad (4-9)$$

At a horizontal distance r meters from the source, the intensity is:

Figure 4-3 Spreading loss in refraction. (From Clay and Medwin[2])

$$I_r = \frac{P}{2\pi r L} = \frac{P}{2\pi r \Delta r |\sin \theta_1|} = \frac{P}{2\pi r \Delta z \cos \theta_1} \quad (4-10)$$

The relation between intensities becomes:

$$I_r = \frac{I_{ref} 2\pi \cos \theta_0 \Delta \theta}{2\pi r \Delta r |\sin \theta_1|} = \frac{I_{ref} \Delta \theta \cos \theta_0}{r \Delta r |\sin \theta_1|} \quad (4-11)$$

The loss due to spreading is:

$$\frac{I_r}{I_{ref}} = \frac{\Delta \theta \cos \theta_0}{r \Delta r |\sin \theta_1|} \quad (4-12)$$

In terms of pressure, $I_r = p_r^2 / \rho_1 c_1$, and $I_{ref} = p_{ref}^2 / \rho_0 c_0$, and therefore

$$\frac{p_r^2}{p_{ref}^2} = \frac{\rho_1 c_1}{\rho_0 c_0} \frac{\Delta \theta \cos \theta_0}{r \Delta r |\sin \theta_1|} \quad (4-13)$$

Since by Snell's law, $\cos \theta_0 / c_0 = \cos \theta_1 / c_1$,

$$\frac{p_r^2}{p_{ref}^2} = \frac{\rho_1}{\rho_0} \frac{\Delta \theta \cos \theta_1}{r \Delta r |\sin \theta_1|} = \frac{\Delta \theta}{r \Delta r |\tan \theta_1|} \quad (4-14)$$

since $\rho_1 / \rho_0 = 1$ in seawater to an excellent approximation.

Applying the dipole model to this spreading loss equation gives

$$p_0^2 = \frac{4\pi^2 \sin^2 \theta_0 \Delta r}{r |\tan \theta_1| \Delta r} \quad (4-15)$$

where $A = F_0 / \lambda$.

Equation 4-15 assumes a unique refractive path between source and hydrophone. In the Arctic there may be other paths due to the non-specular scattering of rays off the ice canopy. Figure 4-4 illustrates how rays normally trapped in a surface duct, may be deflected down to a hydrophone. The minimum vertexing angle calculated from the linearized sound velocity profile of Chapter 3 was 0.064 radians. For a ray to stay in a surface duct above the hydrophone it must be reflected from a slope of less than 0.032 radians or about 2° . It is reasonable to assume that the ice canopy lacks local levelness to this order, so that non-specular rays must be accounted for.

The rays which rebound from the ice canopy experience some loss. The attenuation for the FRAM IV experiment has been reported at 0.1 dB/km at 80 Hz[11]. This attenuation may be converted to a loss per bounce.

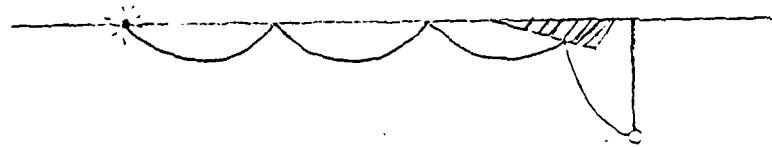
$$\beta = 0.1 \text{ dB/km} = \frac{b}{X} , \quad (4-16)$$

where b = loss per bounce, and
 X = cycle distance.

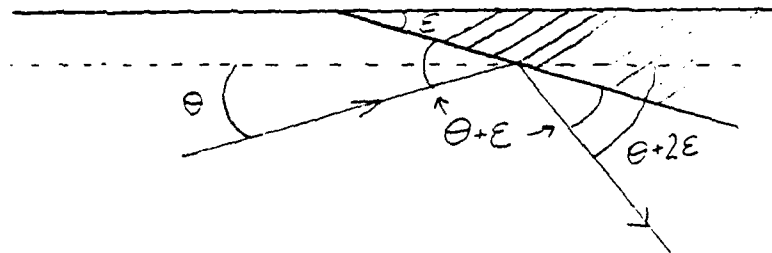
The cycle distance depends on the launch angle and the sound speed gradient. For a launch angle of 0.032 radians and the assumed sound velocity profile of Chapter 3, the cycle distance is 3.7 km. Therefore, the loss per bounce is about 0.4 dB. This loss is low enough that even a ray



specular reflection



non specular reflection



detail of non specular reflection

Figure 4-4 Specular and non-specular reflections from the ice/water interface.

which has bounced several times may contribute a significant amount of energy at the hydrophone. The non-specular rays cannot be ignored. Bounce loss at frequencies less than 80 Hz are even smaller, since the data show a roughly linear dependence on frequency.

To account for the non-specular rays the spreading loss is calculated using the ray averaging technique[5]. The pressure from a particular ray at a given depth and horizontal range, assuming a dipole source model, is

$$p^2(r,z) = \frac{A^2 \sin^2 \theta_0}{r |\tan \theta_1|} \frac{d\theta}{dr} \frac{dr}{X/2} \quad (4-17)$$

The term $\frac{dr}{X/2}$ represents the probability that a ray bundle will cross a certain depth, as shown in Figure 4-5. For a single linear sound speed gradient the cycle distance can be written as

$$X = \frac{2c_v}{g} \sin \theta_0 = 2r_c \sin \theta_0 \approx 2r_c \theta_0 \quad (4-18)$$

where r_c is the radius of curvature, to a good approximation constant for all small angle rays in a linear sound speed gradient.

Applying equation 4-18 to equation 4-17, and using the small angle approximation, gives

$$p^2(r,z) = \frac{A^2 |\theta_0| d\theta_0}{r_c r |\theta_1|} \quad (4-19)$$

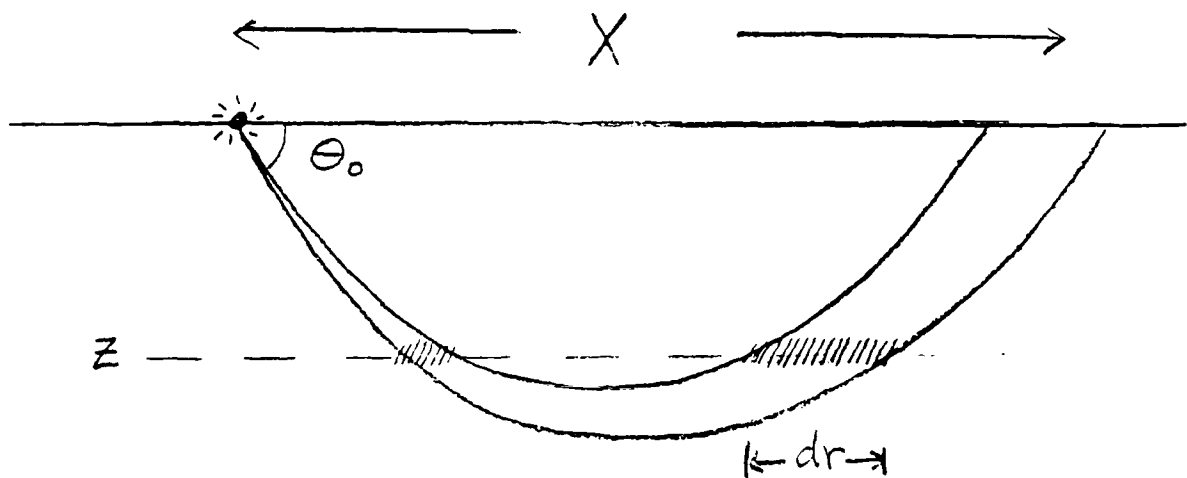


Figure 4-5 Probability of a ray bundle crossing a certain depth at a given horizontal range.

In order to average the contributions of the possible rays, this pressure is integrated over all possible angles for a given receiver depth, and then averaged over depth down to the hydrophone at z_0 .

$$p^2(r) = \frac{2 A^2}{r r_c} \frac{1}{z_0} \int_0^{z_0} dz \int_{\theta_m}^{\theta_v} \frac{\theta_0}{|\theta_1|} d\theta_0, \quad (4-20)$$

where θ_v is the maximum launch angle of a ray that will hit the hydrophone at a given range, and θ_m is the minimum launch angle.

The angle θ_1 is a function of θ_0 and z

$$z = r_c [\cos \theta_1 - \cos \theta_0] \quad (4-21)$$

Using the small angle approximation for cosine leads to

$$\theta_1 = \sqrt{\theta_0^2 - \frac{2z}{r_c}} \quad (4-22)$$

Substituting this into equation 4-20 and evaluating the integral over angle gives

$$p^2(r) = \frac{2 A^2}{r r_c z_0} \int_0^{z_0} \left[\sqrt{\theta_v^2 - \frac{2z}{r_c}} - \sqrt{\theta_m^2 - \frac{2z}{r_c}} \right] dz \quad (4-23)$$

$\theta_m^2 = \frac{2z}{r_c}$ for all z so the second term within the integral is always zero. Evaluating the first term over depth gives an expression for pressure in terms of r and θ_v .

$$p^2(r) = \frac{2 A^2}{3 r z_0} \left[\theta_v^3 - \left[\theta_v^2 - \frac{2z_0}{r_c} \right]^{3/2} \right] \quad (4-24)$$

This expression can be used to find the source strength.

$$A^2 = p^2 \frac{3 r z_0}{2 \left[\theta_v^3 - \left[\theta_v^2 - \frac{2z_0}{r_c} \right]^{3/2} \right]} = G(r) p^2 \quad (4-25)$$

The spreading function, G , is presented as a function of r alone since θ_v depends on r . For each r there is a unique θ_v , and therefore, a unique G . The spreading function was calculated for horizontal ranges from 300 m to 20,000 m, and tabulated in Appendix D. The spreading function is shown in a log-log plot in Figure 4-6. For comparison the equivalent spherical spreading for a dipole source is also shown. From this one can see that source strengths calculated using the spherical spreading law lead to an unrealistic dependence on range.

In order to get θ_v and r_c a linear sound speed gradient of 0.054 sec^{-1} was chosen. This gradient gives the same θ_v at $r = 3 \text{ km}$ as the multiple step profile used in Chapter 3. Three kilometers was chosen since it was the median horizontal range for the noise events.

The spreading loss function and measured peak pressure magnitudes were used to calculate dipole strength.

$$F_0 = 2\lambda A = 2\lambda p_0 \sqrt{G(r)} \quad (4-26)$$

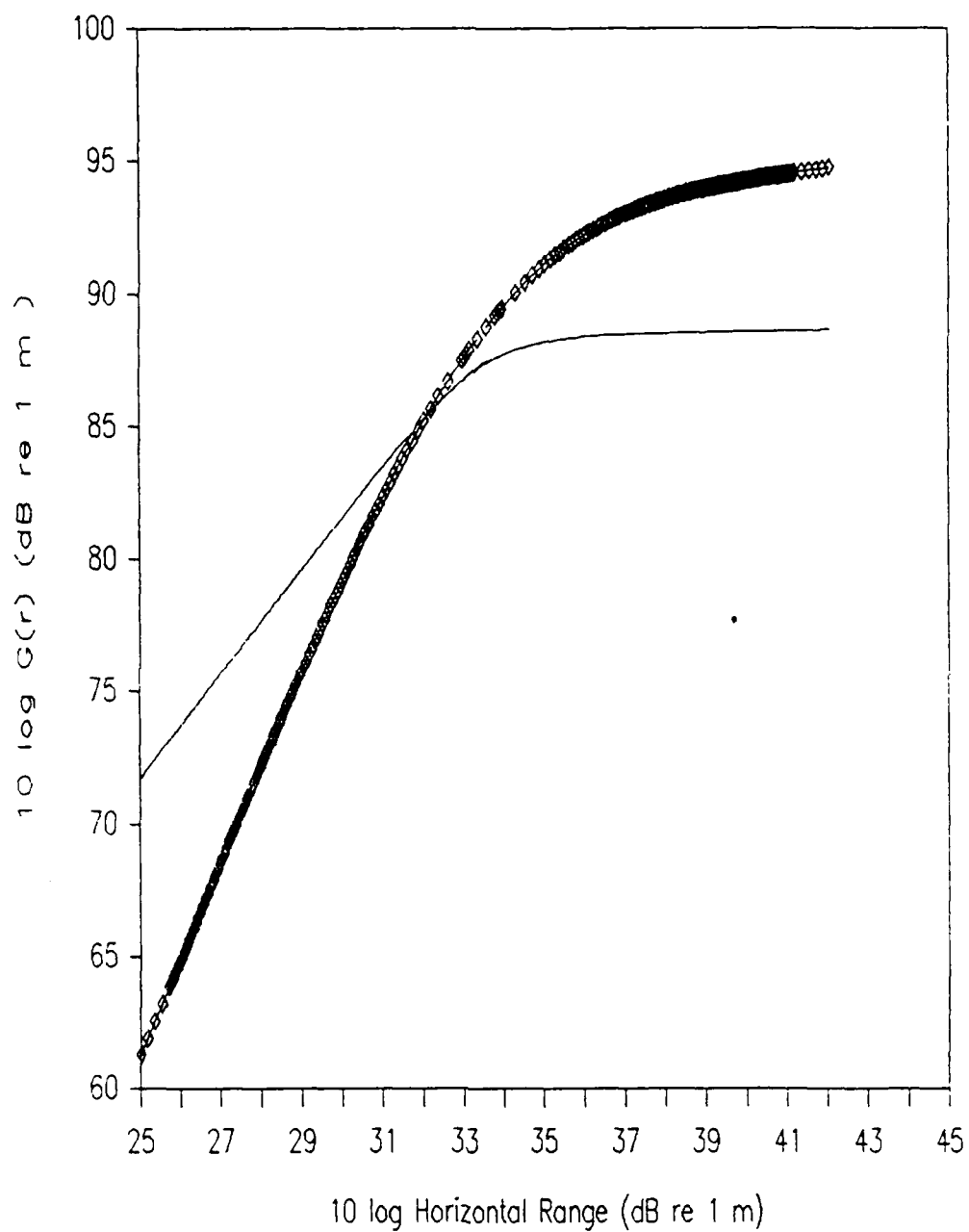


Figure 4-6 Spherical (heavy line) and refractive spreading loss, $G(r)$, as a function of horizontal range.

For a particular event the source strength was calculated from each hydrophone, and then the average taken as the source strength for the event. The standard deviation within each event ran from 2% to 125% of the mean value. An event-by-event summary of Appendix C lists the mean measured peak pressure, the mean dipole strength, along with the standard deviation of these values for each event.

Strength of Background Noise

I was interested to find out what effect that environmental loading might have had on the temporal, spatial and strength statistics. It has been shown by Marris and Dyer(10) that low frequency (10-20 Hz band) ambient noise rms pressure, averaged over a long time, correlates well with environmental stresses and moments. Since I had ambient noise pressure for most of the period of the FRAM IV experiment, and since I had environmental stresses and moments available for only a part of the time, I chose to use the 20-80 Hz long-time-average rms pressure as my environmental indicator.

The 10 to 20 Hz band ambient noise pressure was converted to 20 to 80 Hz band pressure in the following manner. Figure 4-7 shows the typical spectrum for central Arctic pack ice noise. The portion of the spectrum between 10 and 100 Hz can be approximated by a straight line.

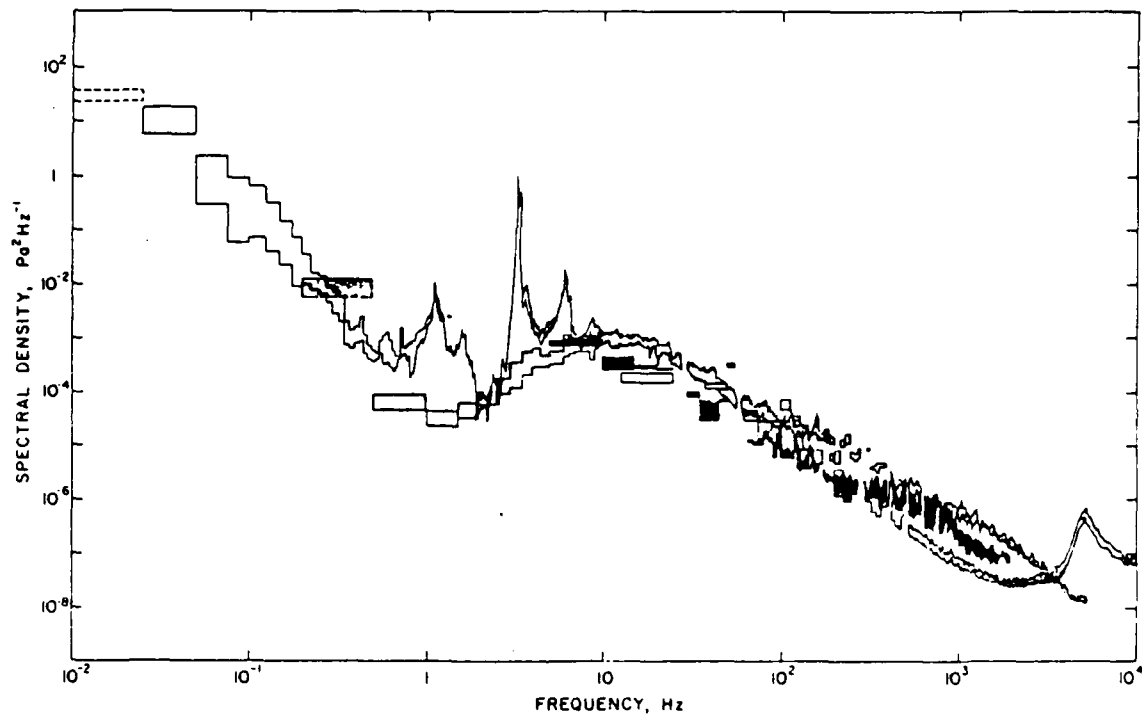


Figure 4-7 Composite central Arctic ambient noise spectrum observed during the FRAM IV experiment. (From Dyer[6])

$$\log S = A [\log f] + B , \quad (4-27)$$

$$\text{where } A = \text{slope} = -1.7273 \text{ Pa}^2/\text{Hz}^2 ,$$

$$B = \text{intercept} = -1.0909 \text{ Pa}^2/\text{Hz} ,$$

or

$$S = 10^{B_f A} . \quad (4-28)$$

The band rms pressure relates to the spectral level by:

$$p_{\text{rms},b}^2 = \int_b S df . \quad (4-29)$$

I have assumed that as the sound pressure level changes from time to time the intercept B changes, but the slope remains the same. By substituting equation 4-28 into 4-29, and using the known 10 to 20 Hz ambient noise band, B can be written in terms of the known pressure.

$$B = \log \left[\frac{p_{\text{rms},10-20}^2}{K_1} \right] , \quad (4-30)$$

where

$$K_1 = \left[\frac{20^{(A+1)} - 10^{(A+1)}}{A+1} \right] = 0.1020 \text{ Hz} .$$

The ambient noise rms pressure for the 20 to 80 Hz band may now be found.

$$p_{\text{rms},20-80}^2 = \int_{20}^{80} 10^{B_f A} df . \quad (4-31)$$

$$= p_{rms,10-20}^2 \frac{K_2}{K_1} ,$$

where

$$K_2 = \left[\frac{80(A+1) - 20(A+1)}{A+1} \right] = 0.0988 \text{ Hz} ,$$

or finally,

$$P_{rms,20-80} = P_{rms,10-20} \sqrt{\frac{K_2}{K_1}} . \quad (4-32)$$

$$P_{rms,20-80} = 0.98 P_{rms,10-20} .$$

Thus the band from 20 to 80 Hz is virtually identical to the one from 10 to 20 Hz in rms pressure, for long-time-averages, and in turn, is an acceptable surrogate for environmental forcing (applied stresses and moments). The 20 to 80 Hz band ambient noise rms pressure for each of the tapes investigated is found in Table 4-1.

Table 4-1 20 to 80 Hz Band Ambient Noise rms Pressure

Tape #	Date Recorded	P _{rms} , 20-80 (Pa)
4001	3-27-82	Not Available
2001	3-29-82	Not Available
2009	3-30-82	0.022
3001	3-31-82	0.019
4003	4-01-82	0.044
4005	4-01-82	0.035
4007	4-01-82	0.022
4009	4-02-82	0.010
4011	4-02-82	0.010
4013	4-03-82	0.013
2023	4-08-82	0.037
4015	4-09-82	0.040
3047	4-13-82	0.010
4016	4-15-82	0.017
4019	4-15-82	0.016
4021	4-19-82	0.013
4023	4-19-82	0.011
4024	4-19-82	0.011
4027	4-20-82	0.012
4029	4-20-82	0.012
4031	4-20-82	0.012
4033	4-20-82	0.012
4040	4-21-82	0.034
4047	4-21-82	0.114
4049	4-21-82	0.140
4051	4-21-82	0.140
4053	4-22-82	0.080
4055	4-22-82	0.082
4057	4-22-82	0.053
4059	4-22-82	0.065
4061	4-22-82	0.034
4063	4-22-82	0.028
4065	4-22-82	0.027
4067	4-22-82	0.015

CHAPTER 5

ANALYSIS OF NOISE EVENTS

Detection Analysis

A total of 34 tapes was examined, for a total time of 662 minutes. (For a few of these tapes the entire 20 minutes was not used.)

There was a total of 499 detections of events flagged on at least 50% of the hydrophone channels. Of these, 139 were man-made artifacts, and 125 were false alarms (detections which were so weak that no pattern for taking time delays could be discerned). There were 199 unique events, and 36 multiple detections of those events. Stated in another way, of the detections which were not artifacts, 65.3% were strong enough to support analysis and 34.7% were too weak to reasonably analyze, and hence labeled false alarms.

Since the detection process depends on signal-to-noise ratio, the level of background ambient noise should affect the event detection rate. Figure 5-1 shows normalized ambient noise pressure, number of false alarms per tape, and number of unique events per tape for each tape examined. *There is some trend for more events being found when the ambient pressure is low, and more false alarms declared when the ambient pressure is high.*

This is more clearly seen in Figure 5-2, which shows the average number of false alarms and unique events found

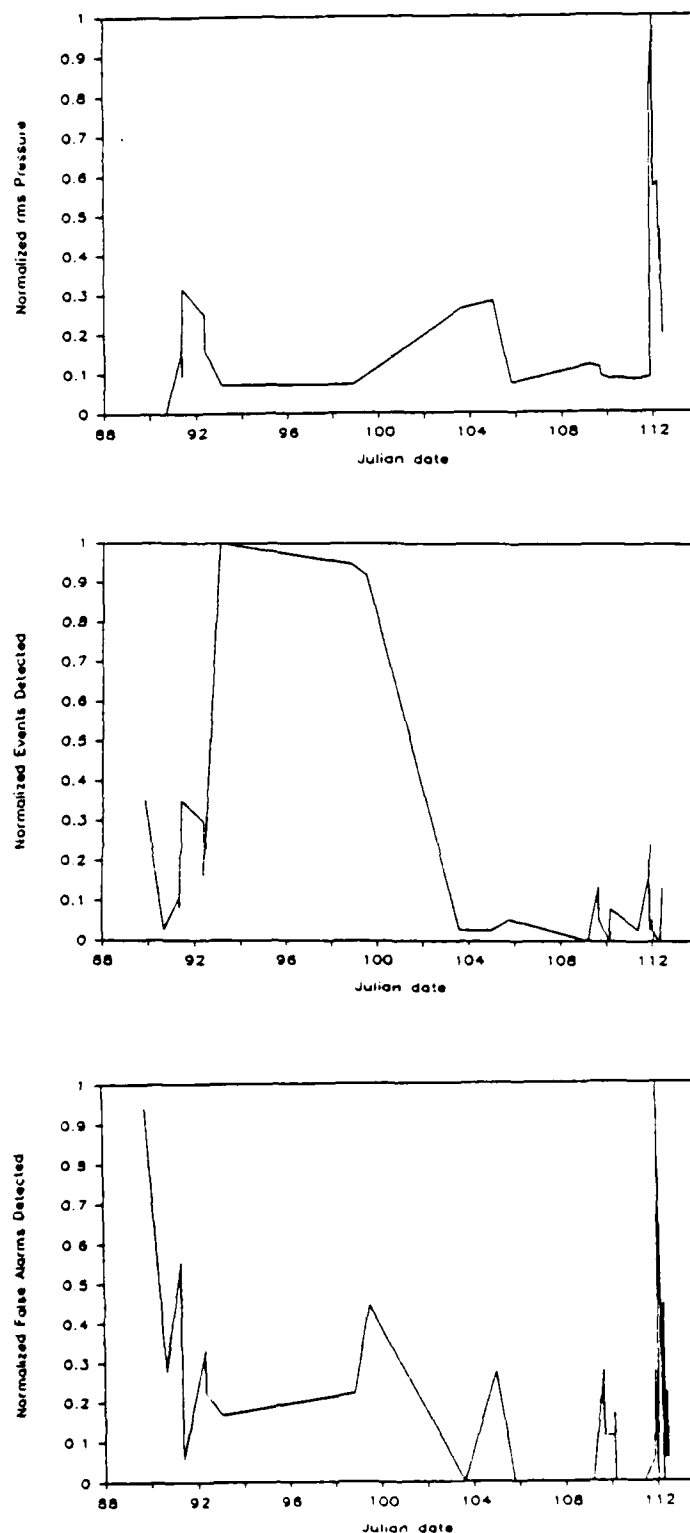


Figure 5-1 Normalized ambient noise pressure, number of unique events per tape, and number of false alarms per tape for each data tape examined.

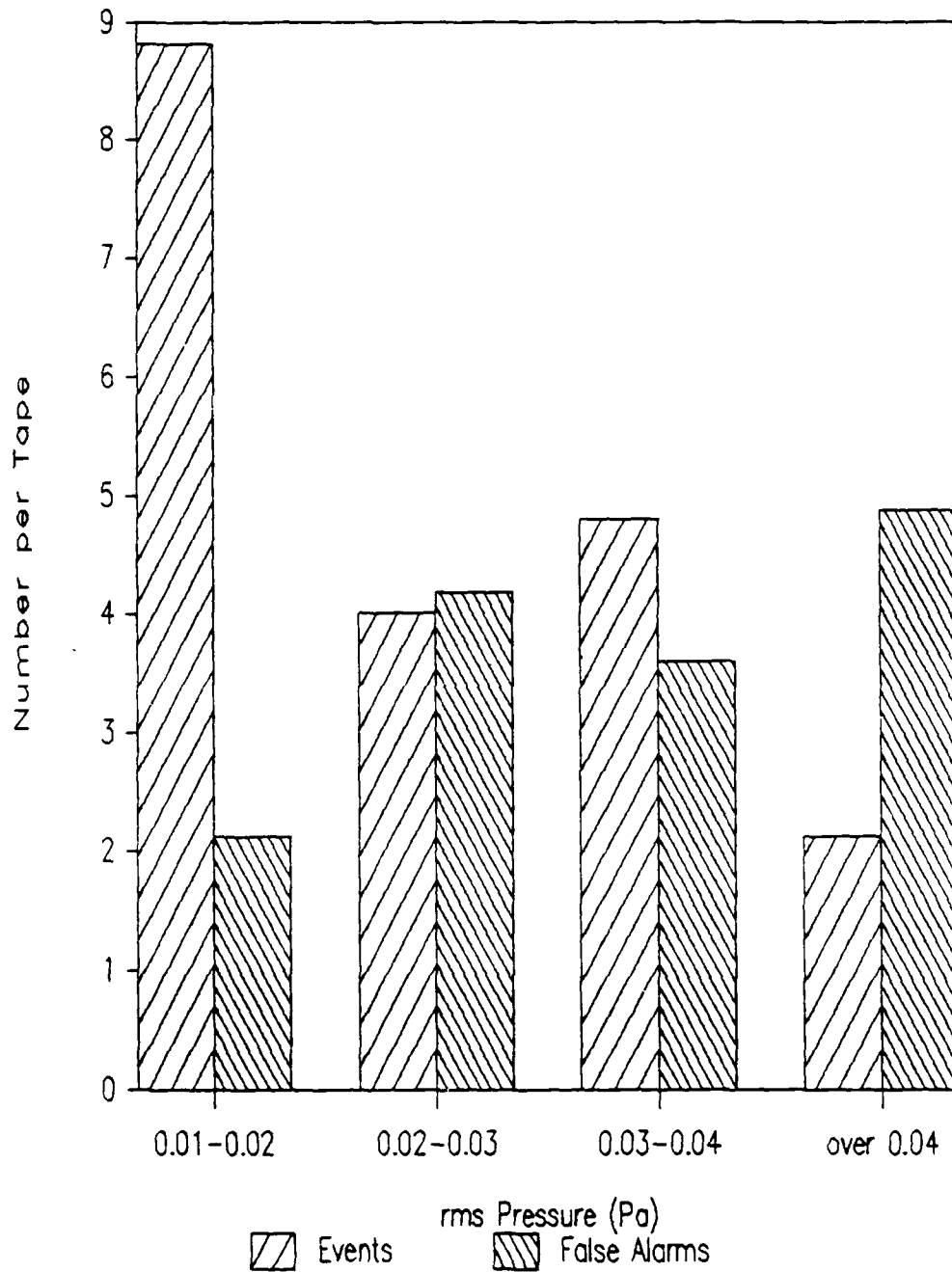


Figure S-2 Average number of false alarms and unique events per data tape for four ranges of ambient noise pressure.

per tape in each of four background noise pressure ranges. The 0.01-0.02 Pa range used 15 tapes to compute its average, the 0.02-0.03 Pa range 4 tapes, the 0.03-0.04 Pa range 5 tapes, and the over 0.04 Pa range 8 tapes. Two tapes were recorded during the first few days of the FRAM IV experiemnt, before the 10-20 Hz band ambient noise recordings were started.

A breakdown of detections for each tape is found in Appendix C.

Temporal Analysis

The interarrival time between events ranged from 1 to 1064 seconds. Each event time was taken to the nearest second, and no events were taken as having the same event time. If two events happened in the same second, one was judged to be earlier, and the two events were given event times one second apart. The interarrival time for a particular event was measured from the previous event, except for the first event of a tape, which was measured from the start of the tape.

The interarrival times were divided into bins of 20 seconds. The first bin ("0") contained events which had interarrival times from 0 to 19 seconds, the second bin from 20 to 39 seconds, and so on. The number of events per bin is presented in Table 5-1 and shown graphically in Figure 5-3. A complete listing of interarrival times for

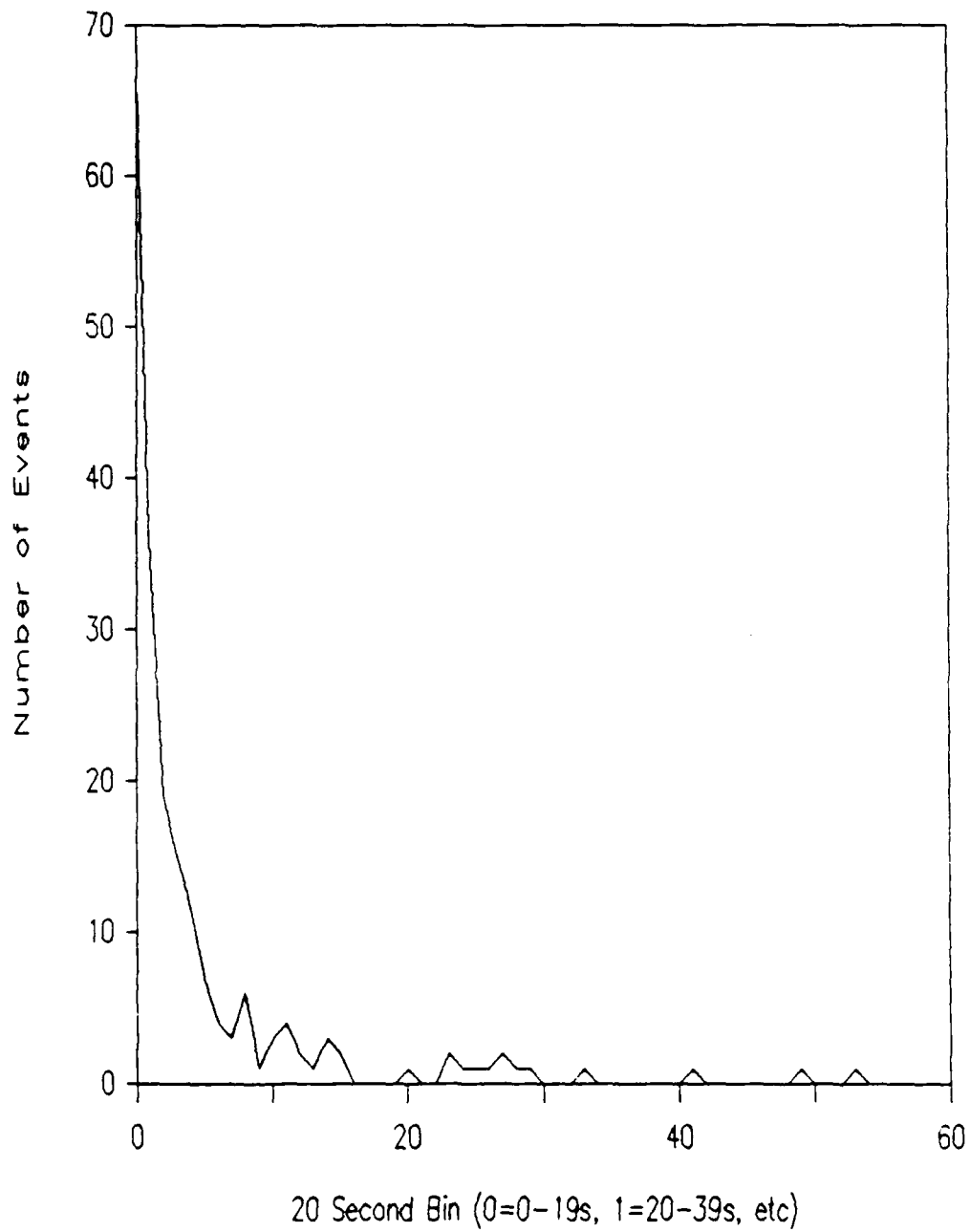


Figure 5-3 Number of events found per interarrival time bin.

each event is found in Appendix C. The mean of the interarrival times (μ) is 100 seconds, and the standard deviation (σ) 166 seconds. In terms of bins, the mean is 5 and the standard deviation 8. The standard deviation is 1.66 times the mean.

Table 5-1 Number of Events per Interarrival Time Bin

Bin	Events	Bin	Events
0	67	31	0
1	36	32	0
2	19	33	1
3	15	34	0
4	12	35	0
5	7		
6	4	36	0
7	3	37	0
8	6	38	0
9	1	39	0
10	3	40	0
11	4	41	1
12	2	42	0
13	1	43	0
14	3	44	0
15	2	45	0
16	0	46	0
17	0	47	0
18	0	48	0
19	0	49	1
20	1	50	0
21	0	51	0
22	0	52	0
23	2	53	1
24	1	54	0
25	1	55	0
26	1	56	0
27	2	57	0
28	1	58	0
29	1	59	0
30	0		

Three different probability density functions were investigated to find an appropriate fit for Figure 5-3. They were 1) a half-gaussian distribution, 2) an exponential distribution and 3) a J shaped distribution.

The half-gaussian probability density function is[3]:

$$p(t) = \frac{2}{\sqrt{2\pi}t_0} e^{-t^2/2t_0^2} . \quad (5-1)$$

The general equations for mean, mean square value and variance (σ^2) can be used to solve for the unknown constant, t_0 :

$$\mu = \int_0^{\infty} t p(t) dt . \quad (5-2)$$

$$\text{mean square value} = \int_0^{\infty} t^2 p(t) dt . \quad (5-3)$$

$$\begin{aligned} \sigma^2 &= \int_0^{\infty} (t - \mu)^2 p(t) dt . \\ &= \text{mean square value} - \mu^2 . \end{aligned} \quad (5-4)$$

Substituting equation 5-1 into equations 5-2, 5-3 and 5-4 leads to the following relations:

$$t_0 = \frac{\sqrt{2\pi}\mu}{2} ; \text{ mean square value} = t_0^2 . \quad (5-5)$$

$$\sigma^2 = \left[\frac{\pi - 2}{\pi} \right] t_0^2 ; \quad \sigma = 0.756 \mu .$$

This value for t_0 was used in equation 5-1, and the probability density function integrated over appropriate limits to get the number of events in each 20 second bin. The result is plotted against the experimental distribution in Figure 5-4.

The second distribution (the exponential) belongs to the family of gamma distribution functions [15]:

$$p = \frac{1}{t_0^{\alpha+1} \Gamma(\alpha+1)} t^{\alpha} e^{-t/t_0} . \quad (5-6)$$

When $\alpha = 0$, this becomes the exponential probability density function

$$p = \frac{1}{t_0} e^{-t/t_0} . \quad (5-7)$$

Again using equations 5-2, 5-3 and 5-4 leads to:

$$\begin{aligned} \mu &= t_0 ; \quad \text{mean square value} = 2\mu^2 . \\ \sigma^2 &= \mu^2 ; \quad \sigma = \mu . \end{aligned} \quad (5-8)$$

The exponential probability density function was integrated over the bins, and the results are shown in Figure 5-5.

Another demonstration of the fit of the exponential probability distribution is shown in Figure 5-6. Taking the natural log of the function should lead to a straight line when plotted against time or bin number. The straight line

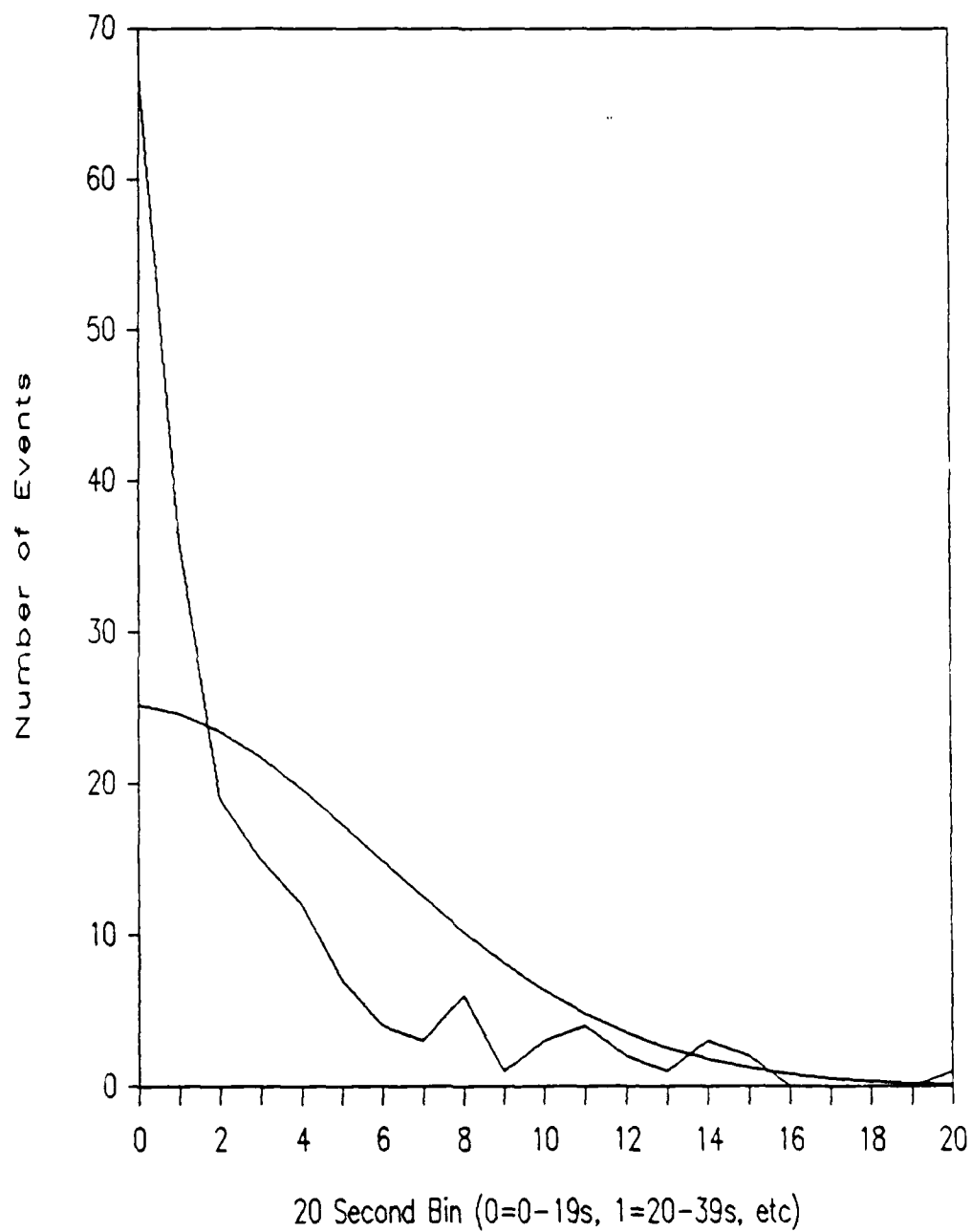


Figure 5-4 Half-gaussian distribution compared with experimental values.

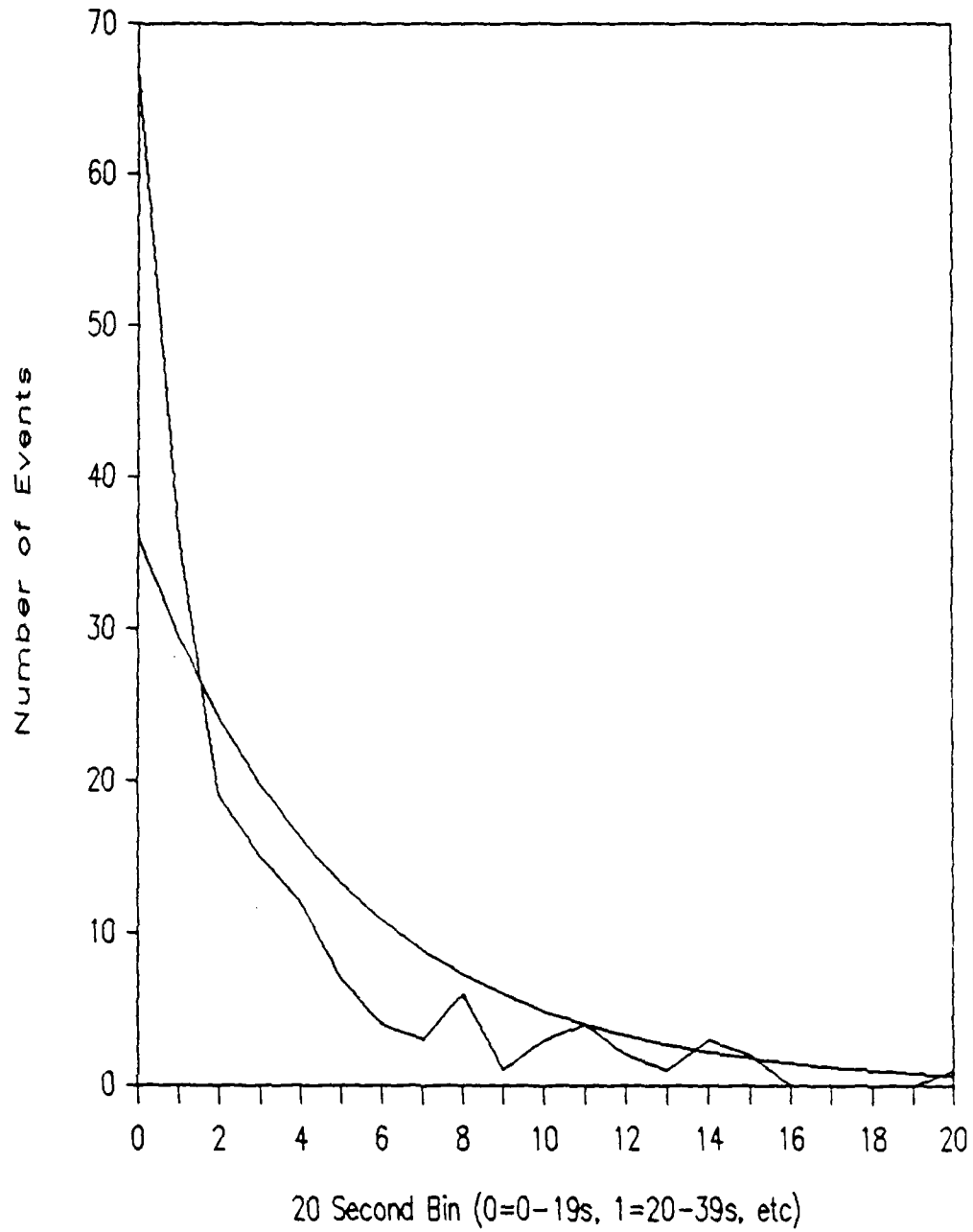


Figure 5-5 Exponential distribution compared with experimental values.

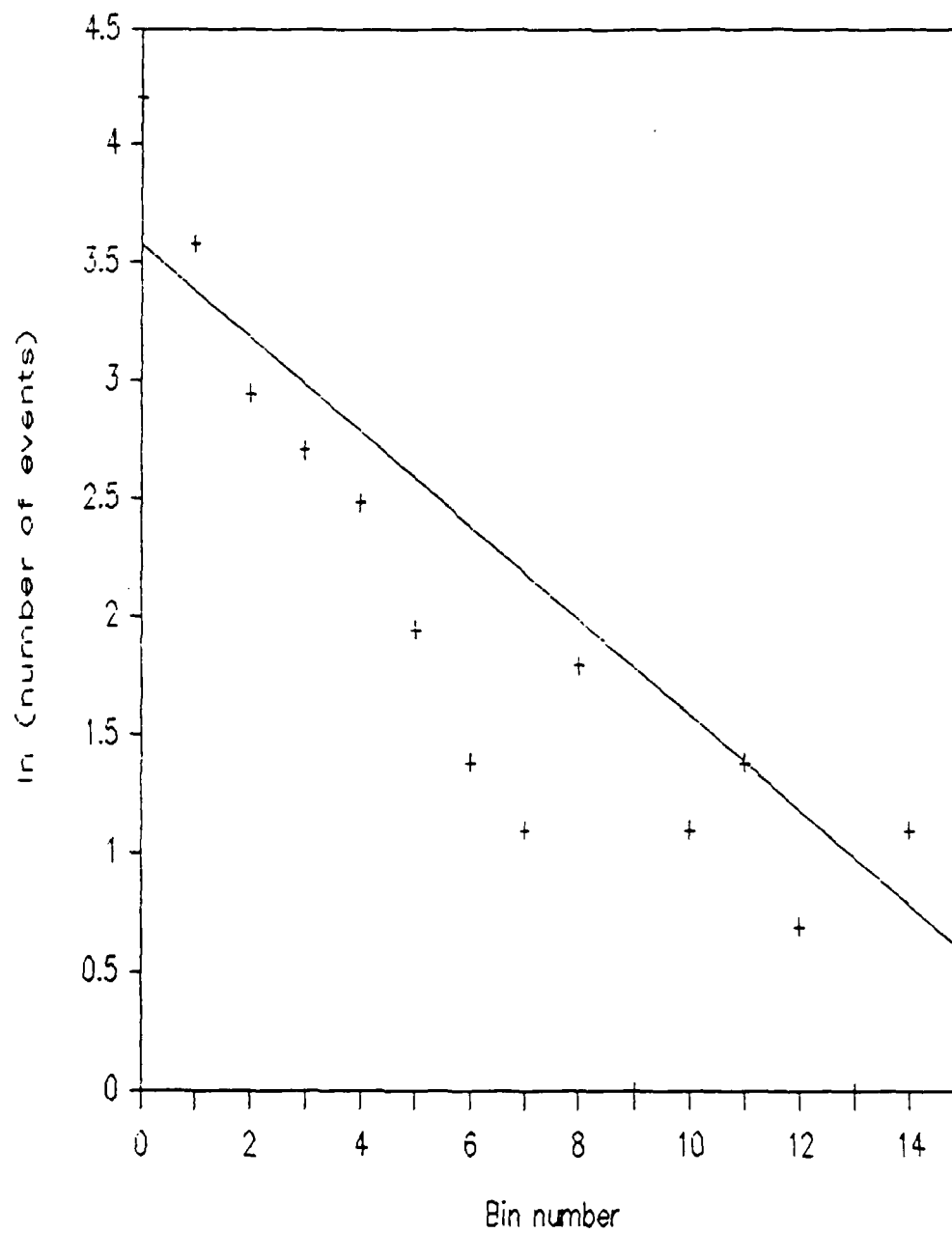


Figure 5-6 Semi log plot of exponential distribution and experimental values against bin number.

in Figure 5-6 is a plot of the natural log of the points calculated using the exponential probability density function. The experimental points seem to curve rather than lie on a straight line.

The last distribution (J shaped) is also a gamma distribution. The J shaped distributions are characterized by $\alpha < 0$. I chose a fairly common distribution with $\alpha = -0.5$. The probability density function is:

$$p(t) = \frac{1}{\sqrt{t_0\pi}} t^{-1/2} e^{-t/t_0}, \quad (5-9)$$

and the key parameters are:

$$t_0 = 2\mu \quad ; \quad \text{mean square value} = \frac{3t_0^2}{4}, \quad (5-10)$$

$$\sigma^2 = \frac{t_0^2}{2} \quad ; \quad \sigma = \sqrt{2}\mu.$$

This distribution is plotted against the experimental values in Figure 5-7. The natural log of both calculated and experimental points are plotted against bin number in Figure 5-8. This distribution seems to fit the experimental points best of all. The J shaped probability density function goes to infinity at zero, but it is integrable.

A Chi square goodness of fit test was done on all three distributions. The results are summarized in Table

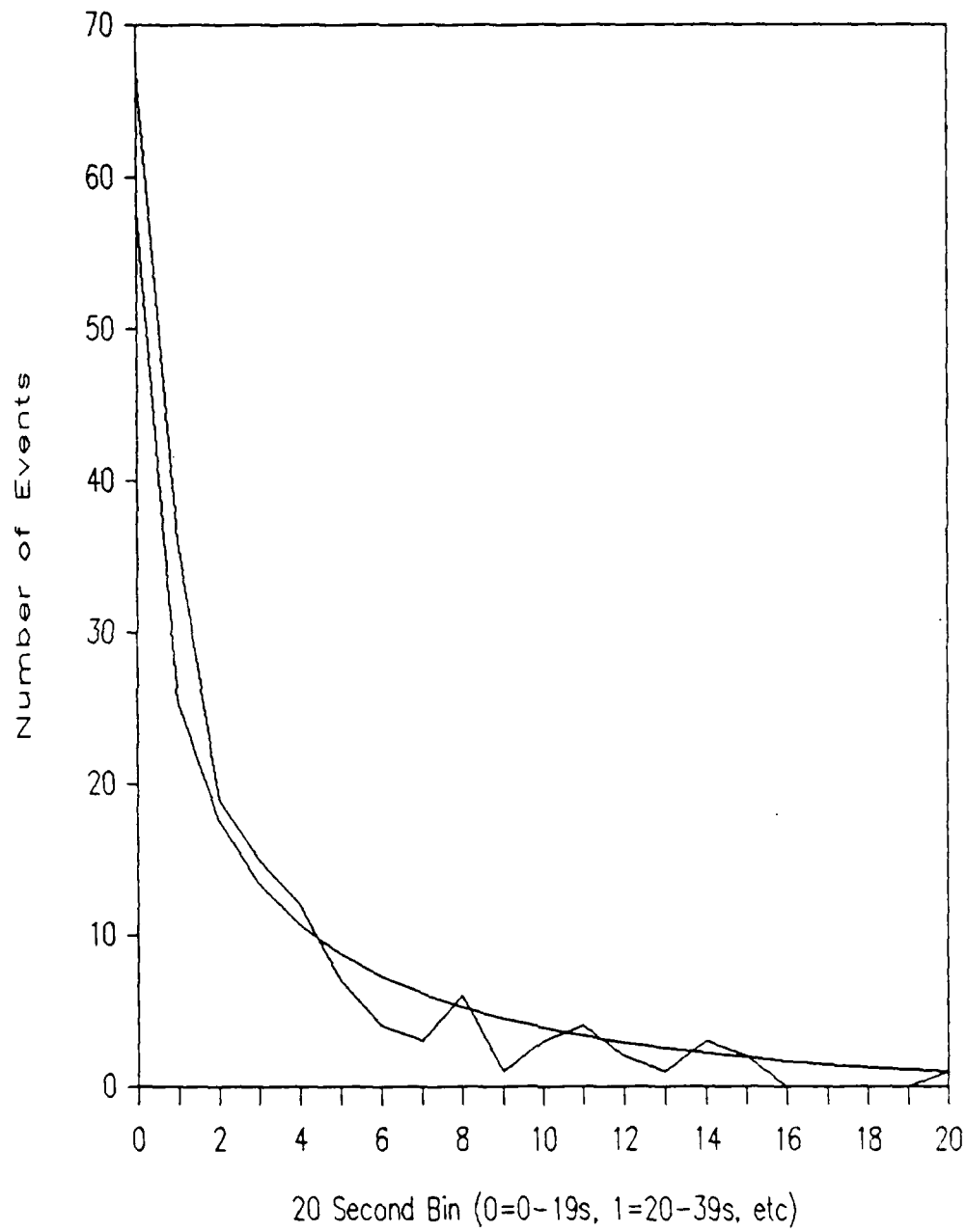


Figure 5-7 J shaped distribution compared with experimental values.

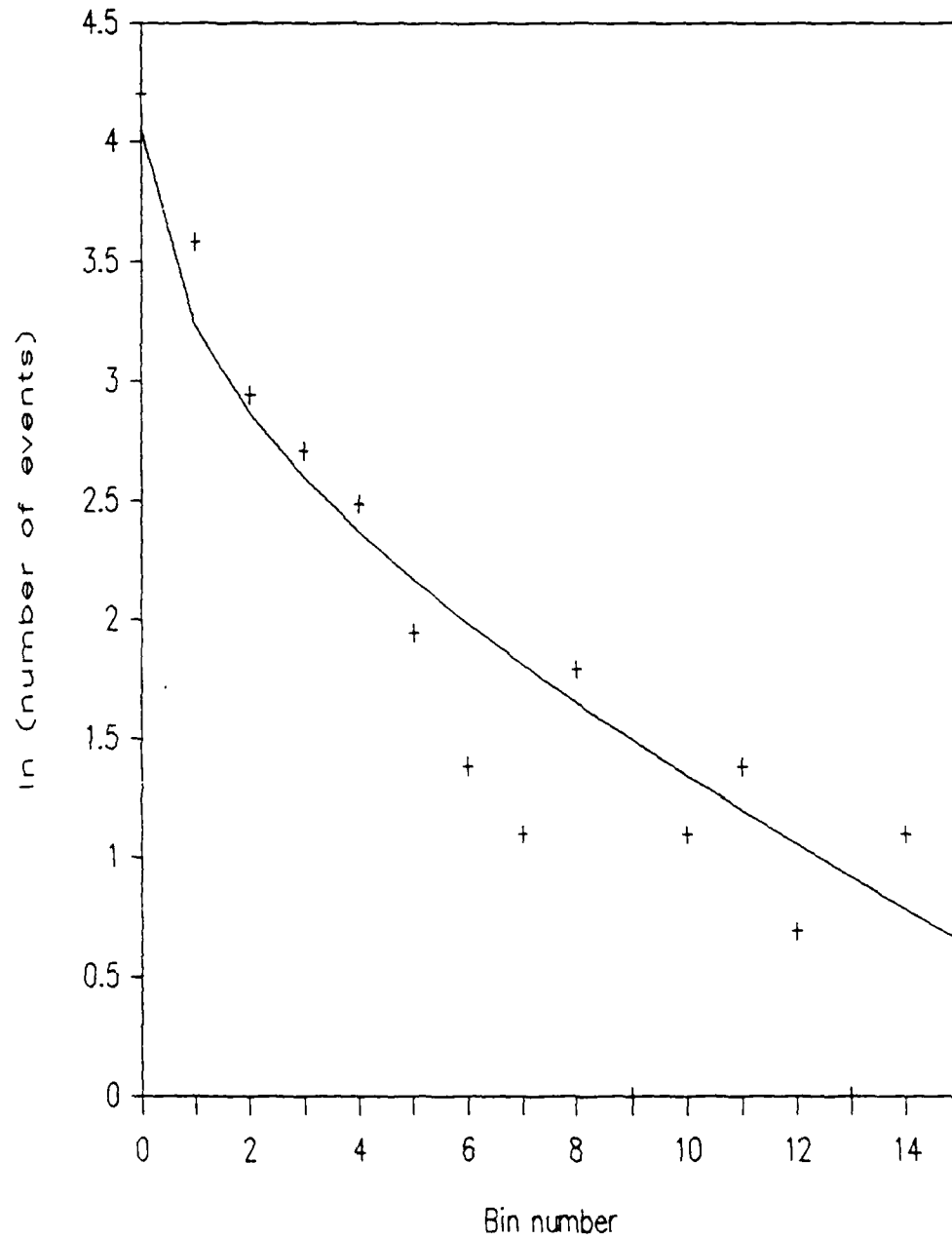


Figure 5-8 Semi log plot of J shaped distribution and experimental values against bin number.

5-2. Also presented in Table 5-2 are the ratios of standard deviation to mean.

Table 5-2 Comparison of Distribution Functions

	Chi square	σ/μ
Experimental	---	1.66
Half-gaussian	127.17	0.76
Exponential	45.69	1.00
J shaped	10.65	1.41

For a distribution to pass a goodness of fit test it must have a Chi square less than a prescribed limit. The limit for my test (9 degrees of freedom, $\alpha = 0.005$) was 23.6[16]. Only the J shaped distribution passed the Chi square test. It also has σ/μ closest to the experimental values. In summary, the interarrival data reasonably fit a J shaped distribution given by:

$$p(t) = \frac{1}{\sqrt{2\pi\mu}} t^{-1/2} e^{-t/2\mu} \quad (5-11)$$

Since event detection rate depended on ambient noise level, interarrival time between events should also show environmental dependence. Table 5.3 gives average and standard deviation of the interarrival time for different ambient noise pressure levels.

Table 5-3 Background Noise Level Dependence of Interarrival Time

Ambient Noise rms pressure (20-80 Hz) (Pa)	Interarrival Time	
	mean (sec)	standard deviation (sec)
0.01-0.02	67	129
0.02-0.03	190	153
0.03-0.04	147	143
over 0.04	183	318

The tapes having a background noise level of 0.01 to 0.02 Pa have a significantly shorter interarrival time than tapes in the other three pressure groups. As with detection rate, *the interarrival time does depend on ambient noise level.*

Spatial Analysis

After removing nonlocatable events and events located outside a horizontal range of 20,000 meters, 164 events remained. These were grouped by horizontal range into 42 annuli of equal area as shown in Figure 5-9. Each annulus is a 30 square km ring centered at the array origin. The first annulus ("0") went from 0 to 3090 meters, the second from 3090 to 4370 meters, and so on.

Table 5-4 shows the number of events per annulus and Figure 5-10 shows this distribution graphically.

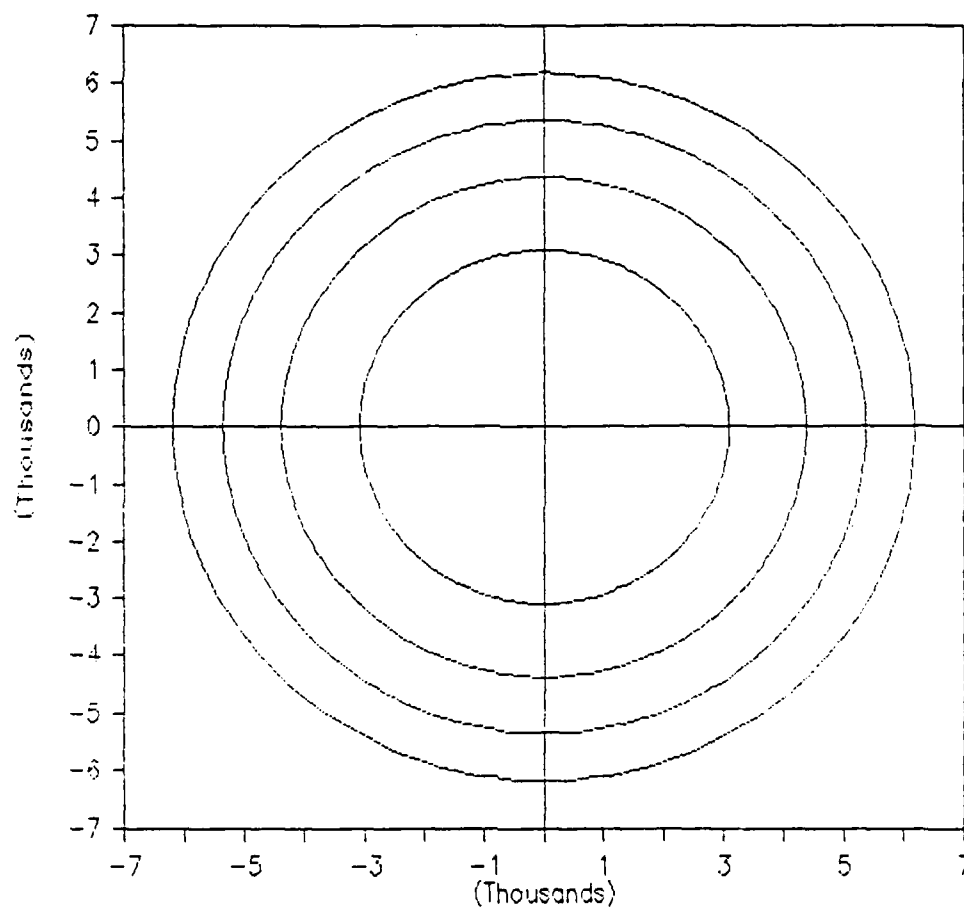


Figure 5-9 Scheme for annuli each of area equal to 30 km^2 .

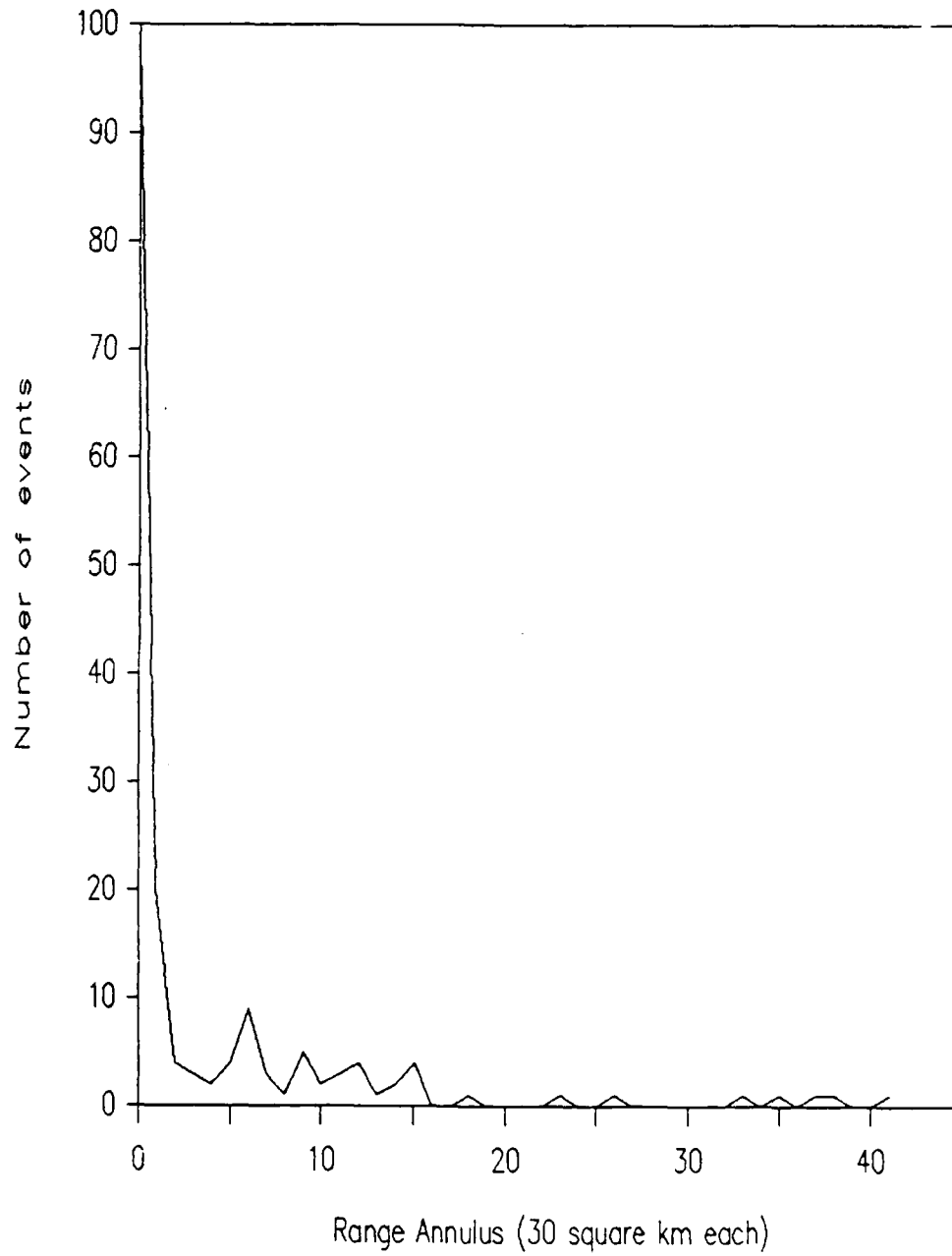


Figure 5-10 Number of events per radius annulus.

Table 5-4 Number of Events per Annulus

Annulus	Events	Annulus	Events
0	91	21	0
1	19	22	0
2	4	23	1
3	3	24	0
4	2	25	0
5	4	26	1
6	9	27	0
7	3	28	0
8	1	29	0
9	5	30	0
10	2	31	0
11	3	32	0
12	4	33	1
13	1	34	0
14	1	35	1
15	4	36	0
16	0	37	1
17	0	38	1
18	1	39	0
19	0	40	0
20	0	41	1

The average number of events per annulus is 3.93 and the standard deviation is 14.15 events. Figure 5-10 shows that *the number of events found is highly dependent on their range from the array.* In the center annulus there were over 20 times the mean number of events.

The dependence on range is not a surprise, since spreading (and possibly scattering and other losses) will reduce the strength of weak transients down to the ambient noise level. For this reason, the center annulus is probably the best indicator of actual event density. In this ring there were 91 events per 10 square kilometers per 662 minutes of observation or approximately 0.3 events per

square kilometer per hour.

The average number of events per annulus and the number of events per square kilometer per hour should depend on background noise level. The average number of events per annulus was found for each ambient noise rms pressure range, and adjusted to reflect the number of events in a 662 minute period. The results are seen in Table 5-5. The number of events per square kilometer per hour for the center annulus are also shown in Table 5-5.

Table 5-5 Average Number of Events per Annulus for 4 Ambient Noise Levels

Ambient Noise rms pressure (20-80 Hz)	Events per Annulus	Minutes of tape Examined	Adjusted Events per Annulus	# Events per km ² per hr
0.01-0.02 Pa	2.60	287.5	5.98	0.452
0.02-0.03 Pa	0.29	77	2.46	0.260
0.03-0.04 Pa	0.45	100	3.99	0.150
over 0.04 Pa	0.36	157.5	1.50	0.076
Entire Population	3.93	662	3.93	0.275

The average number of events per annulus and the number of events per square kilometer per hour both reflect the effect of signal-to-noise ratio on the detection scheme.

The entire population of events was investigated for angular dependence. Figures 5-11 and 5-12 show the number

NO-A190 253

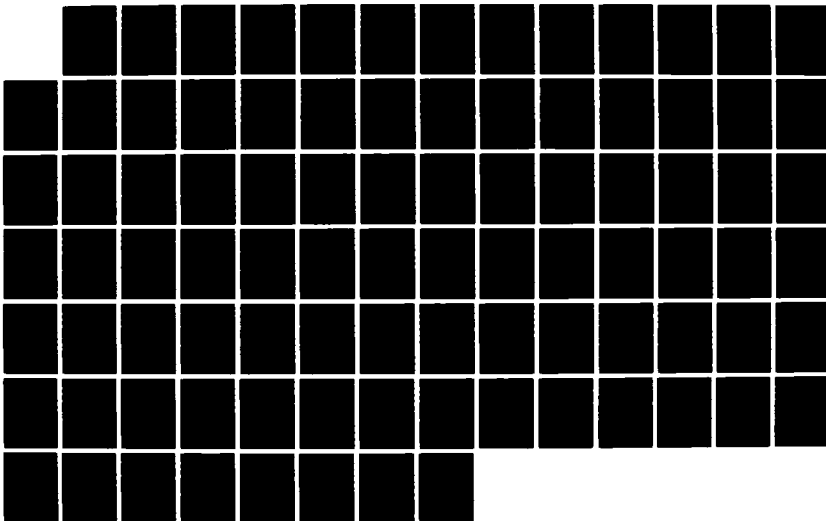
ANALYSIS OF CENTRAL ARCTIC NOISE EVENTS(U)
MASSACHUSETTS INST OF TECH CAMBRIDGE DEPT OF OCEAN
ENGINEERING N TOWNSEND-MANNING JUN 87 N00220-85-0-3262

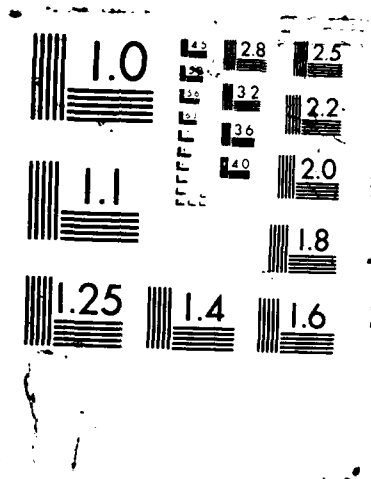
2/2

UNCLASSIFIED

F/O 20/1

HL





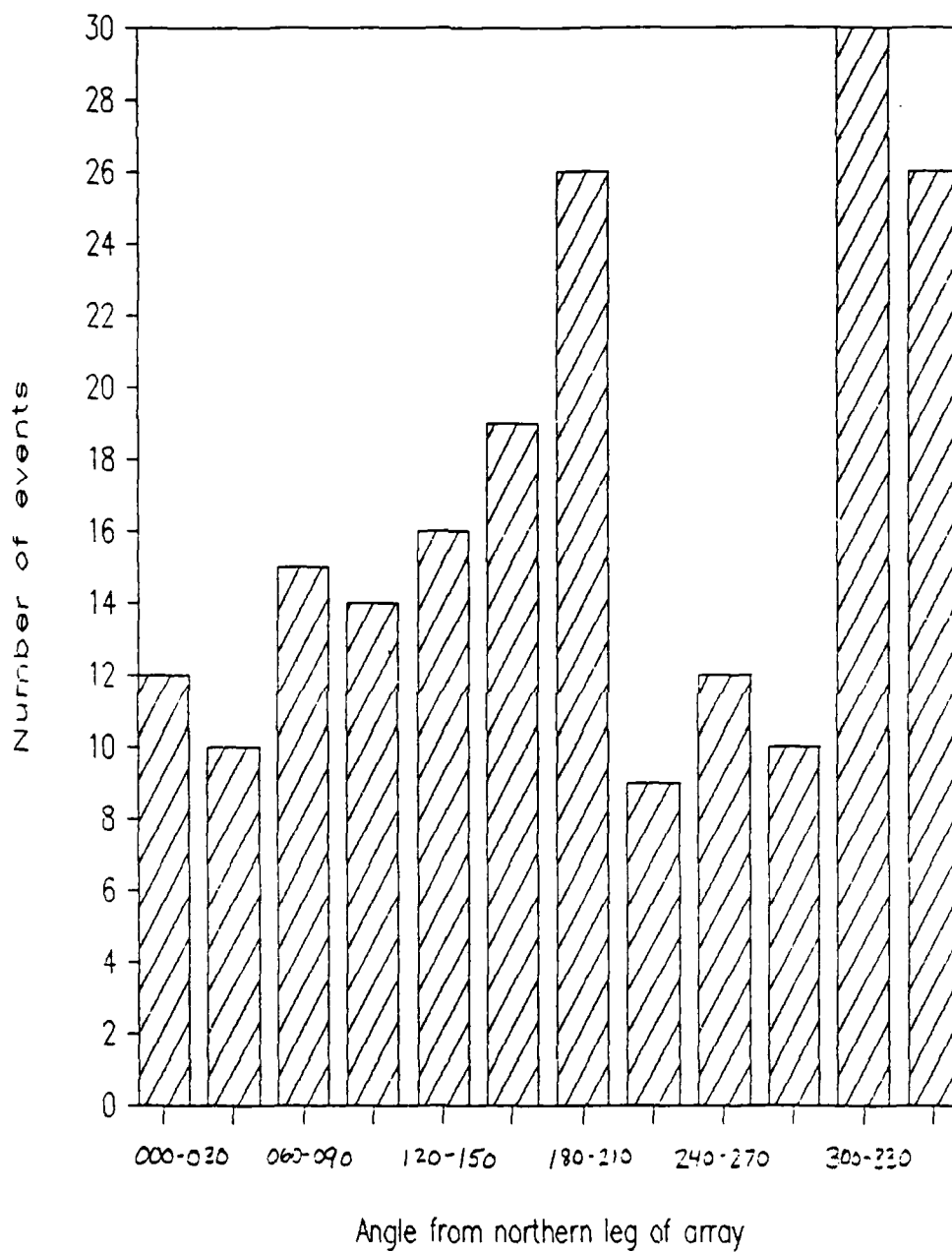


Figure 5-11 Number of events per 30° sector. Angles are measured from the northern leg of the hydrophone array.

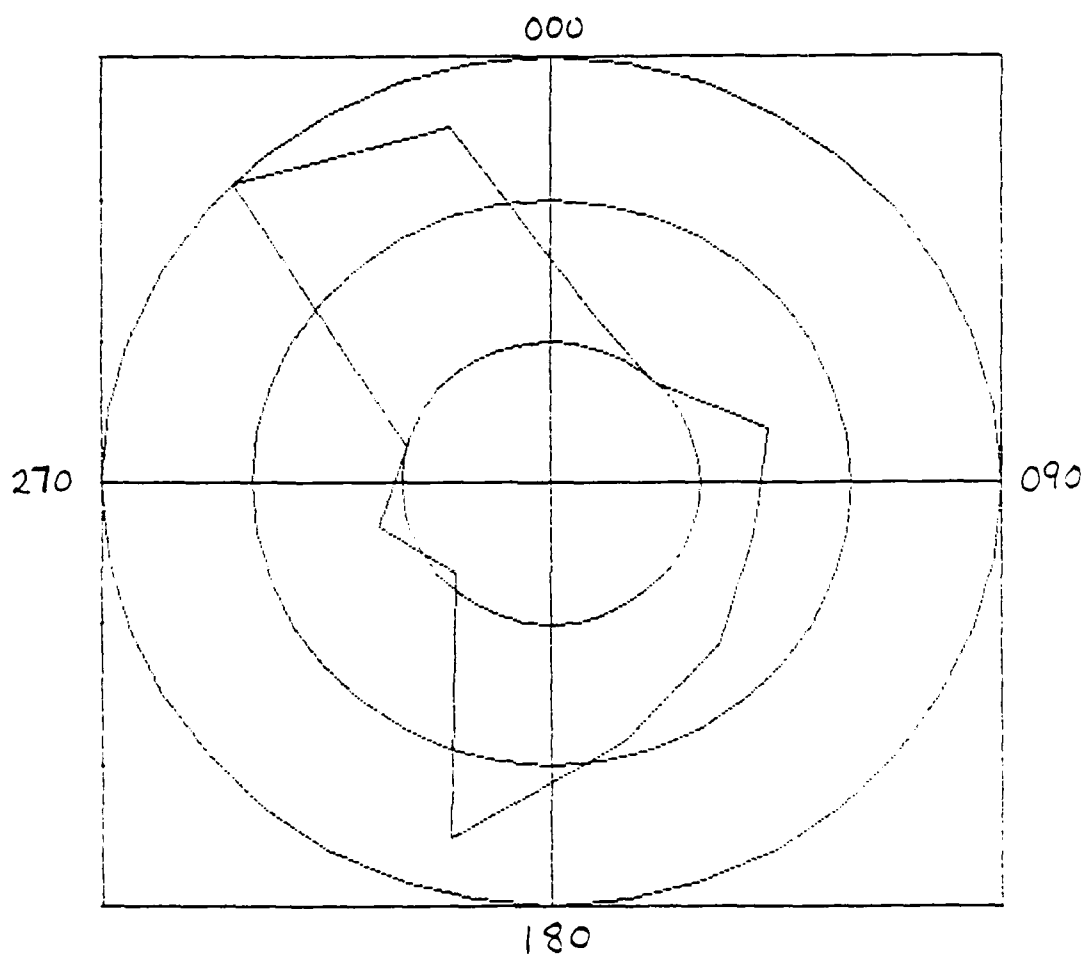


Figure 5-12 Number of events per 30° sector. Radius gives the number of events, while angle indicates the sector measured from the northern leg of the array. Each ring represents 10 events.

of events found per 30° sector. In the polar diagram (Figure 5-12) the radius shows the number of events. The angles are measured from the northern leg of the array. Figure 5-13 is a polar plot showing the number of events per 10° sector. *There was no predominant angular direction found.* However, some preference can be seen for bearings of 330° and 190° from the northern leg of the array.

Strength Analysis

The mean hydrophone peak pressure magnitude for each event fell within a fairly narrow band of values. The mean peak pressures ranged from 1.32 to 0.16 Pa, with an average of 0.36 Pa and a standard deviation of 0.20 Pa. Figure 5-14 shows the mean hydrophone peak pressure values for all events located between 100 m and 20,000 m plotted against range from the array origin.

The different symbols shown in Figure 5-14 represent events during each of the four ambient pressure categories. *The events with a higher mean hydrophone peak pressure have a tendency to occur during higher ambient noise levels.* This can be seen in Table 5-6, where the maximum, minimum, average and standard deviation of the mean hydrophone peak pressure values are given for each of the four ambient noise levels.

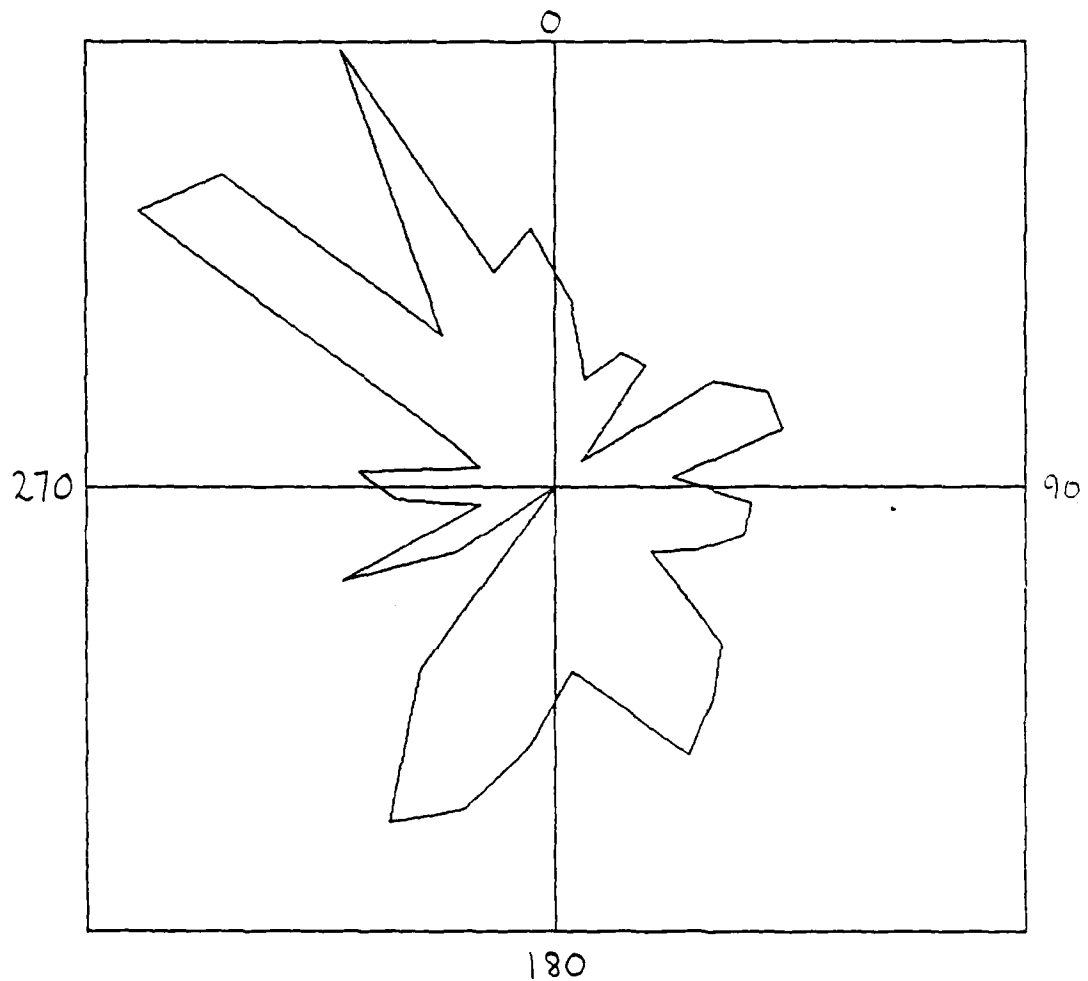
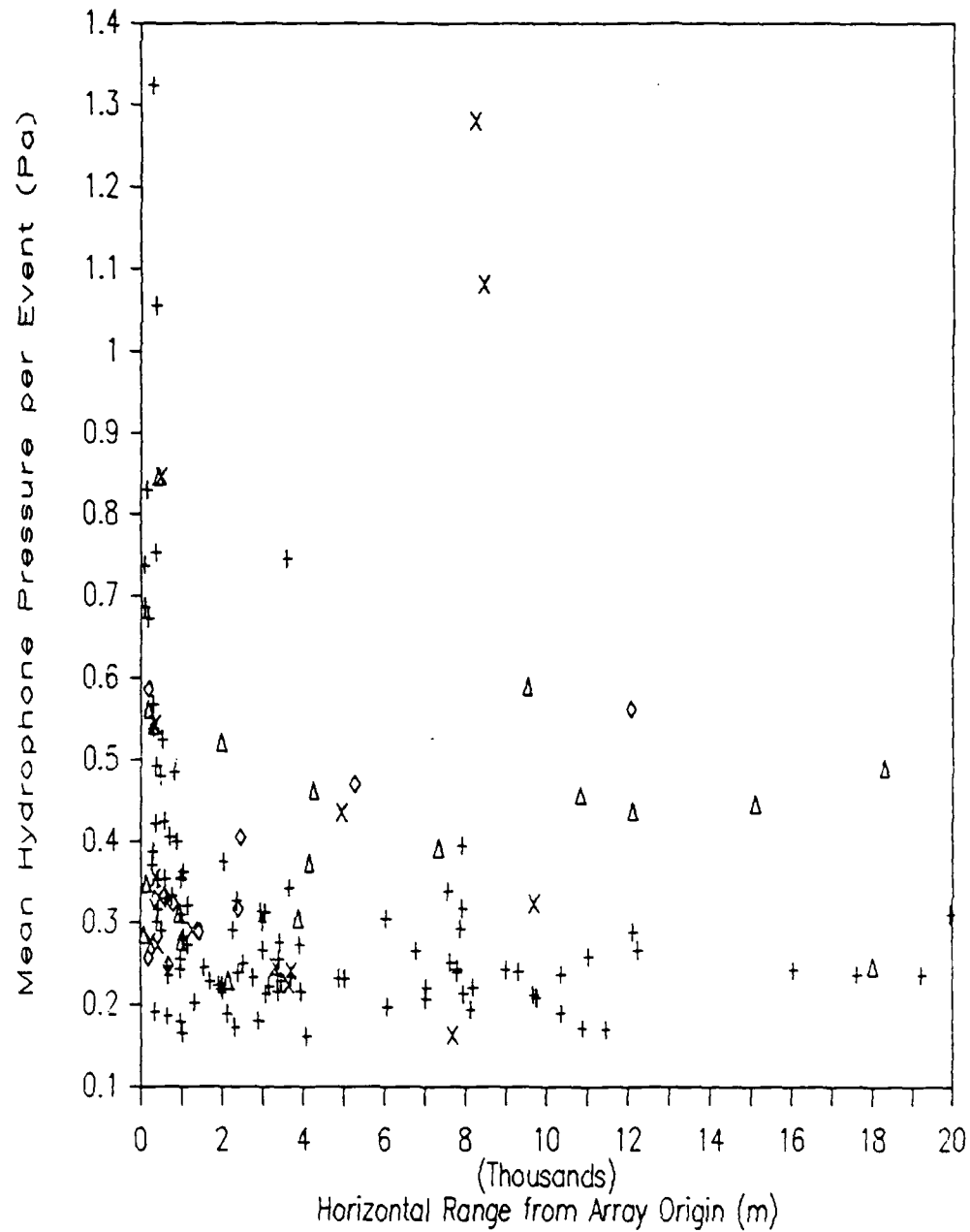


Figure 5-13 Number of events per 10° sector. Radius gives the number of events, while angle indicates the sector measured from the northern leg of the array.



+ 0.01-0.02 Pa ◇ 0.02-0.03 Pa Δ 0.03-0.04 Pa X 0.04+ Pa

Figure 5-14 Mean hydrophone peak pressure measured for events between 100m and 20,000 m, plotted against horizontal range from the FRAM IV array origin.

Table 5-6 Mean Hydrophone Peak Pressure
for 4 Ambient Noise Levels

Ambient Noise rms pressure (20-80 Hz)	Mean Hydrophone Peak Pressure (Pa)			
	max	min	average	std dev
0.01-0.02 Pa	1.32	0.16	0.31	0.17
0.02-0.03 Pa	0.56	0.25	0.36	0.09
0.03-0.04 Pa	0.85	0.23	0.43	0.15
over 0.04 Pa	1.28	0.16	0.49	0.34
Entire Population	1.32	0.16	0.36	0.20

Source strength (F_0) was found for the events which had hydrophone locations between 300 m and 20,000 m from the event.

The dipole strengths ranged from 33 kN to 4.9 MN, with an average of 431 kN and a standard deviation of 555 kN. The distribution of strengths for the 151 events evaluated is shown in Figure 5-15 and in Table 5-7.

Figure 5-16 shows the dipole strength for all events plotted against horizontal range from the array origin. Again, it can be seen that the stronger events occur when the ambient pressure level is high. Table 5-8 gives the strength values for the different ambient noise levels.

Table 5-7 Strength Distribution for a Population of Events

F_0	# of Events
0 to 100 kN	19
100 to 200 kN	29
200 to 300 kN	33
300 to 400 kN	28
400 to 500 kN	8
500 to 600 kN	5
600 to 700 kN	4
700 to 800 kN	5
800 to 900 kN	2
900 to 1000 kN	5
1000 to 1100 kN	3
1100 to 1200 kN	2
1200 to 1300 kN	3
1300 to 1400 kN	1
1400 to 1500 kN	1
1.5 to 3 MN	1
over 3 MN	2

Table 5-8 Dipole Strength versus Ambient Noise Levels

Ambient Noise rms pressure (20-80 Hz)	Dipole Strength (F_0) (kN)			
	max	min	average	std dev
0.01-0.02 Pa	1051	33	259	155
0.02-0.03 Pa	2041	64	649	634
0.03-0.04 Pa	1153	79	643	359
over 0.04 Pa	4939	59	860	1449
Entire Population	4939	33	431	555

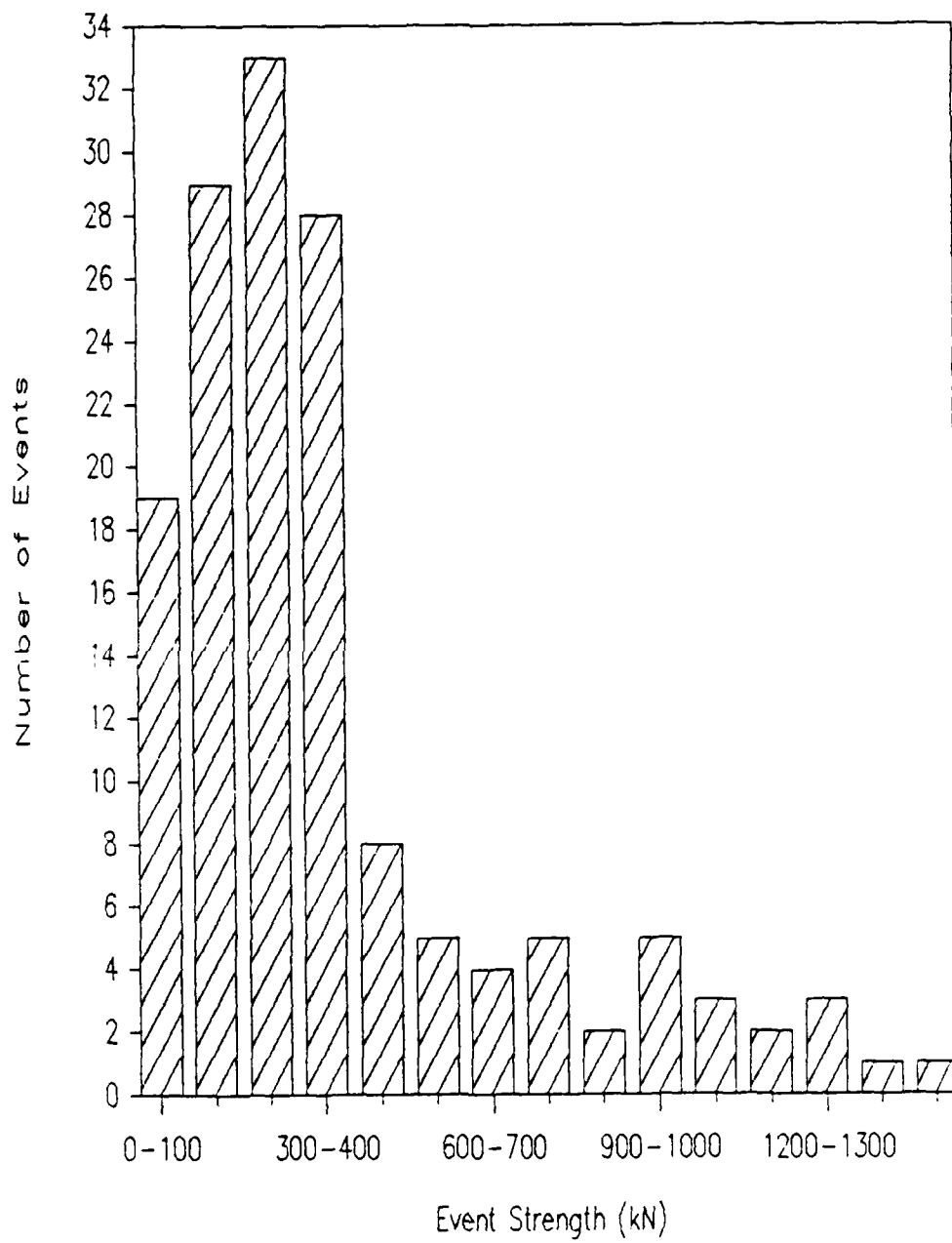
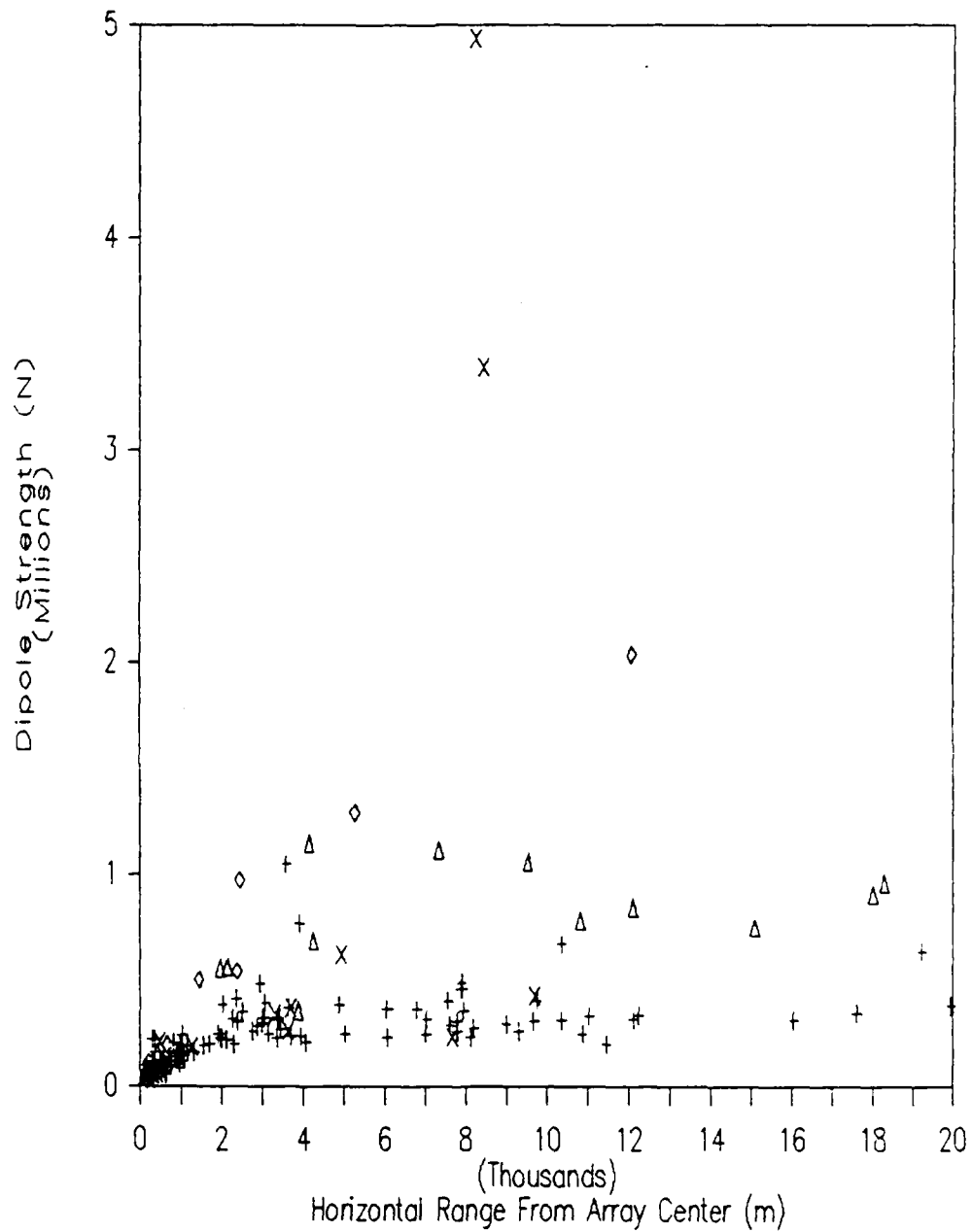


Figure 5-15 Distribution of strength for a population of noise events



+ 0.01-0.02 Pa ◇ 0.02-0.03 Pa Δ 0.03-0.04 Pa X 0.04+ Pa

Figure 5-16 Dipole strength for events between 300 m and 20,000 m, plotted against horizontal range from the array origin.

Most of the events evaluated for strength occurred during the lowest ambient noise levels. Figure 5-17 shows the strength of events that occurred when the ambient noise was 0.01 to 0.02 Pa. The log of the dipole strength is plotted against the log of the horizontal range from the center of the array. The points scatter more so to the upper left rather than lower right, because distance itself filters out weak events. A weak signal from far away would not reach the hydrophone array with enough amplitude to be distinguished from the background noise. And events located farther away would tend to be strong events. However, events located close to the array should have the entire range of source strength levels. This would produce a wedged shaped plot of weaker events close to the array. Indeed, Figure 5-17 shows a general scattering with perhaps a wedge of weaker events near the array origin.

Nonetheless the trend shown in Figure 5-17 suggests that the ray average model used to estimate refractive-surface reflective spreading may need to be replaced with a more refined model. For example, horizontal ranges less than about 1000 m may include too small a loss, and therefore lead to too small a strength, because the reflective contributions may not be as large as imputed. Such a criticism is supported by the notion that for a given slope, ϵ , reflective rays and hence ray averaging occurs only beyond a critical horizontal range.

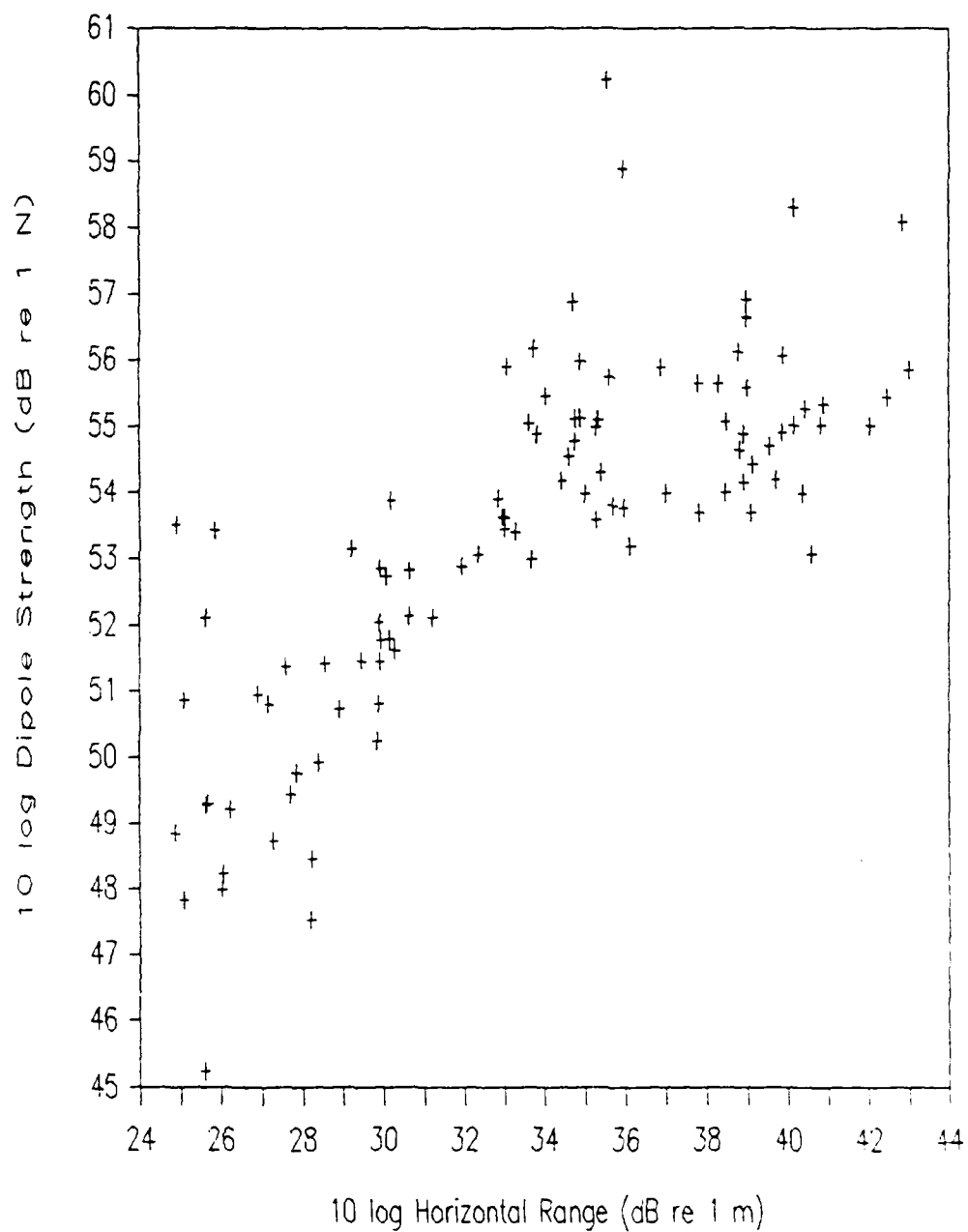


Figure 5-17 10 log of Dipole strength (dB re 1 N) versus 10 log of horizontal range from the array origin (dB re 1 m) for events occurring during an ambient noise level of 0.01 to 0.02 Pa.

The foregoing speculation suggests that the average dipole strength for the lowest ambient noise case is best found from the events farther from the array, and is

$$F_0 \approx 10^{5.5} \text{ N} \approx 320 \text{ kN} , \quad (5-12)$$

with a much smaller standard deviation than in Table 5-8. Presumably corresponding adjustments could be made for the higher ambient noise cases, but the FRAM IV data set contains too few events at higher ambient noise to plot as in Figure 5-17.

The strength analysis is a somewhat ambivalent one because of spreading model uncertainty, and because data on ice slopes are not available. But the dipole picture of an event likely has some validity, and at least rough estimates of its strength have been extracted from the data.

CHAPTER 6

SUMMARY AND THOUGHTS

Through the use of a detection program, visual confirmation and a location program, a population of 199 Arctic noise transients was gathered. There are four major results.

First, more events are found when the ambient pressure is low, and more false alarms when the ambient pressure is high. The interarrival time and the average number of events per unit area also depend on ambient noise level. Since more events are found when the ambient noise is low, the interarrival time decreases, and the spatial density increases.

Second, the interarrival times were fit to several possible probability distributions. The interarrival time distribution best fits a J shaped gamma distribution. The mean interarrival time is 100 seconds.

Third, the number of events per unit area is highly dependent on range, since distance filters out weak transients. The event density in the annulus closest to the center of the array was 0.3 events per square kilometer per hour over all observations and 0.5 events per square kilometer per hour for quiet times. There is no predominant angular dependence to the spatial distribution of events.

Last, the mean dipole strength for the observed events is 430 kN overall and 260 kN during low ambient noise levels. Stronger events occurred during high ambient noise levels. A refinement of the spreading loss model used to calculate these values may lead to values which are slightly higher.

Analysis of Arctic acoustic events is far from complete. Several areas for improvement have been mentioned earlier in the thesis. The detection program needs to be made more robust to eliminate the event time error. A scheme for ignoring artifacts should be included. The location program wastes time looking in the wrong direction, although the bearing accuracy of the program is very good. The algorithm should be changed to quickly find the right bearing, and then search in a sector.

The type of each event, whether it was a pop or a whine, was not recorded. Collecting this information and correlating it with interarrival time and range still needs to be done.

REFERENCES

- [1] Y.M. Chen. *Report for a Study on Sound Speed Profiles of the Arctic Ocean*. Technical Report, MIT Department of Ocean Engineering, June, 1981.
- [2] C.S. Clay and H. Medwin. *Acoustical Oceanography*. John Wiley & Sons, New York, 1977.
- [3] S.H. Crandall and W.D. Mark. *Random Vibration in Mechanical Systems*. Academic Press, New York, 1963.
- [4] F.R. DiNapoli, et.al. TRISTEN/FRAM IV CW Spatial Coherence and Temporal Stability. Scientific and Engineering Studies; Underwater Acoustics in the Arctic. Naval Underwater Systems Center, Newport, RI, 1985.
- [5] I. Dyer. Fundamentals and Applications of Underwater Sound. Course Notes for MIT class by same name (13.851).
- [6] I. Dyer. The Song of Sea Ice and Other Arctic Ocean Melodies. *Arctic Technology and Policy*. Hemisphere Publishing Corporation, Washington, 1984.
- [7] I. Dyer. Arctic Ocean Ambient Noise. *Proceedings of the 12th International Congress on Acoustics*. Toronto, 1986, 24-31 July.
- [8] P.E. Green and R.V. Wood. *Large Aperture Seismic Array Capabilities*. Technical Note 1966-16 Lincoln Laboratories MIT, Lexington, MA, 1966.
- [9] E.J. Kelly. *LASA On-Line Detection, Location and Signal-to-Noise Enhancement*. Technical Note 1966-36 Lincoln Laboratory MIT, Lexington, MA, 1966.
- [10] N.C. Makris and I. Dyer. Environmental Correlates of Pack Ice Noise. *Journal of the Acoustical Society of America*. May, 1986.
- [11] R.H. Mellen. Underwater Acoustics in the Arctic Ocean. Sonar Signal Processing and the Arctic Environment Course Notes. Applied Technology Institute, Columbia, MD, 1987.
- [12] J. Nielsen, et.al. TRISTEN/FRAM IV Arctic Ambient Noise Measurements. *Scientific and Engineering Studies, Underwater Acoustics in the Arctic*. Naval Underwater Systems Center, Newport, RI, 1985.

[13] P.J. Stein. Acoustic Monopole in a Floating Ice Plate
Doctoral thesis, Massachusetts Institute of Technology,
February, 1986.

[14] R.J. Urick. *Principles of Underwater Sound*. McGraw-
Hill Book Company, New York, 1983.

[15] G.P. Wadsworth and J.G. Bryan. *Applications of
Probability and Random Variables*. McGraw-Hill, Inc., New
York, 1974.

[16] *Standard Mathematical Tables*, 27ed. W.H. Beyer, ed. CRC
Press, Inc., Boca Raton, FL, 1984.

[17] Measurements on WHOI Hydrophones Serials 1, 2, and 3.
USRD Calibration Memorandum No. 6628. Naval Research
Laboratory, Orlando, FL, 1982.

ACKNOWLEDGEMENTS

I would like to acknowledge first of all my thesis advisor, Ira Dyer, whose inspirational and gentle guidance kept me eagerly moving forward. I have benefited from his clear thinking and his tremendous knowledge. I am most grateful for the precious gift of time he gave me, especially as this effort drew to a close.

I would like to thank Art Baggeroer for pinch-hitting as my thesis advisor, and for his sincere interest in my project. I thank Greg Duckworth for his valuable advise on signal processing techniques, and for his indirect help with learning the 'c programming language. His clear and concise programs allowed me to learn the language by "copying a master".

I am grateful for all the assistance I received at the Woods Hole Oceanographic Institute, but especially to Eddie Scheer and Nan Galbraith. Both were always helpful, and Eddie's disparaging humor helped me keep things in perspective. Nan was especially patient and responsive. Many mornings I would greet her with a problem, even before her first cup of coffee.

I would like to thank my Arctic acoustics compatriots at MIT. Peter Stein, Chi-Fang Chen, Nick Makris and Andrew Langley were especially supportive in either helping me get started in this work, or with probing questions which

stimulated my efforts.

I would like to thank Wendy Woods for her many long hours helping me complete the strength calculations in this thesis. I value most her quick mind and her dependability.

I must also acknowledge those people who gave me the emotional support I needed to complete this task. I would like to thank Pam Barnes for sharing. I would like to thank my parents and my brothers and sisters for their support and good wishes.

Finally, I would like to thank most of all my devoted husband, Bob, who put up with much and was always there. He has made this work possible.

APPENDIX A

User's Guide for the *hdetect* Program

Figure A-1: Flow Chart of the *hdetect* Program

Source Code for the *hdetect* Program

USER'S GUIDE FOR THE *hdetect* PROGRAM

The purpose of the *hdetect* program is to detect ambient noise transients amidst the background ambient noise recorded on a FRAM data tape. This is done by comparing the short average of data points to the long average of points on a single channel in order to flag a possible detection, and then waiting until 50% of the channels are flagged to declare an actual detection.

The input for the *hdetect* program is a *framread* output file without headers. A FRAM data tape is read into the file by the command

```
framread -head      <RETURN>
```

The program will ask for the input device (tape drive designation), the output file, and the number of data segments to skip and to read. Each segment represents 3.6 seconds of data on 24 channels. The *framread* program reads a first segment which contains no data records, so you should specify skipping one more segment than you would normally calculate. For example, reading the entire first half of a 20 minute FRAM IV tape would require the response of

```
1 160              <RETURN>
```

to the question of "enter #skip, #segments:".

Once this input file has been created the *hdetect* program can be used. The program is started with the

command

hdetect

<RETURN>

The program will ask for the FRAM tape number, the Julian date of the tape, and the start time of the tape in hours, minutes and seconds. The program will then ask you to select the channels you wish to use. In most cases the FRAM data tapes did not have ambient noise hydrophones tied into all channels, and the specific channel that a hydrophone was recorded on changed throughout the experiment. Which channels were in use and for which hydrophones can be found in the experiment logs. The program assumes that the channel number is equal to the hydrophone number, but allows you to change this by inputting the channel number and the proper hydrophone number, or "0" if the channel is not in use. For example, if channel 3 was not used, and channel 7 was used for hydrophone 21, the input would be

3,0	<RETURN>
7,21	<RETURN>
0,0	<RETURN>

The "0,0" ends the changes to the channel selection. You must now hit any key to continue the program.

You will be asked to enter the input device (the input *framread* file), the number of skips and segments, and the name of the output file. The output file does not have to exist before the program is started. It will be created by the program. The number of skips and segments are those

that you would calculate using 3.8 seconds per segment.
For example, to process the entire first half of a 20 minute
FRAM IV tape the number of skips and segments would be

0,160 <RETURN>

This is all of the input required by the user. The
program proceeds from this point without user interaction.

The output of the *hdetect* program is a file containing
a list of detections in the following format:

```
tapenumber Juliadate hour minute seconds
0 eventnumber eventtime
channel hydrophone timedelay amplitude
channel hydrophone timedelay amplitude
channel hydrophone timedelay amplitude
.
.
channel hydrophone timedelay amplitude
0 eventnumber eventtime
channel hydrophone timedelay amplitude
.
.
channel hydrophone timedelay amplitude
0 eventnumber eventtime
.
.
-1
```

The "0" at the start of a line indicates a new event
detection, and the "-1" at the start of a line indicates an
end of file. Each channel that was flagged for a
particular event is listed with its hydrophone number,
timedelay from the earliest channel signal arrival, and its
peak voltage amplitude. This outfile can be used as the
input file for the location programs without modification.

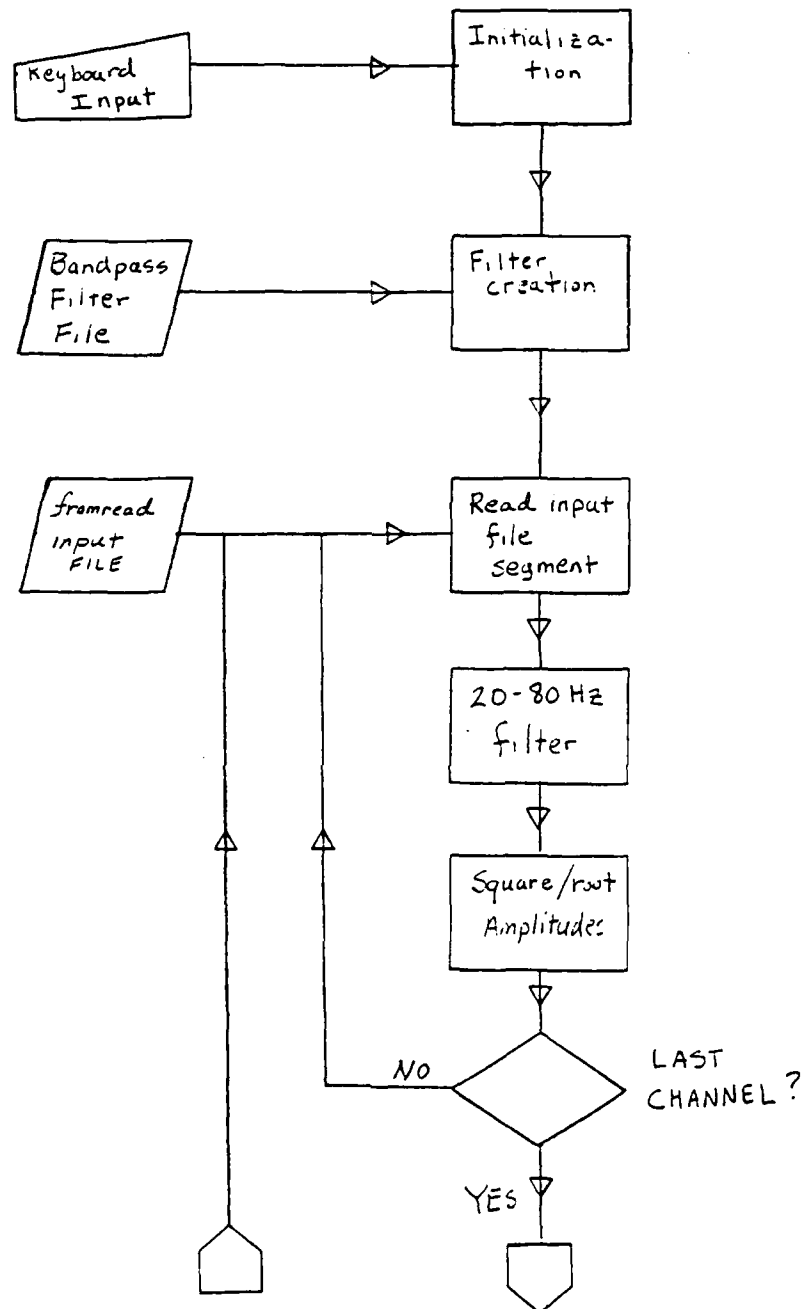


Figure A-1 Flow chart of the hdetect program.

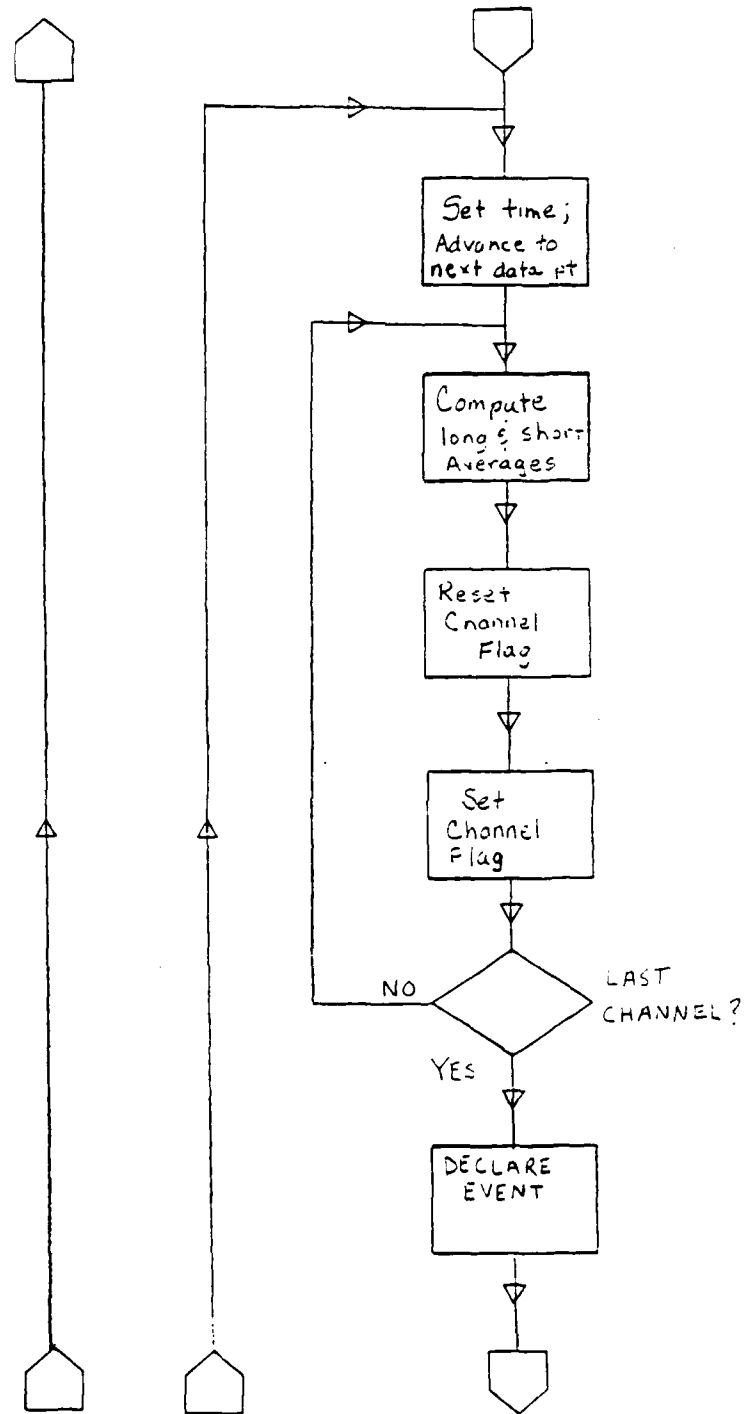


Figure A-1 Flow chart of the hdetect program.

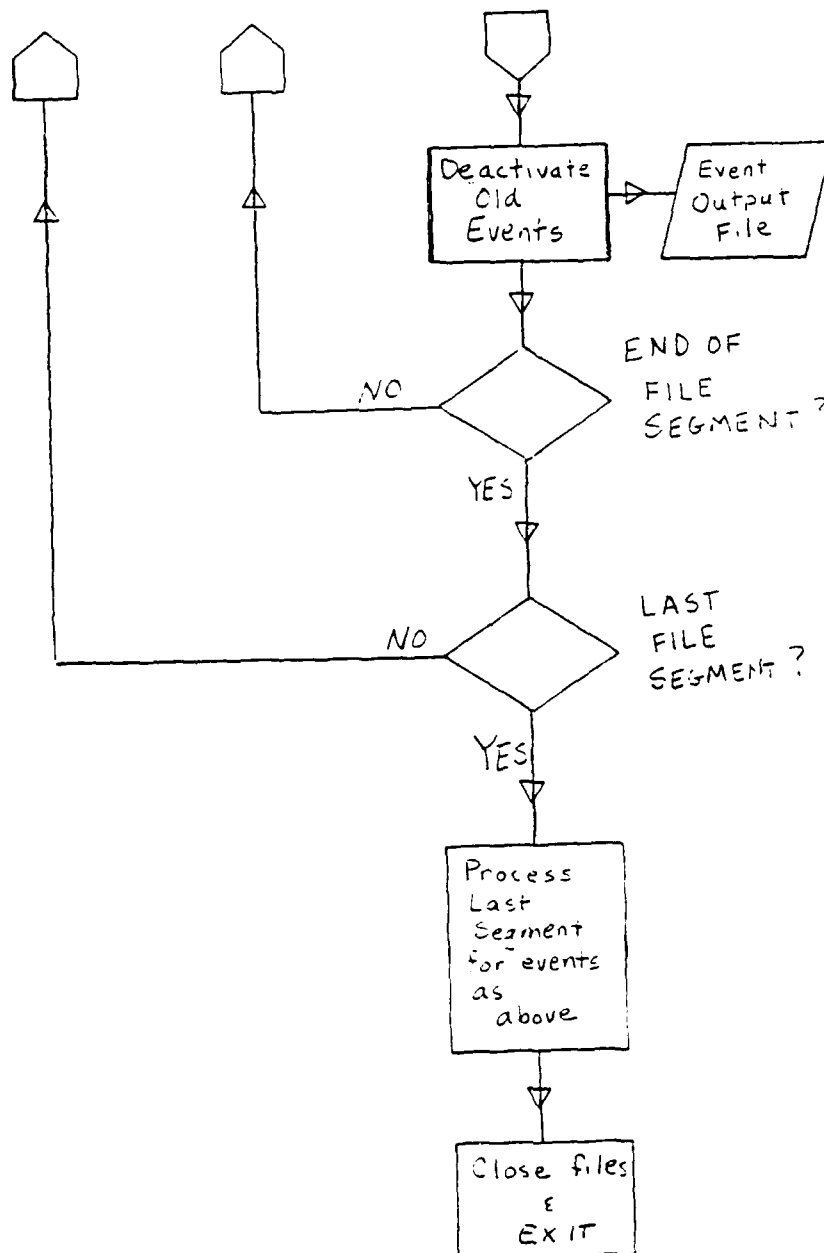


Figure A-1 Flow chart of the hdetect program.

```
/* startdoc
hdetect.c

program to read whoi-segy format data tapes from the fram IV program.

usage:
        hdetect

program is interactive.

by Mary Townsend-Manning

enddoc
*/

#include <stdio.h>
#include <math.h>
#define NCHAN 25
#define RECLN 950 /* number of samples per trace (4 bytes per sample)*/
#define OBYTES 3800 /* number of bytes per record output */
#define ZERO 0
#define LONGFILTLN 64 /* length of long average filter */
#define FLN 64
#define MAXEVENTS 4
#define RESET_DELAY 0.3
#define RATIO 2.38
#define SIG_DELAY 0.02
#define THRESHOLD 0.5
#define EVENT_DELAY 0.5
#define END -1

double vconv(x,y,n)
    register float *x, *y;
    register int n;
{
    register double sum = 0.;

    if(n > 0)
    {
        do {
            sum += *x++ * *y--;
        } while(--n > 0);
    }
    return(sum);
}

main()
{
```

Source code for the *hdetect* program.

```
float l_ave[NCHAN], sh_ave, timeofflag[NCHAN];
float amptofflag[NCHAN], firsttime, timedelay[NCHAN];
float chaneventtime[MAXEVENTS][NCHAN];
float chaneventamp[MAXEVENTS][NCHAN], eventtime[MAXEVENTS];
int flag[NCHAN];
int num_active_events;
int m, n;
int event_flag[MAXEVENTS][NCHAN], flag_sum, number_of_events;
int event_number[MAXEVENTS];
int nchan = 0;
int chan[NCHAN], k, j, i, tid, date, hour, min, sec, l;
int channel, data, toggle;
char answer;
float h[FLN], longfilt[LONGFILTLN];
int nskip, nseg;
char oddobuf[NCHAN][OBYTES], evenobuf[NCHAN][OBYTES];
int count, error;
char fname[80], iname[80];
FILE *iptr, *ptr, *fp, *fopen();
float timeseries[NCHAN][RECLN+2*FLN];
float time = 0.;

num_active_events = 0;

for (i=1; i<25; i++) {
    chan[i] = (i);
    flag[i] = 0;
    for (m=1; m<MAXEVENTS; m++) {
        event_flag[m][i] = 0;
        chaneventtime[m][i] = 0;
        chaneventamp[m][i] = 0;
    }
}

/* Program initialization from keyboard */

fprintf(stderr, "Program Initialization\n");
fprintf(stderr, "enter FRAM tape #\n");
fscanf(stdin, "%d", &tid);

fprintf(stderr, "enter Julian date\n");
fscanf(stdin, "%d", &date);
fprintf(stderr, "enter time - HR, MN, SC\n");
fscanf(stdin, "%d, %d, %d", &hour, &min, &sec);

fprintf(stderr, "default values for channels and phones\n");
fprintf(stderr, "are channel # = phone #.\n");

fprintf(stderr, "enter channel, phone to change.\n");
fprintf(stderr, "enter '0' for phone, to eliminate a channel.\n");
fprintf(stderr, "enter '0,0' to quit.\n");
fscanf(stdin, "%d, %d", &j, &k);

while (j != 0 && j < 25) {
    chan[j] = k;
```

Source code for the *hdetect* program.

```
fscanf(stdin,"%d,%d",&j,&k);
}

fprintf(stderr,"FRAM TAPE %d    Julian Date: %d\n",tid,date);
fprintf(stderr,"                Time:      %d:%d:%d\n",hour,min,sec);
for(i=1;i<13;i++)
    fprintf(stderr,"CH %d PH %d    CH %d PH %d\n",
        i,chan[i],i+12,chan[i+12]);

/* Check to make sure inputs are correct -- Change if necessary */

fscanf(stdin,"%c",&answer);
fprintf(stderr,"Hit any key and RETURN, when ready.");
fscanf(stdin,"%c",&answer);

for(i=1;i<NCHAN;i++) {
    if(chan[i] != 0) nchan++;
}

fprintf(stderr,"enter input device: ");
scanf("%s",iname);

if((iptr = fopen(iname, "r")) == NULL)
{
    fprintf(stderr,"can't open %s\n",iname);
    exit(1);
}

fprintf(stderr,"enter #skip, #segments: \n");
fprintf(stderr,"values of 0 and 320 will read entire tape\n");
scanf("%d,%d",&nskip,&nseg);

/* load bandwidth filter */

if((fp=fopen("PMfloat","r")) == NULL) {
    printf ("cannot open bandwidth filter file\n");
    exit(0);
}
for(i=0;i<64;i++)
    fscanf(fp,"%f",&h[i]);
fclose(fp);

/* load averaging filter */

for(i=0;i<LONGFILTLN;i++)
    longfilt[i] = 1.0/(float)LONGFILTLN;

/* Open output file */
```

Source code for the *hdetect* program.


```
fprintf(stderr,"enter out-file: ");
scanf("%s",fname);
if((ptr = fopen(fname, "w")) == NULL)
{
    fprintf(stderr,"can't open %s\n",fname);
    exit(1);
}

fprintf(ptr,"%d %d %d %d %d\n", tid, date, hour, min, sec);

time = time + 3.8 * (nskip-1) ;

/* enter first record */

if (nskip%2 == 1){
    for(j=1;j<NCHAN;j++){
        fread(&evenobuf[j][0], sizeof(float), RECLN, iptr);
    }
    toggle = 1;
}
else {
    for(j=1;j<NCHAN;j++){
        fread(&oddbuf[j][0], sizeof(float), RECLN, iptr);
    }
    toggle = 0;
}

/* ENTERING RECORD READING MODULE */
time = time + 0.504;

/*      fprintf(stderr,"using buffer size %d bytes\n",sizeof(buf)); */
for(i=1; i < nseg; i++)
{
    fprintf(stderr,"time = %f\n", time);
    fprintf(stderr,"processing record %d\n", nskip+i); /*
/* read next record into appropriate buffer */

if (toggle == 1){
    for(j=1;j<NCHAN;j++){
        fread(&oddbuf[j][0], sizeof(float), RECLN, iptr);
    }
    toggle = 0;
}
else {
    for(j=1;j<NCHAN;j++){
        fread(&evenobuf[j][0], sizeof(float), RECLN, iptr);
    }
    toggle = 1;
}

/* filter and square data */
```

Source code for the *hdetect* program.

```
if (toggle == 1) {
  for(j=1;j<NCHAN;j++) {
    if(chan[j] != 0) {

      sq_filt(&oddbuf[j][0],&evenobuf[j][0],h,
&timeseries[j][0]);
      l_ave[j] = vconv(&longfilt[0],&timeseries[j][2*(FLN-1)],
LONGFILTLEN);
    }
  }
} else {
  for(j=1;j<NCHAN;j++) {
    if(chan[j] != 0) {
      sq_filt(&evenobuf[j][0],&oddbuf[j][0],h,
&timeseries[j][0]);
      l_ave[j] = vconv(&longfilt[0],&timeseries[j][2*(FLN-1)],
LONGFILTLEN);
    }
  }
}

/* ENTERING EVENT DETECTION MODULE */

for(k=0;k<RECLN;k += 4) {

  for(l=1;l<NCHAN;l++) {
    if (chan[l] != 0) {
      l_ave[l] = (63.0*l_ave[l] + timeseries[l][2*(FLN-1)+k])/64.0;
      sh_ave = (timeseries[l][2*(FLN-1)+k] +
timeseries[l][2*(FLN-1)+k-1] + timeseries[l][2*(FLN-1)+k-2] +
timeseries[l][2*(FLN-1)+k-3])/4.0;

/* reset old flags */

      if (flag[l] == 1 && (time - timeofflag[l]) > RESET_DELAY)
        flag[l] = 0;

/* set flag if RATIO of signals is reached */

      if ((sh_ave/l_ave[l])>=RATIO) {
        if (flag[l] == 1) {
          if (sh_ave > ampoflag[l]) {
            timeofflag[l] = time;
            ampoflag[l] = sh_ave;
          }
        }
      } else {
        if (num_active_events == 0) {
          flag[l] = 1;
        }
      }
    }
  }
}
```

Source code for the *hdetect* program.

```
        timeofflag[l] = time;
        ampoflag[l] = sh_ave;
    }
    else {
        for (m=1;m<(num_active_events + 1);m++) {
            if (event_flag[m][l] == 1) {
                if ((time - chaneventtime[m][l])
                    <= SIG_DELAY) {
                    if (sh_ave > chaneventamp[m][l]) {
                        chaneventtime[m][l] = time;
                        chaneventamp[m][l] = sh_ave;
                    }
                }
            }
            else {
                flag[l] = 1;
                timeofflag[l] = time;
                ampoflag[l] = sh_ave;
            }
        }
    }
    else {

        event_flag[m][l] = 1;
        chaneventtime[m][l] = time;
        chaneventamp[m][l] = sh_ave;
        m = num_active_events;
    }
}
}
}
}
}

/* end of set flag module */

/* start new event module */

flag_sum = 0;

for (l=1;l<NCHAN;l++) {
    if (flag[l] == 1) flag_sum++;
}
if (((float)flag_sum/(float)nchan) >= THRESHOLD) {
    num_active_events++;
    eventtime[num_active_events] = time;
    number_of_events++;
    event_number[num_active_events] = number_of_events;

    for (l=1;l<NCHAN;l++) {
        event_flag[num_active_events][l] = flag[l];
        chaneventtime[num_active_events][l] = timeofflag[l];
        chaneventamp[num_active_events][l] = ampoflag[l];
        flag[l] = 0;
        timeofflag[l] = 0;
        ampoflag[l] = 0;
    }
}
```

Source code for the *hdetect* program.

```

    }
}

/* end of new event module */

/* start of deactivate old event module */

    if (num_active_events > 0 && (time - eventtime[l]) > EVENT_DELAY) {
        fprintf (ptr,"%d %d %f\n",ZERO,
                event_number[l],eventtime[l]);
    /*   fprintf (stderr,"%d %f\n",event_number[l],eventtime[l]); */

/*
        find time delays by finding earliest channel event
        time, and subtracting that from the other channel
        times

*/

        firsttime = 10000.0;

        for(l=1;l<NCHAN;l++) {
            if(chan[l] != 0 && event_flag[l][l] != 0 &&
                chaneventtime[l][l] < firsttime)
                firsttime = chaneventtime[l][l];
        }

        for(l=1;l<NCHAN;l++) {
            if(chan[l] != 0 && event_flag[l][l] != 0) {
                timedelay[l] = ((chaneventtime[l][l]) - firsttime);
                fprintf(ptr,"%d %d %f %f\n",l,chan[l],
                    timedelay[l], chaneventamp[l][l]);
            }
        }

/*
        print to file to indicate end of event */

        for (l=1;l<num_active_events;l++) {
            for (m=1; m<NCHAN;m++) {
                event_flag[l][m] = event_flag[l+1][m];
                chaneventtime[l][m] = chaneventtime[l+1][m];
                chaneventamp[l][m] = chaneventamp[l+1][m];
            }
            eventtime[l] = eventtime[l+1];
            event_number[l] = event_number[l+1];
        }
        num_active_events--;
    }
    time += 0.004*4.0;
}
/* EXIT MODULE */

```

Source code for the *hdetect* program.

```

/* fprintf(stderr,"processing record %d\n", nskip+nseg); */
if(toggle == 1) {
    for(j=1;j<NCHAN;j++) {
        if(chan[j] != 0) {
            for(k=0;k<OBYTES;k++)
                oddobuf[j][k] = 0;
            sq_filt(&evenobuf[j][0],&oddobuf[j][0],h,&timeseries[j][0]);
            l_ave[j] = vconv(&longfilt[0],&timeseries[j][2*(FLN-1)],
                            LONGFILTLEN);
        }
    }
}
else {
    for(j=1;j<NCHAN;j++) {
        if(chan[j] != 0) {
            for(k=0;k<OBYTES;k++)
                evenobuf[j][k] = 0;
            sq_filt(&oddobuf[j][0],&evenobuf[j][0],h,&timeseries[j][0]);
            l_ave[j] = vconv(&longfilt[0],&timeseries[j][2*(FLN-1)],
                            LONGFILTLEN);
        }
    }
}

for(k=0;k<(RECLN-2*(FLN-1));k+=4) {
    for(l=1;l<NCHAN;l++) {
        if (chan[l] != 0) {
            l_ave[l] = (63.0*l_ave[l] + timeseries[l][2*(FLN-1)+k]) / 64.0;
            sh_ave = (timeseries[l][2*(FLN-1)+k] +
timeseries[l][2*(FLN-1)+k-1] + timeseries[l][2*(FLN-1)+k-2] +
timeseries[l][2*(FLN-1)+k-3]) / 4.0;
        }
    }
}

/* reset old flags */
if (flag[l] == 1 && (time - timeofflag[l]) > RESET_DELAY)
    flag[l] = 0;

/* set flag if RATIO of signals is reached */

if ((sh_ave/l_ave[l])>=RATIO) {
    if (flag[l] == 1) {
        if (sh_ave > ampoflag[l]) {
            timeofflag[l] = time;
            ampoflag[l] = sh_ave;
        }
    }
    else {
        if (num_active_events == 0) {
            flag[l] = 1;
            timeofflag[l] = time;
        }
    }
}

```

Source code for the hdetect program.

```

        ampoofflag[l] = sh_ave;
    }
    else {
        for (m=1;m<(num_active_events + 1);m++) {
            if (event_flag[m][1] == 1) {
                if ((time - chaneventtime[m][1])
                    <= SIG_DELAY) {
                    if (sh_ave > chaneventamp[m][1]){
                        chaneventtime[m][1] = time;
                        chaneventamp[m][1] = sh_ave;
                    }
                }
            }
            else {
                flag[l] = 1;
                timeofflag[l] = time;
                ampoofflag[l] = sh_ave;
            }
        }
        else {

            event_flag[m][1] = 1;
            chaneventtime[m][1] = time;
            chaneventamp[m][1] = sh_ave;
            m = num_active_events;
        }
    }
}

/* end of set flag module */

/* start new event module */

flag_sum = 0;

for (l=1;l<NCHAN;l++) {
    if (flag[l] == 1) flag_sum++;
}
if (((float)flag_sum/(float)nchan) >= THRESHOLD) {
    num_active_events++;
    eventtime[num_active_events] = time;
    number_of_events++;
    event_number[num_active_events] = number_of_events;

    for (l=1;l<NCHAN;l++) {
        event_flag[num_active_events][1] = flag[l];
        chaneventtime[num_active_events][1] = timeofflag[l];
        chaneventamp[num_active_events][1] = ampoofflag[l];
        flag[l] = 0;
        timeofflag[l] = 0;
        ampoofflag[l] = 0;
    }
}

```

Source code for the *hdetect* program.

```
    }

/* end of new event module */

/* start of deactivate old event module */

    if (num_active_events > 0 && (time - eventtime[l]) > EVENT_DELAY) {
        fprintf (ptr,"%d %d %f\n", ZERO,
                event_number[l],eventtime[l]);
/*    fprintf (stderr,"%d %f\n",event_number[l],eventtime[l]); */

/*        find time delays by finding earliest channel event
        time, and subtracting that from the other channel
        times

*/

        firsttime = 10000.0;

        for(l=1;l<NCHAN;l++) {
            if(chan[l] != 0 && event_flag[l][l] != 0 &&
                chaneventtime[l][l] < firsttime)
                firsttime = chaneventtime[l][l];
        }

        for(l=1;l<NCHAN;l++) {
            if(chan[l] != 0 && event_flag[l][l] != 0) {
                timedelay[l] = ((chaneventtime[l][l]) - firsttime);
                fprintf(ptr,"%d %d %f %f\n",l,chan[l],
                    timedelay[l], chaneventamp[l][l]);
            }
        }

/*    print to file to indicate end of event */

        for (l=1;l<num_active_events;l++) {
            for (m=1; m<NCHAN;m++) {
                event_flag[l][m] = event_flag[l+1][m];
                chaneventtime[l][m] = chaneventtime[l+1][m];
                chaneventamp[l][m] = chaneventamp[l+1][m];
            }
            eventtime[l] = eventtime[l+1];
            event_number[l] = event_number[l+1];
        }
        num_active_events--;

        time += 0.004*4.0;
    }
/* print out all events */

if(num_active_events > 0) {
```

Source code for the hdetect program.

```
for(k=1;k<(num_active_events + 1);k++) {
    fprintf(ptr,"%d %d %f\n", ZERO,
            event_number[k],eventtime[k]);
/*      fprintf (stderr,"%d %f\n",event_number[k],eventtime[k]); */

/*      find time delays by finding earliest channel event
      time, and subtracting that from the other channel
      times

*/

    firsttime = 10000.0;

    for(l=1;l<NCHAN;l++) {
        if(chan[l] != 0 && event_flag[k][l] != 0 &&
           chaneventtime[k][l] < firsttime)
            firsttime = chaneventtime[k][l];
    }

    for(l=1;l<NCHAN;l++) {
        if(chan[l] != 0 && event_flag[k][l] != 0) {
            timedelay[l] = ((chaneventtime[k][l]) - firsttime);
            fprintf(ptr,"%d %d %f %f\n",l,chan[l],
                    timedelay[l], chaneventamp[k][l]);
        }
    }
}

/* final summary to screen */

fprintf(ptr,"%d", END);
fclose(ptr) ;
fclose(iptr) ;
exit(0) ;

}

sq_filt(first,second,filter,output)
/* filters and squares two data arrays */

float first[RECLN], second[RECLN], filter[FLN];
float output[RECLN+2*FLN];

{
```

Source code for the hdetect program.


```
/* put zeros in first (FLN -1) places of output */

    int j, i;
    float transition[2*FLN];
    float sum;

    for(i=0;i<FLN-1;i++)
        output[i] = 0.0 ;

/* put in first data */

    for(i=FLN-1;i<RECLN;i++) {
        sum = vconv(&filter[0],&first[i],FLN);
        output[i] = sqrt(sum * sum);
    }

/* put in transition from first to second data */

    for(j=0;j<FLN-1;j++) {
        transition[j] = first[RECLN-(FLN-1)+j];
        transition[j+FLN-1] = second[j];
    }

    for(i=0;i<FLN-1;i++){
        sum = vconv(&filter[0],&transition[i+FLN-1],FLN);
        output[i+RECLN] = sqrt(sum * sum);
    }

/* put in second data */

    for(i=FLN-1;i<2*FLN;i++) {
        sum = vconv(&filter[0],&second[i],FLN);
        output[RECLN+i] = sqrt(sum * sum);
    }

}
```

Source code for the *hdetect* program.

APPENDIX B

User's Guide for the *location*, *farlocate* and *finelocate*
Programs

Source Code for the *farlocate* Program

**USER'S GUIDE FOR THE *location*, *farlocate*,
and *finelocate* PROGRAMS**

The purpose of the location programs is to find the spatial location of an event from the time delays between signal arrival at different hydrophones. The program assumes a test location and computes the slant range to the individual hydrophones. The slant ranges are plotted against the experimental time delays and a least squares fit is done. The test location with the best least squares fit is considered the location of the event.

The input to the location programs is the output file of the detection program. Manual time delays may be substituted for the program generated time delays in this file, but this editing must be done before the location program is invoked.

This location program is very user interactive. The user starts the location program with the command

`location <RETURN>`

The program asks for the input and output file names. It then reads the input file and asks whether the user would like to locate the first event. This allows the user to skip down to the event of interest. The program then allows the user to adjust which hydrophone time delays will be used in the location process. This is very handy for removing questionable time delays, in order to get a better location solution. With the hydrophone channels chosen,

the program proceeds with the actual location algorithm. In the *finelocate* and *farlocate* programs the user is asked to specify which quadrant or direction is to be searched.

The *location* program tries test locations in a large grid, and when the "best" location is found, then searches a smaller grid around this "best" location. The *location* and *farlocate* programs have 4 levels of grids and the *finelocate* program has 3 levels. Intermediate answers are displayed for each level.

The intermediate and final answers display the x and y coordinates of the best location, the standard deviation of the least squares fit (σ), the group speed (which should be around 1440 m/s), and the y intercept of the time delay / slant range plot. After the final answer the user is asked whether or not he would like to remove outlying points. If this option is selected the program removes hydrophones with a deviation from the least squares fit of more than 3 times the standard deviation, and the group speed and the standard deviation are recalculated and displayed.

The user is then asked if he would like to locate the event with different hydrophones, and if so returns the user to the start of the channel selection process. The user may repeat this location scheme as many times as necessary for a particular event. Once the user is satisfied with the location answer, and declines to locate

the event with different phones, the program calculates the event strength based on the amplitudes in the input file, the location of the event and spherical spreading losses. The location parameters and the strength are then written to an outfile.

At this point the user is given the option to exit the program or locate the next event in the input file. The location process continues until the user exits or until the last event in a file is located.

```
/* location.c

program to locate the spatial position of an event based on
time delays taken from "detection".

Source strength is also computed.

*/

#include <stdio.h>
#include <math.h>

#define PHONES 31
#define LEVEL 4
#define FINENESS 20
#define DEPTH 91.0
#define SENSITIVITY 0.0000000112202

main()
{
    float amp[PHONES], phonex[PHONES], phoney[PHONES];
    float timedelay[PHONES], r[PHONES], bestrange[PHONES];
    float sumtime, sumr, sumrsq, sumtimer, slope, yintr;
    float sigma, bestsigma, bestslope, bestyintr;
    float bestamp, N, source[PHONES], sumsource;
    float xgs, ygs, xcctr, ycctr, a, b, bestx, besty;
    float level, gridsize, xfineness, yfineness, time, gpspeed;

    int i, j, tape, date, hour, min, sec, event, flag;
    int phone, num, l, n, m, bestflag;
    int phoneflag[PHONES];
    int eventselect, rerun, change, answer, bye, quadrant;

    char iname[80], oname[80];

    FILE *ptr, open(), *locptr, *optr;

/* PROGRAM INITIALIZATION */

    bye = 0;

    fprintf(stderr, "input file = \n");
    scanf("%s", iname);
    fprintf(stderr, "output file = \n");
    scanf("%s", oname);

/* open files */

    if((ptr = fopen(iname, "r")) == NULL) {
        fprintf(stderr, "can't open %s\n", iname);
        exit(1);
    }
}
```

Source code for the *farlocate* program

```
if((optr = fopen(oname, "w")) == NULL) {
    fprintf(stderr, "can't open %s\n", oname);
    exit(1);
}

if((locptr = fopen("array_loc", "r")) == NULL) {
    fprintf(stderr, "can't open array_loc file\n");
    exit(1);
}

/* read hydrophone locations into array */

for (i=1; i<PHONES; i++) {
    fscanf(locptr, "%d %f %f", &phone, &phonex[i], &phoney[i]);
}

/* read input file header */

fscanf(ptr, "%d %d %d %d %d", &tape, &date, &hour, &min, &sec);

/* read event header */

fscanf(ptr, "%d ", &flag);

while(byte != -1) {

    eventselect = 0;
    while(eventselect != 1) {

        if(flag < 0)
            exit(0);

        for (i=1; i<PHONES; i++) {
            phoneflag[i] = 0;
        }

        fscanf(ptr, "%d %f", &event, &time);

        for(i=1; i<PHONES; i++) {
            fscanf(ptr, "%d", &flag);

            if(flag > 0) {
                fscanf(ptr, "%d", &j);
                phoneflag[j] = 1;
                fscanf(ptr, "%f %f", &timedelay[j], &amp[j]);
            }
            else {
                i = PHONES;
            }
        }

        fprintf(stderr, "event = %d, time = %f\n", event, time);
    }
}
```

Source code for the *farlocate* program

```
fprintf(stderr,"Do you wish to locate this event? (1 = yes)\n");
scanf("%d", &eventselect);
}

/* channel selection */

rerun = 1;
while (rerun == 1) {
    change = 1;
    while (change == 1) {

        fprintf(stderr,"    phone          delay      \n");
        for(i=1; i<PHONES; i++) {
            if(phoneflag[i] != 0) {

                fprintf(stderr,"    %d          %f \n",i,timedelay[i]);
            }
        }

        fprintf(stderr,"Do you wish to change status? (1 = yes)\n");
        scanf("%d", &change);
        if (change == 1) {

            fprintf(stderr,"change status by typing phone#\n");
            fprintf(stderr,"type -1 to quit\n");
            scanf("%d", &j);

            while (j != -1) {
                if (phoneflag[j] != 0) {
                    phoneflag[j] = 0;
                }
                else {
                    phoneflag[j] = 1;
                }
                scanf("%d", &j);
            }
        }
    }
}

/* locate event */

num = 0;
sumtime = 0.0;

for (i=1; i<PHONES; i++) {
    if (phoneflag[i] != 0) {
        num++;
        sumtime += timedelay[i];
    }
}
fprintf(stderr,"select quadrant to search (1=NE, 2=NW, 3=SW, 4=SE\n");
fprintf(stderr,"5=N, 6=S, 7=E, 8=W)\n");
scanf("%d",&quadrant);
if (quadrant == 1) {
```

Source code for the farlocate program


```
    xcctr = 10000.0;
    ycctr = 10000.0;
}
else if (quadrant == 2) {
    xcctr = -10000.0;
    ycctr = 10000.0;
}
else if (quadrant == 3) {
    xcctr = -10000.0;
    ycctr = -10000.0;
}
else if (quadrant == 4) {
    xcctr = 10000.0;
    ycctr = -10000.0;
}
else if (quadrant == 5) {
    xcctr = 0.0;
    ycctr = 10000.0;
}
else if (quadrant == 6) {
    xcctr = 0.0;
    ycctr = -10000.0;
}
else if (quadrant == 7) {
    xcctr = 10000.0;
    ycctr = 0.0;
}
else if (quadrant == 8) {
    xcctr = -10000.0;
    ycctr = 0.0;
}
else {
    xcctr = 0.0;
    ycctr = 0.0;
}

bestflag = 0;

for(l=0; l<LEVEL; l++) {
    level = LEVEL-l-1;
    gridsize = pow(10.0,level);

    for(m=0; m<FINENESS; m++) {
        yfineness = m - (FINENESS/2);
        ygs = ycctr + yfineness * gridsize;

        for(n=0; n<FINENESS; n++) {
            xfineness = n - (FINENESS/2);
            xgs = xcctr + xfineness * gridsize;
            sumr = 0.0;
            sumrsq = 0.0;
            sumtimer = 0.0;
            for (i=1; i<PHONES; i++) {
                if(phoneflag[i] != 0) {
                    a = xgs-phonex[i];
```

Source code for the farlocate program

```

    b = ygs-phoney[i];
    r[i] = sqrt(pow(a,2.0) + pow(b,2.0) + pow(DEPTH,2.0));

    sumr += r[i];
    sumrsq += pow(r[i],2.0);
    sumtimer += (r[i] * timedelay[i]);
}

}

N = num;
slope = ((N * sumtimer) - (sumr * sumtime))/
        ((N * sumrsq) - pow(sumr,2.0));
yintr = (sumtime - (slope * sumr))/N;

sigma = 0.0;
for(i=1; i<PHONES; i++) {
    if(phoneflag[i] != 0) {
        sigma += pow((timedelay[i]-yintr-(slope * r[i])),2.0);
    }
}
sigma = sqrt(sigma/N);

if (bestflag == 0) {
    bestx = xgs;
    besty = ygs;
    bestsigma = sigma;
    bestslope = slope;
    bestyintr = yintr;
    for (i=1; i<PHONES; i++) {
        if (phoneflag[i] != 0) {
            bestrange[i] = r[i];
        }
    }
    bestflag = 1;
}

else {
    if (sigma < bestsigma) {
        bestx = xgs;
        besty = ygs;
        bestsigma = sigma;
        bestslope = slope;
        bestyintr = yintr;
        for (i=1; i<PHONES; i++) {
            if (phoneflag[i] != 0) {
                bestrange[i] = r[i];
            }
        }
    }
}
}
}
}

```

Source code for the farlocate program

```
gpspeed = 1.0/bestslope;

fprintf(stderr,"bestx = %f, besty = %f, sigma = %f\n",
        bestx, besty, bestsigma);
fprintf(stderr,"group velocity = %f\n", gpspeed);
fprintf(stderr,"y intercept = %f\n", bestyintr);
xcntr = bestx;
ycntr = besty;

}

fprintf(stderr,"Do you wish to remove outlying points? (1=yes)\n");
scanf("%d",&answer);
if (answer == 1) {
    num = 0;
    sumr = 0.;
    sumtime = 0.;
    sumrsq = 0.;
    sumtimer = 0.;

    for (i=1; i<PHONES; i++) {
        if(phoneflag[i] != 0) {
            if (sqrt(pow((timedelay[i]-bestyintr-(bestslope*bestrange[i])),
                2.0)) < 2.5*bestsigma) {
                num++;
                sumtime += timedelay[i];
                sumr += bestrange[i];
                sumrsq += bestrange[i]*bestrange[i];
                sumtimer += bestrange[i]*timedelay[i];
            }
            else {
                fprintf(stderr,"outlying phone # %d\n",i);
            }
        }
    }
    N = num;
    bestslope = ((N*sumtimer)-(sumr*sumtime))/
        ((N*sumrsq)-(sumr*sumr));
    bestyintr = (sumtime-(bestslope*sumr))/N;
    gpspeed = 1.0/bestslope;
    fprintf(stderr,"bestx = %f, besty = %f, sigma = %f\n",
        bestx, besty, bestsigma);
    fprintf(stderr,"group velocity = %f\n", gpspeed);
    fprintf(stderr,"y intercept = %f\n", bestyintr);
}

fprintf(stderr,
    "Do you wish to relocate with different phones? (1=yes)\n");
scanf("%d",&rerun);

}
```

Source code for the *farlocate* program

```
/* finding source amplitude */
for(i=1; i<PHONES; i++) {
    if (phoneflag[i] != 0) {
        source[i] = (amp[i]/SENSITIVITY) * bestrange[i];
        sumsource += source[i];
    }
}
bestamp = sumsource/N;

fprintf(optr, "%d %d %f %f %f %f\n", event, date, time,
        bestx, besty, bestamp);
fprintf(optr, "%f %f %f\n", bestsigma, gpspeed, bestyintr);

fprintf(stderr, "Do you wish to exit? (-1 = exit)\n");
scanf("%d", &bye);
}

fclose(ptr);
fclose(optr);
fclose(locptr);

exit(0);
}
```

Source code for the *farlocate* program

APPENDIX C

Table C-1: Event Location Summary

Table C-2: Tape Summary

Table C-3: Event Interarrival Time Summary

Table C-4: Event Strength Summary

Table I- Event Location Summary

Name (Tape #, event #)	x (m)	y (m)	r (m)	R (m)	phi (degrees)	sigma (sec)	sigma (m)	c (m/sec)	Hydrophones Removed
------------------------------	----------	----------	----------	----------	------------------	----------------	--------------	--------------	------------------------

Name is the FRAM IV tape number followed by the time into the tape the event occurred.
 x and y are Cartesian coordinates, with the east leg of the array being the positive x axis.
 r is the horizontal range, and R is the slant range.
 phi is the bearing in degrees from the northern leg of the array.
 sigma (sec) is the standard deviation of the time delays within an event.
 sigma (m) is sigma (sec) times the sound speed c.
 c is the sound speed, the slope of the regression for slope.

* indicates that an event is considered non-locatable.

4001,63	16741	-18783	25310	25311	139	0.0039	5.62	1425	5,17,22
4001,126	4418	-5702	6901	6902	140	0.0034	5.02	1471	8,19,22
4001,175	-1041	-9921	9975	9976	185	0.0014	2.07	1485	2,3
4001,177	-1380	-10148	10241	10242	188	0.0058	8.23	1471	3
4001,195	589	-2191	2271	2272	165	0.0034	5.01	1450	5,11,17,22
4001,558	565	-2101	2109	2111	162	0.0016	2.29	1444	22
4001,818	5417	-9681	11615	11615	146	0.0019	2.60	1452	5,11,17,22
4001,895	-3352	-10100	10642	10642	198	0.0025	3.67	1472	none
4001,1066	3200	-19380	20176	20176	171	0.0012	1.77	1472	17
4001,1131	-9352	9574	13391	13391	316	0.0017	3.91	1465	11,22
4001,1156	773	-2101	2105	2107	165	0.0077	11.27	1457	5
4001,1194	-10159	10760	12204	12205	722	0.0047	6.75	1473	22
4001,1215	2129	-10591	10811	10811	174	0.0074	10.64	1475	none
4003,21	54	-748	758	770	166	0.0174	25.71	1471	7
4003,52	-2821	-9297	9716	9716	197	0.0079	11.58	1451	none
4003,280*	-216	-80	270	248	250	0.0059	8.14	1708	13
4003,264	-1101	-544	1275	1279	240	0.0097	14.08	1477	22
4003,285	265	214	341	353	51	0.0168	25.15	1403	7
4003,301	407	145	432	442	70	0.0050	7.11	1435	13,18
4003,419	791	4890	4954	4954	9	0.0026	3.76	1445	none
4003,515	1421	-7001	7320	7322	155	0.0053	7.64	1474	none
4003,534	-5210	4515	7681	7681	306	0.0037	5.35	1451	none
4003,575	2150	-7001	7715	7715	144	0.0054	7.81	1421	7,12
4003,768	2657	2070	3650	3652	52	0.0045	6.54	1477	12,17
4003,895	19955	1070	20075	20075	35	0.0127	18.45	1447	13,22,24
4003,1057	-105	145	177	187	775	0.0075	10.81	1447	17

Table C-1 Event Location Summary

Name (Tape #, event #)	X (m)	Y (m)	Z (m)	R (m)	phi (degrees)	sigma (sec)	sigma (m)	c (m/sec)	Hydrophones Removed
4005.219	-312	3890	3902	3904	355	0.0107	15.48	1441	none
4005.241	-103	-178	206	226	210	0.0059	8.39	1430	none
4005.395	-342	890	953	958	339	0.0239	34.96	1464	7
4005.808	-88	296	309	323	340	0.0111	16.09	1450	none
4005.916	-785	616	398	1002	308	0.0087	12.21	1404	none
4005.997	-15099	-3810	18005	18006	237	0.0171	24.51	1477	none
4005.1012	-1061	-812	2158	2161	246	0.0127	46.87	1474	none
4005.1097	-4791	-19807	20060	20063	194	0.0017	2.50	1447	none
4005.1169	1890	-586	1979	1981	107	0.0089	12.40	1399	none
4005.1175	-49	-140	146	175	139	0.0025	3.57	1409	7
4005.1183	-47	-101	111	145	205	0.0010	1.42	1478	4, 9, 10, 11
4007.204	323	167	364	375	63	0.0144	21.21	1469	none
4007.444	791	-108	798	804	98	0.0059	8.47	1449	none
4007.582	-205	-74	218	237	250	0.0150	20.98	1398	none
4007.794	-197	-73	210	230	250	0.0156	21.87	1400	none
4007.820	327	466	584	591	34	0.0125	17.06	1417	8
4007.935	-77	-67	75	106	246	0.0110	17.84	1466	5, 6, 7, 12, 13, 14

Table C-1 Event Location Summary

Name (Tape #, event #)	X (m)	Y (m)	r (m)	R (m)	phi (degrees)	sigma (sec)	sigma (m)	sigma (m/sec)	Hydrophones Removed
4009,100	7690	715	3955	3955	50	0.0041	5.38	1450	7.11,12.00,12.14
4009,172	-193	313	370	382	328	0.0026	3.74	1447	13
4009,173	890	427	997	992	64	0.0051	7.40	1464	15
4009,193	-2629	920	2735	2787	289	0.0046	6.66	1448	none
4009,194	-587	-1001	1160	1164	210	0.0082	11.59	1422	6.7,12.17,24
4009,205	8250	-7021	12257	12257	177	0.0062	8.86	1472	none
4009,211	-531	-2107	16031	16031	162	0.0035	4.82	1427	none
4009,290	252	150	297	308	59	0.0070	4.57	1421	17
4009,330	6553	3889	11046	11047	76	0.0077	10.21	1455	none
4009,384	-407	890	779	983	335	0.0118	17.49	1481	none
4009,335	-1575	-3001	3339	3390	208	0.0051	7.46	1479	13
4009,397	3171	121	3174	3175	88	0.0135	19.49	1441	none
4009,410	-175	460	492	501	339	0.0071	10.10	1414	none
4009,447	6989	-3654	7887	7887	116	0.0022	3.16	1431	17
4009,476	-736	488	883	888	304	0.0049	6.82	1368	1.5,7.12
4009,493	773	-2201	2333	2335	161	0.0032	4.79	1476	6.7,10.18
4009,579	-2551	2612	3651	3652	316	0.0030	4.04	1457	none
4009,603	-17	-75	77	106	200	0.0027	4.09	1420	none
4009,608	23	-1771	1971	1973	179	0.0040	5.17	1427	none
4009,620	-1567	2990	3376	3377	332	0.0047	6.57	1435	12
4009,621	589	-71	593	699	95	0.0057	8.21	1417	5
4009,626	460	574	727	747	79	0.0066	10.15	1379	13.21
4009,657	1065	-1000	2717	2769	148	0.0075	10.84	1471	12.13
4009,677	-11	-177	178	199	219	0.0061	11.69	1474	none
4009,725	-746	167	2012	2014	103	0.0050	11.03	1451	9.11
4009,726	-170	744	735	736	332	0.0073	9.77	1410	none
4009,802	2142	1351	2597	2598	77	0.0217	20.46	1473	none
4009,817	709	7502	7924	7924	5	0.0076	10.51	1414	none
4009,828	390	-776	966	971	117	0.0101	14.72	1424	none
4009,876	-160	117	198	219	306	0.0160	22.98	1499	15.16,15.19,15.21
4009,916	-25	223	229	248	154	0.0122	13.72	1502	5.16
4009,948	-1679	-3001	3419	3421	209	0.0070	10.29	1477	17
4009,949	3999	-120	4004	4004	92	0.0036	5.02	1459	5
4009,967	-914	-7510	7565	7566	187	0.0072	4.62	1452	none
4009,982	105	488	499	508	12	0.0143	19.45	1364	18.20,21
4009,1041	1897	646	1997	2000	71	0.0167	15.11	1419	none
4009,1120	551	162	577	581	74	0.0065	9.07	1416	12

Table D-1. Event Location Summary

Case Case #, event #	Lat	Long	Lat	Long	Lat degrees	Long sec	Signa S	Signa N	Notes Hydrophones Removed
4011.137*	2870	-5899	2870	2875	1.4	1.0017	27.41	100	none
4011.168	-922	-5901	5071	5072	169	0.1052	7.81	140	none
4011.169	-5201	5349	3187	3134	711	0.0060	3.75	1448	none
4011.215	-96	-591	407	417	194	0.0040	5.25	1492	24
4011.241	2890	-592	2897	2898	145	0.0018	15.68	1471	none
4011.250	-420	39	484	489	775	1.0078	5.60	1491	7
4011.257	-50	788	788	788	75	1.0078	5.67	1455	none
4011.273	-534	-5001	1159	1161	21	1.0077	24.07	1471	100
4011.282	2190	-5011	3721	3724	144	1.0072	4.62	1451	7
4011.307	3250	5890	5772	5773	29	1.0060	8.84	1468	5.5.7
4011.344	1990	765	2172	2174	69	0.1059	10.29	1431	15.13
4011.362	5372	-10007	11454	11455	151	0.0097	14.17	1457	13
4011.385	-829	-4001	4056	4067	191	0.1077	11.02	1463	none
4011.510	19870	13790	24136	24187	55	0.1069	23.52	1797	5.5.7, 19.7.1.21
4011.532	-581	244	612	619	294	0.0068	9.93	1475	none
4011.541	-258	607	660	666	337	0.0084	11.50	1423	15.13
4011.573*	14471	-11409	21373	21372	179	0.1055	3.81	1573	5.1.5, 16.1.9, 20.1.22, 22.1.24
4011.585	355	-82	757	775	137	1.0012	4.77	1478	22
4011.515	3212	-4473	7530	7537	125	0.1020	21.32	1475	10.13
4011.516	-670	2890	2559	2559	748	0.1232	27.55	1447	none
4011.565	2991	1566	3375	3377	62	0.0057	7.81	1473	13
4011.564	165	155	768	780	46	0.0035	4.37	1757	22
4011.597	30	579	579	5791	1	1.0007	7.66	1452	21
4011.615*	1424	7161	7160	7167	77	1.0048	5.41	1475	1
4011.721	-216	-1249	710	726	221	0.1032	26.27	1444	none
4011.811	-796	399	374	379	775	0.1079	11.75	1452	7
4011.881	17666	-5391	2196	2091	179	0.1070	17.11	1421	9.1.21, 7.11
4011.883	734	-701	1015	1019	174	0.1112	15.67	1440	none
4011.885	990	345	1048	1057	71	0.0057	7.41	1491	13.21.22
4011.985	5741	-8212	10375	10376	142	0.0079	5.81	1423	none
4011.992	-1301	1390	2294	2296	325	0.0273	17.52	1408	7.12.24
4011.1040	-555	1890	2000	2001	341	0.1049	7.25	1467	7.12.17, 22.12-
4011.1061	-52	107	119	151	334	0.1020	2.70	1737	2.4.5.5.20
4011.1128	-636	452	750	786	305	0.1047	5.72	1441	none
4011.1137	-2101	-133	3004	3035	257	0.1097	17.79	1416	22.14

Table C-1 Event Location Summary

Name (Tape #, event #)	x (m)	y (m)	r (m)	R (m)	phi (degrees)	sigma (sec)	sigma (m)	c (m/sec)	Hydrophones Removed
4013,120	-833	-4970	5039	5040	190	0.0091	13.11	1447	none
4013,177	370	-1896	1932	1934	169	0.0035	5.00	1437	2,8,9,10
4013,277	-393	366	537	545	313	0.0045	6.38	1418	8,9,14,16,22,23,24
4013,317	1326	-12	1326	1329	91	0.0028	3.99	1445	none
4013,351	-54	-99	113	146	209	0.0070	9.72	1396	none
4013,354	1534	761	1712	1715	64	0.0016	2.31	1447	21
4013,373	216	683	716	722	18	0.0028	4.11	1450	none
4013,381	1248	-2815	3079	3081	156	0.0051	7.41	1442	none
4013,403	2602	-5450	6039	6040	154	0.0067	9.56	1420	none
4013,464	842	2261	2413	2414	20	0.0083	12.03	1454	none
4013,478	-52	662	664	671	356	0.0076	10.56	1388	none
4013,518	175	492	522	530	20	0.0082	12.05	1472	14,16,17
4013,661	6890	3658	7801	7801	62	0.0030	4.34	1463	none
4013,664	-1001	1205	1567	1569	320	0.0114	16.72	1473	19,20,22
4013,671	19866	-8441	21585	21585	113	0.0104	14.72	1416	none
4013,694	-675	9290	9314	9315	356	0.0039	5.62	1437	none
4013,723	3100	-1533	3458	3460	116	0.0059	8.51	1447	none
4013,755*	264	168	313	326	58	0.0151	23.00	1520	24
4013,776	7989	-5590	9750	9751	125	0.0052	7.48	1446	none
4013,797	-389	7013	7024	7024	357	0.0052	7.56	1461	none
4013,801	-400	-133	422	432	252	0.0078	11.58	1479	none
4013,866	38	307	309	323	7	0.0062	8.92	1448	none
4013,875	49	320	324	337	9	0.0031	4.27	1397	none
4013,908	9854	17869	20406	20406	29	0.0066	9.26	1414	7,12
4013,922*	13	26	29	97	27	0.0090	13.61	1514	8,9,10,11,12,18
4013,950	1165	-2253	2536	2538	153	0.0037	5.30	1442	none
4013,979	7890	920	7943	7944	83	0.0084	11.99	1432	none
4013,1014	-143	2890	2894	2895	357	0.0091	12.80	1413	none
4013,1018	-137	574	590	597	347	0.0169	24.97	1476	none
4013,1107	-701	453	835	840	303	0.0081	11.51	1427	none
4013,1124	-9001	8142	12137	12137	312	0.0064	9.43	1478	none
4013,1166	870	-7001	7055	7055	173	0.0050	7.39	1468	18
4013,1187	-696	693	982	987	315	0.0063	9.34	1472	17,18
4013,1203	7789	-2315	8126	8126	107	0.0035	5.11	1480	none
4015,232	-101	422	434	444	347	0.0026	3.62	1406	21,22

4015 no events

Table C-1 Event Location Summary

Name (Tape #, event #)	x (m)	y (m)	r (m)	R (m)	phi (degrees)	sigma (sec)	sigma (m)	c (m/sec)	Hydrophones Removed
4019,178	-8416	-18097	19958	19958	205	0.0038	5.52	1473	none
4019,679*	-17789	10549	20682	20682	301	0.0023	3.50	1533	none
4019,689	-20109	11680	23255	23255	300	0.0026	3.70	1428	none
4019,776	-21087	12642	24586	24586	301	0.0037	5.13	1394	none
4019,841*	-3001	-88	3002	3004	268	0.0061	9.10	1503	none
4021,81	-7356	15998	17608	17608	325	0.0103	14.68	1430	none
4021,154	-6508	18999	20083	20083	341	0.0062	8.84	1436	13
4023	no events								
4024	no events								
4027,28	-1001	-371	1068	1072	250	0.0145	20.81	1434	24
4029,666	-4250	-10010	10875	10875	203	0.0075	11.20	1489	3,6,11,13,29
4029,897	347	-110	364	376	108	0.0244	33.82	1385	none
4029,1059	-3318	-9110	9695	9696	200	0.0040	5.71	1439	29
4031,823	159	-373	405	416	157	0.0076	11.32	1493	none
4033,490	-2532	4190	4896	4897	329	0.0047	6.61	1408	13,18,29,30
4033,1041	-21010	767	21024	21024	272	0.0119	17.80	1493	9,11,13,19,23,24,27,28,29,30
4033,1048	-10309	1017	10359	10359	276	0.0054	7.91	1451	16,22,23,24
4033,1053	-285	120	309	323	293	0.0042	6.10	1451	13
4033,1126	-21090	1075	21117	21118	273	0.0020	2.91	1465	13
4033,1173	-20905	805	20920	20921	272	0.0085	12.89	1515	13,29
4040,26	-20488	19987	28622	28622	314	0.0125	17.63	1410	6
4040,148	-6001	4252	7355	7355	305	0.0030	4.32	1426	10
4040,385	1462	-4010	4268	4269	160	0.0054	8.03	1486	none
4040,398	-9001	8110	12116	12116	312	0.0150	21.35	1427	13
4040,714	-5432	-14089	15100	15100	201	0.0056	8.38	1497	none
4040,730	6468	-17109	18291	18291	159	0.0126	17.76	1411	6
4040,871	-3424	-8910	9545	9546	201	0.0022	3.20	1446	none
4040,1114	-20973	16769	26853	26853	309	0.0061	9.03	1469	11
4040,1157	-7408	7891	10823	10824	317	0.0075	11.26	1493	none
4047,984	-457	200	499	507	294	0.0230	31.93	1387	none
4049,1064	-2320	-3110	3435	3436	196	0.0068	9.75	1415	none
4049,1066	-1889	-8001	8221	8221	193	0.0150	21.91	1401	9,11,13

Table C-1 Event Location Summary

Name (Tape #, event #)	x (m)	y (m)	r (m)	R (m)	phi (degrees)	sigma (sec)	sigma (m)	c (m/sec)	Hydrophones Removed
4051	no events								
4053,3	-16878	18965	25388	25388	318	0.0021	3.11	1461	7
4055	no events								
4057	no events								
4059	no events								
4061,571	-8393	-20923	22544	22544	202	0.0127	18.29	1445	21,22,23
4061,879	-3355	-2455	4157	4158	234	0.0027	3.91	1445	5,6,23
4063,296	-10503	17985	20827	20827	330	0.0090	12.91	1441	none
4063,824	-16793	14787	22375	22376	311	0.0043	6.29	1455	none
4063,864	-2001	1346	2412	2413	304	0.0043	6.18	1424	18
4063,933	-9077	7976	12083	12084	311	0.0111	15.60	1408	none
4063,936	-1130	912	1452	1455	309	0.0037	5.42	1450	18
4065	no events								
4067	no events								
2001,543	-3455	-5112	6170	6171	214	0.0026	3.77	1452	2
2009,189	-1997	-20987	21082	21082	185	0.0036	5.40	1487	none
2009,453	874	-5201	5274	5275	170	0.0070	9.80	1402	18
2009,455	1441	-2001	2466	2468	144	0.0045	6.55	1445	12
2009,925	-105	-673	681	687	189	0.0193	27.43	1422	none
2023,74	15430	-16460	22561	22562	137	0.0104	15.13	1458	7,11
3001,11	-3921	75	3922	3923	271	0.0125	17.92	1434	none
3001,16	-20103	-9471	22222	22222	245	0.0137	19.92	1450	none
3001,301	-3001	698	3081	3083	283	0.0149	21.13	1418	4,5,6,7,20,21,22,23
3047,169	-19109	-2181	19233	19233	263	0.0073	10.56	1453	23
3047,751	990	-538	1040	1044	121	0.0134	19.52	1460	none
N =						199	199	199	
mean =						0.0077	11.13	1444	
std dev =						0.0055	7.82	34	

Table D-2 Page Summary

Page #	Minutes Examined	Julian Date	Detections	Artifacts	Events	Multiple Responses	False Alarms	Final (20-30 Hz Pa
4001	20	86	35	0	13	5	7	Not Avail
2901	20	86	6	0	1	0	5	Not Avail
2009	20	89	15	0	4	1	10	0.022
3001	10	90	5	0	3	0	2	0.013
4005	20	91	15	0	13	1	1	0.044
4005	20	91	24	5	11	2	6	0.075
4007	17	91	11	0	6	1	4	0.021
4008	20	91	35	7	27	5	7	0.031
4011	20	91	47	7	35	1	4	0.031
4017	20	93	48	1	34	5	3	0.034
2023	20	98	1	0	1	0	0	0.037
4015	20	99	14	8	1	1	5	0.047
4047	17.5	100	2	0	2	0	0	0.017
4016	20	105	3	0	0	0	0	0.017
4019	20	105	14	3	5	1	5	0.016
4021	20	109	6	0	2	2	2	0.017
4023	20	109	22	20	0	0	2	0.011
4024	20	109	14	11	0	0	0	0.011
4027	20	110	26	25	1	1	1	0.012
4029	20	110	11	8	7	0	0	0.012
4031	20	110	11	10	1	0	0	0.012
4033	20	110	19	12	5	0	1	0.012
4040	20	111	27	10	5	1	7	0.014
4047	20	111	6	0	1	1	5	0.014
4049	20	111	5	0	2	0	0	0.014
4051	20	111	1	0	1	1	5	0.014
4053	20	112	21	0	1	2	15	0.014
4055	17.5	112	0	0	0	0	0	0.014
4057	20	112	9	1	0	0	5	0.015
4059	20	112	1	0	0	0	1	0.015
4061	20	112	6	0	2	0	4	0.014
4063	20	112	9	0	5	0	1	0.013
4065	20	112	7	2	0	0	1	0.017
4067	20	112	6	5	0	0	0	0.013
Total	662		499	119	199	26	125	

Detection is declared when at least 50% of the hydrophones have a signal.

Artifacts are machine noises, shifts, and other alarms.

Events are detections and/or alarms to analyze.

Multiple Responses are multiple detections of an already counted event.

False alarms are detections too weak to analyze.

Table D-2 Event Interarrival Time Summary

Name (Tape #, event #)	Event Time (sec)	Interarrival Time (sec) (20s bin)		Horizontal Range (m)
4001.63	63	63	3	25310
4001.126	126	63	3	6901
4001.175	175	49	2	9975
4001.177	177	2	0	10241
4001.195	195	18	0	2271
4001.658	658	463	23	2109
4001.918	918	160	8	11615
4001.935	935	77	3	10641
4001.1066	1066	171	8	20136
4001.1131	1131	65	3	13391
4001.1156	1156	25	1	3196
4001.1194	1194	38	1	23204
4001.1215	1215	21	1	19011
4003.21	21	21	1	358
4003.52	52	31	1	9716
4003.283	283	231	11	230
4003.334	334	1	0	1076
4003.335	335	1	0	741
4003.301	301	16	0	432
4003.419	419	118	5	4954
4003.516	516	97	4	3310
4003.534	534	18	5	7681
4003.535	535	1	0	7715
4003.703	703	77	3	7611
4003.995	995	287	14	21075
4003.1057	1057	58	2	272
4005.219	219	219	10	3902
4005.241	241	22	1	206
4005.395	395	154	7	953
4005.908	908	413	20	789
4005.916	916	108	5	998
4005.997	997	81	4	15006
4005.1012	1012	15	0	2159
4005.1097	1097	85	4	20090
4005.1169	1169	72	3	1079
4005.1177	1177	4	0	143
4005.1187	1187	17	0	711
4007.444	444	247	12	755
4007.592	592	148	6	218
4007.77	77	212	10	31
4007.77	77	7	0	571
4007.77	77	212	10	31

Table C-3 Event Interarrival Time Summary

Name (Tape #, event #)	Event Time (sec)	Interarrival Time (sec) (20s bin)		Horizontal Range (m)
4009,100	100	100	5	3955
4009,172	172	72	3	370
4009,178	178	6	0	987
4009,193	193	15	0	2795
4009,194	194	1	0	1150
4009,278	278	84	4	12253
4009,292	292	14	0	1531
4009,300	300	8	0	180
4009,360	360	60	4	11046
4009,384	384	4	0	979
4009,385	385	1	0	3289
4009,397	397	12	0	3174
4009,410	410	13	0	492
4009,447	447	37	1	7987
4009,476	476	29	1	883
4009,493	493	17	0	2333
4009,579	579	86	4	3651
4009,600	600	21	1	37
4009,608	608	8	0	1871
4009,620	620	12	0	1076
4009,621	621	1	0	693
4009,626	626	5	0	707
4009,667	667	41	2	2367
4009,677	677	10	0	175
4009,706	706	29	2	5070
4009,735	735	28	2	335
4009,802	802	16	0	3597
4009,817	817	15	0	7574
4009,826	826	11	0	966
4009,878	878	50	2	198
4009,916	916	38	1	229
4009,948	948	32	1	7419
4009,949	949	1	0	9064
4009,967	967	18	0	7565
4009,982	982	15	0	169
4009,1041	1041	59	2	1397
4009,1150	1150	119	5	507

Table D-3 Event Interarrival Time Summary

Name (Tape #, event #)	Event Time (sec)	Interarrival Time (sec) (20s bin)		Horizontal Range (m)
4011.133	133	87	4	2973
4011.168	168	35	4	3071
4011.169	169	1	0	3183
4011.215	215	46	2	403
4011.241	241	26	1	2997
4011.250	250	9	0	934
4011.259	259	9	0	79.6
4011.273	273	14	1	1157
4011.287	287	5	0	7727
4011.307	307	24	1	6732
4011.344	344	37	1	2132
4011.362	362	18	0	11454
4011.385	385	23	1	4086
4011.510	510	125	6	24186
4011.532	532	22	1	612
4011.541	541	9	0	660
4011.573	573	32	1	21878
4011.595	595	22	1	767
4011.615	615	20	1	7607
4011.618	618	1	0	2653
4011.653	653	47	2	3375
4011.664	664	1	0	368
4011.697	697	25	1	6793
4011.709	709	12	0	7612
4011.721	721	12	0	777
4011.811	811	90	4	671
4011.861	861	50	2	27613
4011.867	867	6	0	1115
4011.885	885	22	1	1046
4011.985	985	100	5	17375
4011.992	992	7	0	2294
4011.1046	1046	54	2	3000
4011.1061	1061	15	0	119
4011.1128	1128	67	3	780
4011.1167	1167	59	2	3004

Table C-3 Event Interarrival Time Summary

Name (Tape #, event #)	Event Time (sec)	Interarrival Time (sec) (20s bin)		Horizontal Range (#)
4013.120	120	120	6	5039
4013.177	177	57	2	1972
4013.277	277	100	5	537
4013.317	317	40	2	1325
4013.351	351	34	1	112
4013.354	354	3	0	1712
4013.377	377	19	0	716
4013.378	378	1	0	2179
4013.407	407	20	1	5779
4013.454	454	51	3	2410
4013.478	478	14	0	664
4013.518	518	40	2	522
4013.661	661	143	7	7801
4013.664	664	3	0	1567
4013.671	671	7	0	21585
4013.694	694	23	1	9314
4013.723	723	29	1	3458
4013.755	755	32	1	217
4013.776	776	21	1	3751
4013.797	797	21	1	5924
4013.801	801	4	0	422
4013.866	866	65	3	219
4013.875	875	9	0	224
4013.908	908	33	1	20415
4013.922	922	14	0	27
4013.951	951	29	1	2876
4013.979	979	28	1	7540
4013.1014	1014	35	1	2394
4013.1018	1018	4	0	599
4013.1107	1107	89	4	835
4013.1124	1124	17	0	12137
4013.1166	1166	42	2	7055
4013.1187	1187	21	1	982
4013.1200	1200	13	0	5126
4015.272	272	272	11	474
4015	none			

Table D-3 Event Interarrival Time Summary

name (Tape #, event #)	Event Time (sec)	Interarrival Time (sec) (20s bin)		Horizontal Range (m)
4019,176	176	176	8	14956
4019,379	379	501	25	20382
4019,689	689	10	0	23255
4019,776	776	87	4	24536
4019,841	841	65	3	3002
4021,81	81	81	4	17308
4021,154	154	73	3	22357
4023	none			
4024	none			
4027,28	28	28	1	1068
4029,666	666	666	33	10875
4029,897	897	231	11	364
4029,1059	1059	162	8	9695
4031,327	327	327	16	485
4032,490	490	490	24	4351
4032,1041	1041	551	27	21124
4032,1043	1043	2	0	10059
4032,1057	1057	15	1	213
4032,106	106	77	4	21117
4032,1077	1077	47	2	2132
4040,121	121	121	6	23111
4040,146	146	122	6	7755
4040,185	185	237	11	4268
4040,298	298	17	0	12116
4040,314	314	316	16	15170
4040,377	377	16	0	16291
4040,371	371	141	7	9545
4040,1114	1114	243	12	26653
4040,1157	1157	43	2	10927
4047,884	884	884	44	175
4047,104	104	104	5	1175
4047,106	106	2	0	1021

Table D-3 Event Interarrival Time Summary

Name (Tape #, event #)	Event Time (sec)	Interarrival Time (sec) (20s bin)		Horizontal Range (m)
4051	none			
4053.3	3	3	0	25388
4055	none			
4057	none			
4059	none			
4061.571	571	571	28	22544
4061.879	879	308	15	4157
4063.296	296	296	14	20827
4063.824	824	528	26	22375
4063.864	864	40	2	2412
4063.933	933	69	3	12083
4063.936	936	3	0	1452
4065	none			
4067	none			
2001.543	543	543	27	5170
2009.189	189	189	9	21081
2009.457	457	268	13	5274
2009.458	458	0	0	1456
2009.925	925	467	23	551
2023.74	74	74	3	22521
3001.11	11	11	0	3922
3001.15	15	5	0	22222
3001.301	301	285	14	7081
3047.169	169	169	8	19233
3047.751	751	582	29	1040
N =		177		
mean =				
std dev =		1.5		

Table D-4. Event Strength Summary.

Name (Tape #, event #)	r (m)	Po (Pa)	sigma (Pa)	Po (N)	sigma (N)	f (Hz)
Name is the FRAM IV tape number followed by the time into the tape the event occurred. r is the horizontal range. Po is the average peak hydrophone pressure for an event. sigma (Pa) is the standard deviation of the peak hydrophone pressure within an event. Po is the average peak dipole strength calculated for an event. sigma (N) is the standard deviation of the dipole strength within an event. f is the frequency, explicitly, the axis crossing rate.						
4001.106	6741	0.467	0.092	707640	174109	57
4001.175	9975	0.600	0.109	965109	175081	46
4001.177	10241	0.545	0.194	1002792	357487	42
4001.195	2271	0.556	0.117	896709	135110	42
4001.553	2109	0.665	0.097	1340877	208247	71
4001.818	11615	1.117	0.213	1418009	270070	61
4001.895	19642	0.524	0.085	1094608	177198	37
4001.1131	13391	0.482	0.085	779610	136750	48
4001.1156	3196	0.495	0.069	1222073	165840	70
4001.1215	19011	0.527	0.101	1229059	192517	40
4003.21	353	0.283	0.108	59366	17452	71
4003.52	5716	0.324	0.063	430170	57712	58
4003.284	1276	0.291	0.131	187664	30537	64
4003.285	341	0.362	0.136	61970	14917	57
4003.291	472	0.274	0.057	62354	15395	74
4003.419	4954	0.476	0.150	620760	641514	57
4003.516	3320	0.246	0.045	342405	67394	57
4003.574	7621	0.163	0.048	235652	69027	57
4003.575	3715	0.240	0.144	369396	36291	49
4003.768	3650	0.225	0.063	264698	70731	64
4005.219	3902	0.305	0.271	758094	314257	64
4005.295	953	0.312	0.170	158324	70515	64
4005.308	309	0.465	0.193	79018	27448	74
4005.516	998	0.278	0.084	119218	27205	71
4005.997	18066	0.248	0.059	910298	215670	21
4005.1012	2159	0.230	0.060	564168	147577	27
4005.1159	1979	0.521	0.253	555370	230711	58
4005.204	364	0.27	0.175	64713	111	64
4005.204	73	0.72	0.11	1530	3531	71
4005.2	614	0.77	0.11	17007	3111	71

Table C-4 Event Strength Summary

Name (Tape #, event #)	r (m)	Po (Pa)	sigma (Pa)	Po (N)	sigma (N)	f (Hz)
4009,100	3955	0.217	0.043	237677	47362	69
4009,172	370	0.449	0.240	84708	34086	71
4009,175	987	0.256	0.198	150340	52260	58
4009,193	2785	0.234	0.055	261773	57028	64
4009,194	1160	0.321	0.060	191163	28220	65
4009,273	12253	0.267	0.045	339648	56951	61
4009,292	16351	0.242	0.036	315602	46536	60
4009,330	10146	0.260	0.027	336321	49707	60
4009,384	979	0.311	0.106	159935	50432	63
4009,385	3389	0.256	0.049	322982	62179	59
4009,397	3174	0.223	0.088	250181	98245	66
4009,410	492	0.479	0.179	131094	38345	65
4009,447	7867	0.293	0.048	461103	75739	49
4009,476	883	0.400	0.290	139730	61426	73
4009,493	2333	0.173	0.028	199141	31577	59
4009,579	3651	0.343	0.075	373537	81458	69
4009,608	1971	0.218	0.074	230200	84135	59
4009,620	3376	0.237	0.047	315200	61674	56
4009,621	693	0.226	0.065	98247	18204	58
4009,667	2367	0.328	0.135	414294	234724	64
4009,728	2932	0.375	0.132	386341	138491	56
4009,786	385	0.981	0.466	224139	92413	64
4009,802	3597	0.746	0.618	1050885	852095	63
4009,817	7934	0.313	0.089	459710	129412	67
4009,826	866	0.176	0.035	115661	22172	58
4009,848	3419	0.277	0.039	323295	46413	64
4009,849	9004	0.244	0.043	294474	57917	64
4009,867	7565	0.037	0.030	403141	72666	64
4009,1041	1997	0.224	0.089	221127	70462	64
4009,1160	573	0.425	0.132	137233	31215	63

Table D-4 Event Strength Summary

Name (Tape #, event #)	r (m)	F ₀ (Pa)	sigma (Pa)	F ₀ (N)	sigma (N)	f (Hz)
4011.168	6071	0.198	0.040	234021	46798	55
4011.169	8183	0.222	0.052	276205	54448	52
4011.215	403	0.276	0.079	63100	10454	67
4011.241	2997	0.302	0.128	323546	133350	58
4011.250	984	0.353	0.162	197201	65473	59
4011.259	7908	0.395	0.055	491277	68119	52
4011.278	1159	0.273	0.108	163348	33900	56
4011.285	2721	0.235	0.042	129580	42705	74
4011.297	7880	0.244	0.100	307771	125155	51
4011.344	2132	0.189	0.041	218914	47240	55
4011.352	11454	0.170	0.033	202390	38875	65
4011.385	4088	0.162	0.035	207998	45867	59
4011.500	612	0.316	0.120	95187	24435	66
4011.541	560	0.183	0.033	58921	14260	70
4011.595	367	0.708	0.208	157508	32876	64
4011.615	7633	0.253	0.056	291097	64418	67
4011.616	2958	0.314	0.416	486903	607412	46
4011.663	3375	0.217	0.027	227709	38947	71
4011.664	768	0.277	0.080	51797	14121	57
4011.693	6790	0.266	0.051	355550	70710	56
4011.721	323	0.245	0.067	52222	17894	72
4011.811	974	0.244	0.056	120519	22465	65
4011.863	1015	0.166	0.028	187514	46788	71
4011.885	1048	0.362	0.067	249067	46465	64
4011.886	10375	0.228	0.040	315616	56061	50
4011.892	2294	0.292	0.115	320177	117475	51
4011.9046	2000	0.215	0.055	202667	50113	55
4011.9123	780	0.333	0.082	113280	21571	7
4011.9167	3004	0.267	0.090	299767	58504	65

Table D-4 Event Strength Summary

Name (Tape #, event #)	r (a)	Po (Pa)	sigma (Pa)	Po (N)	sigma (N)	f (Hz)
4013.120	5079	0.232	0.046	249982	49665	71
4013.177	1952	0.224	0.047	246066	59124	58
4013.277	537	0.291	0.065	74729	14232	64
4013.317	1326	0.203	0.037	162763	32443	58
4013.354	1712	0.229	0.045	201933	38367	64
4013.373	716	0.354	0.145	136538	31449	61
4013.381	3079	0.313	0.065	325157	66566	71
4013.417	3177	0.206	0.065	285557	51137	64
4013.464	2410	0.240	0.058	206733	71651	50
4013.478	664	0.247	0.072	70133	14240	75
4013.518	522	0.362	0.115	107996	28307	58
4013.661	7801	0.240	0.078	260305	64007	71
4013.684	1567	0.246	0.075	193674	52565	64
4013.694	9314	0.241	0.058	262115	62356	71
4013.723	3458	0.230	0.053	266779	62309	64
4013.776	9750	0.209	0.040	403424	77526	40
4013.797	7024	0.208	0.050	250307	59563	64
4013.801	422	0.251	0.077	77381	15347	48
4013.866	709	0.157	0.556	213971	82635	67
4013.875	324	0.519	0.247	122952	56241	50
4013.950	2536	0.251	0.045	350436	63028	51
4013.979	7943	0.214	0.042	360405	70664	46
4013.1014	2894	0.186	0.043	284500	63668	46
4013.1015	570	0.295	0.076	87526	16507	71
4013.1017	675	0.485	0.134	266443	51647	64
4013.1024	12137	0.290	0.071	316572	77457	71
4013.1056	7055	0.222	0.063	326351	60645	50
4013.1087	952	0.355	0.160	137420	31011	6
4013.1097	8126	0.194	0.043	234018	52339	64
4015.202	434	0.663	0.223	161500	48620	58
4019.178	14958	0.312	0.054	382727	66870	64
4021.81	17603	0.238	0.049	349159	71641	50
4027.23	1068	0.180	0.195	145002	51964	64
4028.066	11675	0.202	0.027	149799	3571	50
4028.077	1142	0.202	0.052	7772	17773	50
4028.10	1113	0.202	0.054	217103	66411	50
4031.907	405	0.246	0.102	66157	26474	64

Table D-4 Event Strength Summary

Name (Type #, event #)	r (m)	Po (Pa)	sigma (Pa)	Po (N)	sigma (N)	F (Hz)
4033,490	4896	0.232	0.048	366811	80416	45
4033,1046	10359	0.190	0.027	674415	34803	22
4033,1053	309	0.365	0.120	68367	19654	69
4040,148	7355	0.392	0.055	1119069	156867	27
4040,365	4268	0.463	0.082	690510	121747	51
4040,398	12116	0.438	0.119	848671	229537	46
4040,704	15101	0.447	0.116	756799	197551	45
4040,730	18291	0.491	0.105	962290	204667	46
4040,871	9545	0.591	0.093	1061264	167076	47
4040,1157	10823	0.457	0.108	786954	185924	45
4047,984	499	0.759	0.252	214017	54162	60
4049,1064	8435	1.082	0.135	3389218	424279	25
4049,1066	8221	1.291	0.242	4938915	931151	20
4061,879	4157	0.374	0.353	1152689	197727	25
4060,864	2412	0.318	0.056	545747	86019	41
	12087	0.562	0.068	2040664	245977	21
4063,936	1452	0.290	0.027	565945	31058	27
2001,240	6170	0.466	0.065	695237	84461	57
2005,467	8274	0.470	0.067	1294164	167961	28
2005,468	2466	0.405	0.069	397981	166791	27
2005,428	681	0.249	0.041	177106	62704	26
3001,11	3922	0.274	0.045	772736	123159	27
3001,301	3081	0.214	0.039	395029	71946	46
3047,169	19203	0.237	0.027	646540	100864	29
3047,751	1040	0.280	0.112	150767	56491	64

N = 151

Mean = 470251

Std Dev = 167164

Max = 4978915

Min = 771

APPENDIX D

Table D-1: Angles, Ranges and Times for Refractive
Propagation Paths

Table D-2: Spreading Loss Function, $G(r)$

Table D-1 Angles, Ranges and Times for Refractive Propagation Paths

Theta zero Theta 1 Theta 2 Theta 3 Theta 4 z

Theta zero is the surface launch angle.
 Theta 1 is the angle at 80 meters.
 Theta 2 is the angle at the hydrophone (93m).
 Theta 3 is the angle at 254 meters.
 Theta 4 is the angle at 363 meters.
 z is the maximum depth of the ray.
 (See Figure 3-8)

0.0657	0.039	0.001			93
0.0658	0.039	0.004			93
0.0660	0.040	0.006			93
0.0670	0.041	0.013			94
0.0680	0.043	0.018			96
0.0690	0.045	0.021			97
0.0700	0.046	0.024			98
0.0710	0.048	0.027			99
0.0720	0.049	0.030			100
0.0730	0.051	0.032			102
0.0740	0.052	0.034			103
0.0750	0.053	0.036			104
0.0760	0.055	0.038			105
0.0770	0.056	0.040			107
0.0780	0.058	0.042			108
0.0790	0.059	0.044			109
0.0800	0.060	0.046			111
0.0810	0.062	0.047			112
0.0820	0.063	0.049			113
0.0830	0.064	0.051			115
0.0840	0.065	0.052			116
0.0850	0.067	0.054			118
0.0860	0.068	0.056			119
0.0870	0.069	0.057			121
0.0880	0.070	0.059			122
0.0890	0.072	0.060			124
0.0900	0.073	0.062			125
0.0910	0.074	0.063			127
0.0920	0.075	0.064			128
0.0930	0.077	0.066			130
0.0940	0.078	0.067			131
0.0950	0.079	0.069			133
0.0960	0.080	0.070			135
0.0970	0.081	0.071			136
0.0980	0.083	0.073			138
0.0990	0.084	0.074			140
0.1000	0.085	0.075			141
0.1010	0.086	0.077			143

Angles for Refractive Propagation Paths

Theta zero	Theta 1	Theta 2	Theta 3	Theta 4	z
0.1020	0.087	0.073			145
0.1030	0.089	0.079			146
0.1040	0.090	0.081			148
0.1050	0.091	0.082			150
0.1060	0.092	0.083			152
0.1070	0.093	0.085			154
0.1080	0.094	0.086			155
0.1090	0.095	0.087			157
0.1100	0.097	0.088			159
0.1110	0.098	0.090			161
0.1120	0.099	0.091			163
0.1130	0.100	0.092			165
0.1140	0.101	0.093			167
0.1150	0.102	0.094			169
0.1160	0.103	0.096			171
0.1170	0.104	0.097			173
0.1180	0.106	0.098			175
0.1190	0.107	0.099			177
0.1200	0.108	0.100			179
0.1210	0.109	0.101			181
0.1220	0.110	0.103			183
0.1230	0.111	0.104			185
0.1240	0.112	0.105			187
0.1250	0.113	0.106			189
0.1260	0.114	0.108			191
0.1270	0.115	0.109			194
0.1280	0.117	0.110			195
0.1290	0.118	0.111			199
0.1300	0.119	0.112			200
0.1310	0.120	0.113			202
0.1320	0.121	0.115			205
0.1330	0.122	0.116			207
0.1340	0.123	0.117			209
0.1350	0.124	0.118			212
0.1360	0.125	0.119			214
0.1370	0.127	0.120			216
0.1380	0.128	0.121			219
0.1390	0.129	0.123			221
0.1400	0.130	0.124			223
0.1410	0.131	0.125			225
0.1420	0.132	0.126			228
0.1430	0.133	0.127			230
0.1440	0.134	0.128			233
0.1450	0.135	0.129			236
0.1460	0.136	0.130			238
0.1470	0.137	0.131			240

Angles for Refractive Propagation Paths

Theta zero	Theta 1	Theta 2	Theta 3	Theta 4	z
0.1480	0.138	0.133			243
0.1490	0.139	0.134			246
0.1500	0.140	0.135			248
0.1510	0.142	0.136			251
0.1520	0.143	0.137			254
0.1521	0.143	0.137			254
0.1522	0.143	0.137	0.002		254
0.1523	0.143	0.138	0.003		255
0.1524	0.143	0.138	0.003		255
0.1525	0.143	0.138	0.010		256
0.1526	0.143	0.138	0.011		257
0.1527	0.143	0.138	0.013		257
0.1528	0.143	0.138	0.014		258
0.1529	0.144	0.138	0.015		258
0.1530	0.144	0.138	0.016		259
0.1540	0.145	0.139	0.024		265
0.1550	0.146	0.140	0.029		272
0.1560	0.147	0.142	0.034		276
0.1570	0.148	0.143	0.039		284
0.1580	0.149	0.144	0.045		291
0.1590	0.150	0.145	0.046		297
0.1600	0.151	0.146	0.050		304
0.1610	0.152	0.147	0.053		310
0.1620	0.153	0.148	0.056		317
0.1630	0.154	0.149	0.059		327
0.1640	0.155	0.150	0.061		330
0.1650	0.156	0.151	0.064		337
0.1660	0.157	0.152	0.067		347
0.1670	0.159	0.154	0.069		350
0.1680	0.160	0.155	0.071		357
0.1681	0.160	0.155	0.072		358
0.1682	0.160	0.155	0.072		358
0.1683	0.160	0.155	0.072		359
0.1684	0.160	0.155	0.072		360
0.1685	0.160	0.155	0.073		360
0.1686	0.160	0.155	0.073		361
0.1687	0.160	0.155	0.073		362
0.1688	0.160	0.156	0.073	0.005	364
0.1689	0.161	0.156	0.074	0.008	369
0.1690	0.161	0.156	0.074	0.010	371
0.1691	0.161	0.156	0.074	0.011	374
0.1692	0.161	0.156	0.074	0.012	375
0.1693	0.161	0.156	0.074	0.014	381
0.1694	0.161	0.156	0.075	0.015	384
0.1695	0.161	0.156	0.075	0.016	385
0.1696	0.161	0.156	0.075	0.017	386

Angles for Refractive Propagation Paths

Theta zero	Theta 1	Theta 2	Theta 3	Theta 4	z
0.1697	0.161	0.157	0.075	0.018	395
0.1698	0.161	0.157	0.076	0.019	398
0.1699	0.162	0.157	0.076	0.020	401
0.1700	0.162	0.157	0.076	0.021	405
0.1701	0.162	0.157	0.076	0.022	408
0.1702	0.162	0.157	0.076	0.022	411
0.1703	0.162	0.157	0.077	0.023	415
0.1704	0.162	0.157	0.077	0.024	418
0.1705	0.162	0.157	0.077	0.025	421
0.1706	0.162	0.158	0.077	0.025	425
0.1707	0.162	0.158	0.078	0.026	428
0.1708	0.163	0.158	0.078	0.027	432
0.1709	0.163	0.158	0.078	0.027	435
0.1710	0.163	0.158	0.078	0.028	439
0.1711	0.163	0.159	0.078	0.028	442
0.1712	0.163	0.158	0.079	0.029	445
0.1713	0.163	0.158	0.079	0.030	449
0.1714	0.163	0.158	0.079	0.030	452
0.1715	0.163	0.159	0.079	0.031	456
0.1716	0.163	0.159	0.080	0.031	459
0.1717	0.163	0.159	0.080	0.032	462
0.1718	0.164	0.159	0.080	0.032	466
0.1719	0.164	0.159	0.080	0.033	469
0.1720	0.164	0.159	0.080	0.034	473
0.1721	0.165	0.160	0.083	0.038	507
0.1741	0.166	0.161	0.085	0.043	541
0.1750	0.167	0.162	0.087	0.047	576
0.1760	0.168	0.163	0.089	0.050	611
0.1770	0.169	0.164	0.091	0.054	647
0.1780	0.170	0.166	0.093	0.057	682
0.1790	0.171	0.167	0.095	0.060	718
0.1800	0.172	0.168	0.096	0.063	753
0.1900	0.183	0.178			
0.2000	0.193	0.189			
0.2100	0.203	0.200			
0.2200	0.214	0.210			
0.2300	0.224	0.221			
0.2400	0.234	0.231			
0.2500	0.244	0.241			
0.2600	0.255	0.252			
0.2700	0.265	0.261			
0.2800	0.275	0.271			
0.2900	0.285	0.283			
0.3000	0.295	0.293			
0.3100	0.305	0.307			
0.3200	0.315	0.321			

Angles for Refractive Propagation Paths

Theta zero	Theta 1	Theta 2
0.3500	0.356	0.354
0.3800	0.377	0.375
0.4000	0.397	0.395
0.4500	0.447	0.446
0.5000	0.497	0.496
0.5500	0.548	0.546
0.6000	0.598	0.597
0.6500	0.648	0.647
0.7000	0.698	0.697
0.8000	0.799	0.798
0.9000	0.899	0.898
1.0000	0.999	0.999
1.1000	1.099	1.099
1.2000	1.199	1.199
1.3000	1.300	1.299
1.4000	1.400	1.400
1.5000	1.500	1.500
1.5708	1.571	1.571

Ranges for Refractive Propagation Paths

Theta zero	r1	r2	r3	r4	r5	R1	R2
------------	----	----	----	----	----	----	----

r1 is the horizontal projection of the path from the source (6m) to 8m.
r2 is the horizontal projection of the path from 8m to the hydrophone depth.
r3 is the horizontal projection of the path from the hydrophone depth to 254m, or the vertex.
r4 is the horizontal projection of the path from 254m to 362m, or the vertex, if sooner.
r5 is the horizontal projection of the path from 362m to the vertex.
R1 is the horizontal distance to the hydrophone on the downward path of the ray.
R2 is the horizontal distance to the hydrophone on the upward swing of the ray.
(See Figure 3-8)

0.0657	1523.5	640.5	563.7			2164.2	2214.7
0.0658	1519.7	600.9	565.5			2129.6	2251.3
0.0660	1512.0	563.2	672.1			2075.2	2297.1
0.0670	1475.1	476.3	700.0			1951.4	2398.7
0.0680	1440.4	429.2	727.1			1869.6	2465.5
0.0690	1407.8	395.8	753.7			1803.5	2519.4
0.0700	1377.0	369.8	779.7			1746.6	2566.5
0.0710	1347.8	348.6	805.2			1695.4	2609.6
0.0720	1320.1	330.8	830.3			1650.9	2650.0
0.0730	1293.8	315.4	855.1			1609.2	2688.5
0.0740	1268.7	302.0	879.4			1570.6	2725.5
0.0750	1244.7	290.0	903.4			1534.7	2761.6
0.0760	1221.8	279.3	927.1			1501.2	2796.6
0.0770	1199.9	269.6	950.6			1469.5	2831.4
0.0780	1178.9	260.8	973.7			1439.7	2865.1
0.0790	1158.8	252.7	996.5			1411.5	2897.7
0.0800	1139.4	245.2	1019.7			1384.7	2930.3
0.0810	1120.7	238.4	1041.3			1359.2	2961.9
0.0820	1102.8	232.0	1064.1			1334.8	2992.7
0.0830	1085.5	226.0	1086.2			1311.5	3022.8
0.0840	1068.8	220.4	1108.1			1289.2	3054.5
0.0850	1052.7	215.2	1129.8			1267.8	3087.2
0.0860	1037.1	210.2	1151.4			1247.7	3119.7
0.0870	1022.0	205.5	1172.9			1227.6	3152.2
0.0880	1007.4	201.1	1194.2			1208.5	3184.5
0.0890	993.3	196.9	1215.4			1190.2	3217.1
0.0900	979.6	193.0	1236.4			1172.5	3250.4
0.0910	966.3	189.2	1257.3			1155.5	3284.5
0.0920	953.4	185.6	1278.0			1139.7	3319.2
0.0930	940.9	182.1	1298.9			1124.7	3354.5
0.0940	928.7	178.8	1319.5			1110.5	3390.3
0.0950	916.9	175.7	1340.0			1097.0	3426.2
0.0960	905.4	172.7	1360.4			1084.2	3463.1
0.0970	894.2	169.7	1380.8			1072.0	3500.7
0.0980	883.3	166.9	1401.0			1060.2	3538.4
0.0990	872.7	164.3	1421.0			1048.9	3576.3
0.1000	862.3	161.7	1441.0			1038.0	3614.4

Ranges for Refractive Propagation Paths

Theta zero	n1	n2	n3	n4	n5	n1	n2
0.1010	852.3	159.2	1481.3			1011.5	1615.7
0.1020	842.4	156.3	1481.2			999.2	1615.1
0.1030	832.9	154.5	1501.1			987.3	1650.5
0.1040	823.5	152.2	1521.0			975.7	1717.2
0.1050	814.4	150.1	1540.7			964.4	1745.7
0.1060	805.4	148.0	1560.4			953.4	1778.3
0.1070	796.7	145.9	1580.1			942.7	1810.8
0.1080	788.2	144.0	1599.8			932.2	1847.5
0.1090	779.9	142.1	1619.2			921.9	1877.1
0.1100	771.7	140.2	1638.7			912.0	1908.3
0.1110	763.8	138.4	1659.1			902.2	1941.5
0.1120	756.0	136.7	1677.5			892.7	1974.7
0.1130	748.4	135.0	1695.8			883.4	2007.9
0.1140	740.9	133.3	1716.1			874.2	2039.8
0.1150	733.6	131.7	1735.4			865.3	2072.8
0.1160	726.4	130.2	1754.6			856.6	2105.5
0.1170	719.4	128.7	1773.8			848.1	2138.3
0.1180	712.5	127.2	1792.9			839.7	2171.2
0.1190	705.8	125.7	1812.1			831.5	2204.2
0.1200	699.2	124.2	1831.1			823.5	2237.1
0.1210	692.7	122.9	1850.2			815.7	2270.1
0.1220	686.3	121.6	1869.2			808.0	2303.1
0.1230	680.1	120.3	1888.2			800.4	2336.1
0.1240	674.0	119.1	1907.1			793.0	2369.2
0.1250	668.0	117.8	1926.1			785.8	2402.2
0.1260	662.1	116.6	1944.9			778.7	2435.7
0.1270	656.3	115.4	1963.8			771.7	2468.8
0.1280	650.6	114.2	1982.6			764.8	2501.9
0.1290	645.0	113.1	2001.3			758.0	2534.8
0.1300	639.5	112.0	2020.2			751.5	2568.0
0.1310	634.2	110.9	2039.0			745.0	2601.2
0.1320	628.9	109.8	2057.7			738.7	2634.5
0.1330	623.7	108.8	2076.4			732.4	2667.7
0.1340	618.5	107.8	2095.1			726.3	2701.0
0.1350	613.5	106.8	2113.8			720.2	2734.4
0.1360	608.5	105.8	2132.5			714.3	2767.7
0.1370	603.7	104.8	2151.1			708.5	2801.1
0.1380	598.9	103.9	2169.7			702.7	2834.5
0.1390	594.2	102.9	2188.1			697.1	2867.9
0.1400	589.6	102.0	2206.5			691.6	2901.2
0.1410	585.1	101.1	2225.0			686.1	2934.8
0.1420	580.6	100.2	2243.4			680.7	2968.3
0.1430	576.1	99.4	2262.0			675.4	3001.8
0.1440	571.7	98.6	2281.1			670.3	3035.7
0.1450	567.4	97.7	2299.6			665.1	3069.5
0.1460	563.1	96.9	2318.1			660.1	3103.3

Ranges for Refractive Propagation Paths

Theta zero	n1	n2	n3	n4	n5	R1	R2
0.1470	559.0	96.1	2336.6			655.1	5136.1
0.1480	554.9	95.3	2355.0			650.3	5169.7
0.1490	550.9	94.6	2373.5			645.4	5203.3
0.1500	546.9	93.8	2391.9			640.7	5237.0
0.1510	543.0	93.0	2410.4			636.0	5270.7
0.1520	539.1	92.3	2428.8			631.4	5304.4
0.1521	538.7	92.2	2430.6			631.0	5307.8
0.1522	538.4	92.2	2402.6	70.4		630.5	5351.2
0.1527	538.0	92.1	2373.1	104.1		630.1	5537.9
0.1528	537.6	92.0	2299.0	323.4		629.6	5690.0
0.1529	537.2	92.0	2271.3	393.0		629.2	5770.8
0.1526	536.8	91.9	2248.1	452.0		628.7	5845.2
0.1527	536.4	91.8	2227.8	504.2		628.3	5903.7
0.1528	536.1	91.7	2209.5	551.6		627.9	5966.5
0.1529	535.7	91.7	2192.9	595.2		627.4	6020.1
0.1530	535.3	91.6	2177.5	635.8		626.9	6070.3
0.1540	531.6	90.9	2061.7	952.1		622.4	6468.3
0.1550	527.9	90.2	1979.9	1188.4		618.0	6774.1
0.1560	524.2	89.5	1914.3	1386.2		613.7	7035.7
0.1570	520.5	88.8	1858.9	1560.2		609.4	7269.9
0.1580	517.1	88.2	1810.4	1717.7		605.2	7485.1
0.1590	513.5	87.5	1767.2	1862.8		601.1	7686.1
0.1600	510.1	86.9	1728.1	1998.5		597.0	7876.0
0.1610	506.7	86.2	1692.2	2126.0		592.9	8057.0
0.1620	503.3	85.5	1659.1	2247.3		588.9	8230.5
0.1630	500.0	84.9	1628.7	2363.6		585.0	8397.7
0.1640	496.7	84.4	1599.5	2474.1		581.1	8559.5
0.1650	493.5	83.8	1572.5	2581.1		577.3	8716.8
0.1660	490.3	83.2	1546.9	2684.4		573.5	8869.5
0.1670	487.2	82.6	1522.7	2784.6		569.8	9019.2
0.1680	484.0	82.0	1499.7	2881.9		566.1	9165.3
0.1681	483.7	82.0	1497.5	2891.5		565.7	9179.7
0.1682	483.4	81.9	1495.2	2901.1		565.3	9194.1
0.1683	483.1	81.9	1493.0	2910.6		565.0	9208.5
0.1684	482.8	81.8	1490.8	2920.1		564.6	9222.9
0.1685	482.5	81.8	1488.5	2929.6		564.3	9237.2
0.1686	482.2	81.7	1486.4	2939.0		563.9	9251.5
0.1687	481.9	81.6	1484.2	2948.5		563.5	9265.8
0.1688	481.6	81.5	1482.1	2958.5	378.7	563.2	9272.5
0.1689	481.3	81.5	1480.0	2968.5	499.6	562.8	9285.1
0.1690	481.0	81.4	1477.8	2978.5	620.5	562.4	9297.4
0.1691	480.7	81.4	1475.7	2988.5	741.4	562.1	9309.5
0.1692	480.4	81.4	1473.5	2998.5	862.3	561.7	9321.5
0.1693	480.1	81.3	1471.4	3008.5	983.2	561.4	9333.5
0.1694	479.8	81.2	1469.3	3018.5	1104.1	561.1	9345.1
0.1695	479.5	81.2	1467.1	3028.5	1225.0	560.7	9356.7

Ranges for Refractive Propagation Paths

Theta zero	n1	n2	n3	n4	n5	R1	R2
0.1696	479.2	81.1	1465.1	2337.4	3390.2	560.3	14733.5
0.1697	478.8	81.1	1463.1	2307.5	3531.0	559.9	15130.9
0.1698	478.5	81.0	1461.0	2279.5	3762.3	559.5	15485.2
0.1699	478.2	81.0	1458.9	2253.2	3935.4	559.2	15892.3
0.1700	477.9	80.9	1456.9	2228.3	4101.2	558.9	15969.9
0.1701	477.6	80.9	1454.9	2204.7	4260.7	558.5	16237.4
0.1702	477.3	80.8	1452.8	2182.3	4414.6	558.1	16495.9
0.1703	477.0	80.7	1450.8	2160.9	4563.3	557.8	16746.3
0.1704	476.7	80.7	1448.8	2140.4	4707.4	557.4	16989.7
0.1705	476.4	80.6	1446.8	2120.7	4847.4	557.1	17225.5
0.1706	476.1	80.6	1444.8	2101.9	4983.5	556.7	17455.8
0.1707	475.8	80.5	1442.8	2083.7	5116.0	556.4	17680.4
0.1708	475.5	80.5	1440.8	2066.1	5245.3	556.0	17899.7
0.1709	475.2	80.4	1438.8	2049.2	5371.6	555.7	18114.1
0.1710	475.0	80.4	1436.9	2032.8	5495.0	555.3	18324.1
0.1711	474.7	80.3	1434.9	2017.0	5615.8	555.0	18529.9
0.1712	474.4	80.3	1433.0	2001.6	5734.2	554.6	18731.7
0.1713	474.1	80.2	1431.0	1986.7	5850.2	554.3	18929.8
0.1714	473.8	80.1	1429.1	1972.3	5964.0	553.9	19124.7
0.1715	473.5	80.1	1427.2	1958.3	6075.6	553.5	19315.8
0.1716	473.2	80.0	1425.3	1944.5	6185.6	553.2	19503.3
0.1717	472.9	80.0	1423.4	1931.2	6293.5	552.9	19689.0
0.1718	472.6	79.9	1421.5	1918.2	6399.7	552.5	19871.4
0.1719	472.3	79.9	1419.6	1905.5	6504.0	552.2	20051.1
0.1720	472.0	79.8	1417.7	1893.1	6607.2	551.8	20228.7
0.1721	471.7	79.7	1415.8	1880.7	6709.1	551.4	20403.1
0.1722	471.4	79.6	1413.9	1868.5	6809.6	551.0	20574.8
0.1723	471.1	79.5	1412.0	1856.5	6908.6	550.6	20743.2
0.1724	470.8	79.4	1410.1	1844.7	7006.1	550.2	20908.7
0.1725	470.5	79.3	1408.2	1833.1	7102.1	549.8	21071.6
0.1726	470.2	79.2	1406.3	1821.7	7196.6	549.4	21232.2
0.1727	469.9	79.1	1404.4	1810.5	7289.6	549.0	21390.7
0.1728	469.6	79.0	1402.5	1799.5	7381.1	548.6	21547.2
0.1729	469.3	78.9	1400.6	1788.7	7471.1	548.2	21701.8
0.1730	469.0	78.8	1398.7	1778.1	7559.6	547.8	21854.7
0.1731	468.7	78.7	1396.8	1767.7	7646.6	547.4	22005.9
0.1732	468.4	78.6	1394.9	1757.5	7732.1	547.0	22155.5
0.1733	468.1	78.5	1393.0	1747.5	7816.1	546.6	22303.6
0.1734	467.8	78.4	1391.1	1737.7	7898.6	546.2	22450.2
0.1735	467.5	78.3	1389.2	1728.1	7979.6	545.8	22595.4
0.1736	467.2	78.2	1387.3	1718.7	8059.1	545.4	22739.2
0.1737	466.9	78.1	1385.4	1709.5	8137.1	545.0	22881.6
0.1738	466.6	78.0	1383.5	1700.5	8213.6	544.6	23022.7
0.1739	466.3	77.9	1381.6	1691.7	8288.6	544.2	23162.4
0.1740	466.0	77.8	1379.7	1683.1	8362.1	543.8	23300.7
0.1741	465.7	77.7	1377.8	1674.7	8434.1	543.4	23437.6
0.1742	465.4	77.6	1375.9	1666.5	8504.6	543.0	23573.1
0.1743	465.1	77.5	1374.0	1658.5	8573.6	542.6	23707.2
0.1744	464.8	77.4	1372.1	1650.7	8641.1	542.2	23840.0
0.1745	464.5	77.3	1370.2	1643.1	8707.1	541.8	23971.4
0.1746	464.2	77.2	1368.3	1635.7	8771.6	541.4	24101.5
0.1747	463.9	77.1	1366.4	1628.5	8834.6	541.0	24230.2
0.1748	463.6	77.0	1364.5	1621.5	8896.1	540.6	24357.5
0.1749	463.3	76.9	1362.6	1614.7	8956.1	540.2	24483.4
0.1750	463.0	76.8	1360.7	1608.1	9014.6	539.8	24607.9
0.1751	462.7	76.7	1358.8	1601.7	9071.6	539.4	24731.0
0.1752	462.4	76.6	1356.9	1595.5	9127.1	539.0	24852.7
0.1753	462.1	76.5	1355.0	1589.5	9181.1	538.6	24973.0
0.1754	461.8	76.4	1353.1	1583.7	9233.6	538.2	25091.9
0.1755	461.5	76.3	1351.2	1578.1	9284.6	537.8	25209.4
0.1756	461.2	76.2	1349.3	1572.7	9334.1	537.4	25325.5
0.1757	460.9	76.1	1347.4	1567.5	9382.1	537.0	25440.2
0.1758	460.6	76.0	1345.5	1562.5	9428.6	536.6	25553.5
0.1759	460.3	75.9	1343.6	1557.7	9473.6	536.2	25665.4
0.1760	460.0	75.8	1341.7	1553.1	9517.1	535.8	25775.9
0.1761	459.7	75.7	1339.8	1548.7	9559.1	535.4	25885.0
0.1762	459.4	75.6	1337.9	1544.5	9600.6	535.0	25992.7
0.1763	459.1	75.5	1336.0	1540.5	9640.6	534.6	26099.0
0.1764	458.8	75.4	1334.1	1536.7	9679.1	534.2	26203.9
0.1765	458.5	75.3	1332.2	1533.1	9716.1	533.8	26307.4
0.1766	458.2	75.2	1330.3	1529.7	9751.6	533.4	26409.5
0.1767	457.9	75.1	1328.4	1526.5	9785.6	533.0	26510.2
0.1768	457.6	75.0	1326.5	1523.5	9818.1	532.6	26609.5
0.1769	457.3	74.9	1324.6	1520.7	9849.1	532.2	26707.4
0.1770	457.0	74.8	1322.7	1518.1	9878.6	531.8	26803.9
0.1771	456.7	74.7	1320.8	1515.7	9906.6	531.4	26899.0
0.1772	456.4	74.6	1318.9	1513.5	9933.1	531.0	26992.7
0.1773	456.1	74.5	1317.0	1511.5	9958.1	530.6	27085.0
0.1774	455.8	74.4	1315.1	1509.7	9981.6	530.2	27175.9
0.1775	455.5	74.3	1313.2	1508.1	10003.6	529.8	27265.4
0.1776	455.2	74.2	1311.3	1506.7	10024.1	529.4	27353.5
0.1777	454.9	74.1	1309.4	1505.5	10043.1	529.0	27440.2
0.1778	454.6	74.0	1307.5	1504.5	10060.6	528.6	27525.5
0.1779	454.3	73.9	1305.6	1503.7	10076.6	528.2	27609.4
0.1780	454.0	73.8	1303.7	1503.1	10091.1	527.8	27691.9
0.1781	453.7	73.7	1301.8	1502.7	10104.1	527.4	27773.0
0.1782	453.4	73.6	1299.9	1502.5	10115.6	527.0	27852.7
0.1783	453.1	73.5	1298.0	1502.5	10125.6	526.6	27931.0
0.1784	452.8	73.4	1296.1	1502.7	10134.1	526.2	28007.9
0.1785	452.5	73.3	1294.2	1503.1	10141.1	525.8	28083.4
0.1786	452.2	73.2	1292.3	1503.7	10146.6	525.4	28157.5
0.1787	451.9	73.1	1290.4	1504.5	10150.6	525.0	28230.2
0.1788	451.6	73.0	1288.5	1505.5	10153.1	524.6	28301.5
0.1789	451.3	72.9	1286.6	1506.7	10154.1	524.2	28371.4
0.1790	451.0	72.8	1284.7	1508.1	10153.6	523.8	28440.0
0.1791	450.7	72.7	1282.8	1509.7	10151.6	523.4	28507.2
0.1792	450.4	72.6	1280.9	1511.5	10148.1	523.0	28573.0
0.1793	450.1	72.5	1279.0	1513.5	10143.1	522.6	28637.4
0.1794	449.8	72.4	1277.1	1515.7	10136.6	522.2	28699.5
0.1795	449.5	72.3	1275.2	1518.1	10128.6	521.8	28760.2
0.1796	449.2	72.2	1273.3	1520.7	10119.1	521.4	28819.5
0.1797	448.9	72.1	1271.4	1523.5	10108.1	521.0	28877.4
0.1798	448.6	72.0	1269.5	1526.5	10095.6	520.6	28933.9
0.1799	448.3	71.9	1267.6	1529.7	10081.6	520.2	28989.0
0.1800	448.0	71.8	1265.7	1533.1	10066.1	519.8	29042.7
0.1801	447.7	71.7	1263.8	1536.7	10049.1	519.4	29095.0
0.1802	447.4	71.6	1261.9	1540.5	10030.6	519.0	29145.9
0.1803	447.1	71.5	1260.0	1544.5	10010.6	518.6	29195.4
0.1804	446.8	71.4	1258.1	1548.7	9989.1	518.2	29243.5
0.1805	446.5	71.3	1256.2	1553.1	9966.1	517.8	29290.2
0.1806	446.2	71.2	1254.3	1557.7	9941.6	517.4	29335.5
0.1807	445.9	71.1	1252.4	1562.5	9915.6	517.0	29379.4
0.1808	445.6	71.0	1250.5	1567.5	9888.1	516.6	29421.9
0.1809	445.3	70.9	1248.6	1572.7	9859.1	516.2	29463.0
0.1810	445.0	70.8	1246.7	1578.1	9828.6	515.8	29502.7
0.1811	444.7	70.7	1244.8	1583.7	9796.6	515.4	29541.0
0.1812	444.4	70.6	1242.9	1589.5	9763.1	515.0	29577.9
0.1813	444.1	70.5	1241.0	1595.5	9728.1	514.6	29613.4
0.1814	443.8	70.4	1239.1	1601.7	9691.6	514.2	29647.5
0.1815	443.5	70.3	1237.2	1608.1	9653.6	513.8	29680.2
0.1816	443.2	70.2	1235.3	1614.7	9614.1	513.4	29711.5
0.1817	442.9	70.1	1233.4	1621.5	9573.1	513.0	29741.4
0.1818	442.6	70.0	1231.5	1628.5	9530.6	512.6	29769.9
0.1819	442.3	69.9	1229.6	1635.7	9486.6	512.2	29797.0
0.1820	442.0	69.8	1227.7	1643.1	9441.1	511.8	29822.7
0.1821	441.7	69.7	1225.8	1650.7	9394.1	511.4	29847.0
0.1822	441.4	69.6	1223.9	1658.5	9345.6	511.0	29869.9
0.1823	441.1	69.5	1222.0	1666.5	9295.6	510.6	29891.4
0.1824	440.8	69.4	1220.1	1674.7	9244.1	510.2	29911.5
0.1825	440.5	69.3	1218.2	1683.1	9191.1	509.8	29930.2
0.1826	440.2	69.2	1216.3	1691.7	9136.6	509.4	29947.5
0.1827	439.9	69.1	1214.4	1700.5	9080.6	509.0	29963.4
0.1828	439.6	69.0	1212.5	1709.5	9023.1	508.6	29977.9
0.1829	439.3	68.9	1210.6	1718.7	8964.1	508.2	29991.0
0.1830	439.0	68.8	1208.7	1728.1	8903.6	507.8	30002.7
0.1831	438.7	68.7					

Ranges for Reflective Propagation Paths

Theta perc	r1	r2	r3	r4	r5	R1	R2
0.3400	227.6	37.4				264.8	
0.3600	213.7	35.0				248.9	
0.3800	201.3	33.0				234.7	
0.4000	190.1	31.1				221.2	
0.4500	166.2	27.2				193.4	
0.5000	146.9	24.0				170.9	
0.5500	130.8	21.3				152.2	
0.6000	117.2	19.1				136.3	
0.6500	105.4	17.2				122.6	
0.7000	95.1	15.5				110.6	
0.8000	77.8	12.7				90.5	
0.9000	63.6	10.3				73.9	
1.0000	51.4	8.4				59.8	
1.1000	40.8	6.6				47.4	
1.2000	31.1	5.1				36.2	
1.3000	22.2	3.6				25.8	
1.4000	13.8	2.2				16.1	
1.5000	5.7	0.9				5.6	
1.5708	0.0	0.0				0.0	

Times for Refractive Propagation Paths

Theta zero

t1

t2

t3

t4

t5

T1

T2

t1, t2, t3, t4, and t5 correspond to the times required to traverse the paths associated with r1, r2, r3, r4 and r5.

T1 and T2 correspond to the times required to traverse the distances R1 and R2.

(See Figure 3-8)

0.0657	1.051	0.445	0.016			1.516	1.575
0.0658	1.053	0.417	0.046			1.475	1.567
0.0660	1.053	0.391	0.076			1.444	1.595
0.0670	1.027	0.331	0.155			1.358	1.669
0.0680	1.003	0.298	0.207			1.301	1.715
0.0690	0.990	0.275	0.248			1.255	1.752
0.0700	0.959	0.257	0.285			1.216	1.785
0.0710	0.939	0.242	0.317			1.181	1.815
0.0720	0.919	0.230	0.347			1.145	1.847
0.0730	0.901	0.219	0.375			1.120	1.879
0.0740	0.884	0.210	0.401			1.094	1.905
0.0750	0.867	0.202	0.426			1.069	1.930
0.0760	0.851	0.194	0.450			1.046	1.945
0.0770	0.836	0.187	0.473			1.024	1.969
0.0780	0.822	0.181	0.495			1.002	1.992
0.0790	0.808	0.176	0.516			0.980	2.016
0.0800	0.794	0.171	0.537			0.958	2.039
0.081	0.781	0.166	0.558			0.947	2.062
0.0820	0.769	0.161	0.577			0.935	2.085
0.0830	0.757	0.157	0.597			0.914	2.108
0.0840	0.745	0.153	0.616			0.899	2.130
0.0850	0.734	0.150	0.635			0.884	2.152
0.0860	0.723	0.146	0.653			0.869	2.176
0.0870	0.712	0.142	0.671			0.855	2.198
0.0880	0.703	0.140	0.689			0.843	2.221
0.0890	0.693	0.137	0.707			0.830	2.247
0.0900	0.683	0.134	0.724			0.818	2.266
0.0910	0.674	0.132	0.741			0.806	2.288
0.0920	0.666	0.129	0.758			0.794	2.310
0.093	0.657	0.127	0.775			0.782	2.332
0.0940	0.649	0.125	0.792			0.770	2.355
0.095	0.641	0.122	0.809			0.758	2.378
0.096	0.632	0.12	0.826			0.746	2.400
0.0970	0.624	0.118	0.843			0.742	2.422
0.0980	0.617	0.116	0.859			0.732	2.445
0.0990	0.610	0.114	0.875			0.724	2.467
0.1000	0.603	0.112	0.892			0.716	2.489

Times for Refractive Propagation Paths

Theta zero	t1	t2	t3	t4	t5	T1	T2
0.1010	0.595	0.111	0.903			0.706	2.512
0.1020	0.588	0.109	0.919			0.698	2.535
0.1030	0.582	0.108	0.934			0.689	2.557
0.1040	0.575	0.106	0.949			0.681	2.580
0.1050	0.569	0.105	0.964			0.674	2.602
0.1060	0.563	0.103	0.979			0.666	2.625
0.1070	0.557	0.102	0.994			0.658	2.647
0.1080	0.551	0.100	1.009			0.651	2.670
0.1090	0.545	0.099	1.024			0.644	2.692
0.1100	0.539	0.098	1.039			0.637	2.715
0.1110	0.534	0.097	1.054			0.630	2.738
0.1120	0.529	0.095	1.068			0.624	2.760
0.1130	0.523	0.094	1.083			0.617	2.783
0.1140	0.518	0.093	1.097			0.611	2.806
0.1150	0.513	0.092	1.112			0.605	2.828
0.1160	0.508	0.091	1.126			0.599	2.851
0.1170	0.503	0.090	1.140			0.593	2.874
0.1180	0.499	0.089	1.155			0.587	2.896
0.1190	0.494	0.088	1.169			0.582	2.919
0.1200	0.488	0.087	1.183			0.576	2.941
0.1210	0.485	0.086	1.197			0.571	2.963
0.1220	0.480	0.085	1.211			0.565	2.986
0.1230	0.476	0.084	1.225			0.560	3.009
0.1240	0.472	0.083	1.239			0.555	3.031
0.1250	0.468	0.082	1.253			0.550	3.054
0.1260	0.464	0.081	1.267			0.545	3.076
0.1270	0.460	0.081	1.281			0.540	3.099
0.1280	0.456	0.080	1.295			0.535	3.121
0.1290	0.452	0.079	1.309			0.531	3.144
0.1300	0.448	0.078	1.322			0.526	3.167
0.1310	0.444	0.078	1.336			0.522	3.189
0.1320	0.441	0.077	1.349			0.518	3.212
0.1330	0.437	0.076	1.363			0.513	3.234
0.1340	0.434	0.075	1.377			0.509	3.257
0.1350	0.430	0.075	1.390			0.505	3.280
0.1360	0.427	0.074	1.404			0.501	3.302
0.1370	0.423	0.073	1.417			0.497	3.325
0.1380	0.420	0.073	1.431			0.493	3.347
0.1390	0.417	0.072	1.444			0.489	3.370
0.1400	0.414	0.071	1.458			0.485	3.392
0.1410	0.410	0.071	1.471			0.481	3.415
0.1420	0.407	0.070	1.485			0.477	3.437
0.1430	0.404	0.070	1.498			0.474	3.460
0.1440	0.401	0.069	1.511			0.470	3.482
0.1450	0.398	0.068	1.524			0.467	3.505
0.1460	0.395	0.068	1.538			0.463	3.527

Times for Refractive Propagation Paths

Theta zero	t1	t2	t3	t4	t5	T1	T2
0.1470	0.393	0.067	1.551			0.460	3.562
0.1480	0.390	0.067	1.564			0.457	3.565
0.1490	0.387	0.066	1.577			0.455	3.568
0.1500	0.384	0.066	1.591			0.453	3.571
0.1510	0.382	0.065	1.604			0.447	3.574
0.1520	0.379	0.065	1.617			0.444	3.578
0.1521	0.379	0.065	1.618			0.443	3.580
0.1522	0.378	0.065	1.599	0.043		0.447	3.579
0.1523	0.378	0.065	1.587	0.041		0.447	3.577
0.1524	0.378	0.065	1.528	0.022		0.441	3.543
0.1525	0.378	0.064	1.509	0.070		0.442	4.000
0.1526	0.377	0.064	1.493	0.111		0.442	4.080
0.1527	0.377	0.064	1.479	0.147		0.441	4.097
0.1528	0.377	0.064	1.467	0.179		0.441	4.100
0.1529	0.377	0.064	1.455	0.409		0.441	4.170
0.1530	0.376	0.064	1.445	0.437		0.441	4.204
0.1540	0.374	0.064	1.366	0.655		0.437	4.478
0.1550	0.371	0.063	1.310	0.817		0.434	4.668
0.1560	0.369	0.063	1.265	0.957		0.431	4.863
0.1570	0.366	0.061	1.223	1.070		0.428	5.003
0.1580	0.364	0.062	1.195	1.181		0.426	5.177
0.1590	0.361	0.061	1.165	1.281		0.422	5.315
0.1600	0.359	0.061	1.139	1.374		0.420	5.445
0.1610	0.357	0.061	1.115	1.461		0.417	5.571
0.1620	0.354	0.060	1.090	1.548		0.414	5.695
0.1630	0.352	0.060	1.070	1.624		0.411	5.814
0.1640	0.350	0.059	1.052	1.704		0.409	5.918
0.1650	0.348	0.059	1.034	1.774		0.406	6.017
0.1660	0.345	0.058	1.017	1.845		0.404	6.113
0.1670	0.343	0.058	1.001	1.910		0.401	6.206
0.1680	0.341	0.058	0.986	1.980		0.399	6.300
0.1681	0.341	0.058	0.984	1.967		0.399	6.340
0.1682	0.341	0.058	0.980	1.990		0.398	6.350
0.1683	0.340	0.058	0.961	2.000		0.398	6.360
0.1684	0.340	0.058	0.980	2.006		0.398	6.370
0.1685	0.340	0.057	0.973	2.010		0.398	6.380
0.1686	0.340	0.057	0.977	2.015		0.397	6.387
0.1687	0.340	0.057	0.975	2.016		0.397	6.389
0.1688	0.339	0.057	1.074	2.015	0.644	0.397	6.400
0.1689	0.339	0.057	1.070	2.017	0.613	0.397	6.403
0.1690	0.339	0.057	1.070	2.017	0.613	0.396	6.403
0.1691	0.339	0.057	1.070	2.017	0.613	0.396	6.403
0.1692	0.339	0.057	1.070	2.017	0.613	0.396	6.403
0.1693	0.339	0.057	1.070	2.017	0.613	0.396	6.403
0.1694	0.339	0.057	1.070	2.017	0.613	0.396	6.403
0.1695	0.339	0.057	1.070	2.017	0.613	0.396	6.403

Times for Refractive Propagation Paths

Theta zero	t1	t2	t3	t4	t5	T1	T2
0.1696	0.338	0.057	0.962	1.607	2.325	0.395	10.164
0.1697	0.338	0.057	0.961	1.586	2.456	0.395	10.401
0.1698	0.337	0.057	0.960	1.567	2.580	0.394	10.639
0.1699	0.337	0.057	0.958	1.549	2.699	0.394	10.607
0.1700	0.337	0.057	0.957	1.532	2.813	0.394	10.997
0.1701	0.337	0.057	0.956	1.516	2.922	0.394	11.151
0.1702	0.337	0.057	0.954	1.500	3.028	0.393	11.353
0.1703	0.336	0.057	0.953	1.486	3.130	0.393	11.530
0.1704	0.336	0.057	0.952	1.472	3.228	0.393	11.696
0.1705	0.336	0.057	0.950	1.458	3.324	0.392	11.858
0.1706	0.336	0.057	0.949	1.445	3.418	0.392	12.016
0.1707	0.335	0.057	0.948	1.433	3.509	0.392	12.170
0.1708	0.335	0.057	0.946	1.421	3.597	0.392	12.320
0.1709	0.335	0.057	0.945	1.409	3.684	0.392	12.467
0.1710	0.335	0.057	0.944	1.398	3.768	0.391	12.611
0.1711	0.335	0.057	0.942	1.387	3.851	0.391	12.752
0.1712	0.334	0.056	0.941	1.377	3.932	0.391	12.891
0.1713	0.334	0.056	0.940	1.366	4.012	0.391	13.027
0.1714	0.334	0.056	0.938	1.356	4.090	0.390	13.160
0.1715	0.334	0.056	0.937	1.347	4.167	0.390	13.291
0.1716	0.334	0.056	0.936	1.337	4.242	0.390	13.420
0.1717	0.333	0.056	0.935	1.328	4.316	0.390	13.547
0.1718	0.333	0.056	0.933	1.319	4.389	0.389	13.672
0.1719	0.333	0.056	0.932	1.311	4.460	0.389	13.795
0.1720	0.333	0.056	0.931	1.302	4.531	0.389	13.917
0.1721	0.333	0.056	0.929	1.293	4.601	0.389	14.038
0.1722	0.332	0.056	0.928	1.285	4.670	0.388	14.158
0.1723	0.332	0.056	0.927	1.276	4.739	0.388	14.277
0.1724	0.332	0.056	0.926	1.268	4.807	0.388	14.395
0.1725	0.332	0.056	0.925	1.259	4.875	0.388	14.512
0.1726	0.332	0.056	0.924	1.251	4.942	0.388	14.628
0.1727	0.332	0.056	0.923	1.242	5.009	0.388	14.743
0.1728	0.332	0.056	0.922	1.234	5.075	0.388	14.857
0.1729	0.332	0.056	0.921	1.225	5.141	0.388	14.970
0.1730	0.332	0.056	0.920	1.217	5.206	0.388	15.082
0.1731	0.332	0.056	0.919	1.208	5.271	0.388	15.193
0.1732	0.332	0.056	0.918	1.200	5.335	0.388	15.303
0.1733	0.332	0.056	0.917	1.191	5.400	0.388	15.412
0.1734	0.332	0.056	0.916	1.183	5.463	0.388	15.520
0.1735	0.332	0.056	0.915	1.174	5.527	0.388	15.627
0.1736	0.332	0.056	0.914	1.166	5.589	0.388	15.733
0.1737	0.332	0.056	0.913	1.157	5.652	0.388	15.838
0.1738	0.332	0.056	0.912	1.149	5.714	0.388	15.942
0.1739	0.332	0.056	0.911	1.140	5.777	0.388	16.045
0.1740	0.332	0.056	0.910	1.132	5.839	0.388	16.147
0.1741	0.332	0.056	0.909	1.123	5.901	0.388	16.249
0.1742	0.332	0.056	0.908	1.115	5.963	0.388	16.350
0.1743	0.332	0.056	0.907	1.106	6.025	0.388	16.451
0.1744	0.332	0.056	0.906	1.098	6.086	0.388	16.551
0.1745	0.332	0.056	0.905	1.089	6.148	0.388	16.651
0.1746	0.332	0.056	0.904	1.081	6.209	0.388	16.750
0.1747	0.332	0.056	0.903	1.072	6.270	0.388	16.849
0.1748	0.332	0.056	0.902	1.064	6.331	0.388	16.947
0.1749	0.332	0.056	0.901	1.055	6.392	0.388	17.045
0.1750	0.332	0.056	0.900	1.047	6.453	0.388	17.142
0.1751	0.332	0.056	0.899	1.038	6.514	0.388	17.239
0.1752	0.332	0.056	0.898	1.030	6.575	0.388	17.335
0.1753	0.332	0.056	0.897	1.021	6.636	0.388	17.431
0.1754	0.332	0.056	0.896	1.013	6.696	0.388	17.526
0.1755	0.332	0.056	0.895	1.004	6.757	0.388	17.621
0.1756	0.332	0.056	0.894	0.996	6.817	0.388	17.716
0.1757	0.332	0.056	0.893	0.987	6.878	0.388	17.810
0.1758	0.332	0.056	0.892	0.979	6.938	0.388	17.904
0.1759	0.332	0.056	0.891	0.970	7.000	0.388	18.000
0.1760	0.332	0.056	0.890	0.962	7.060	0.388	18.095
0.1761	0.332	0.056	0.889	0.953	7.121	0.388	18.190
0.1762	0.332	0.056	0.888	0.945	7.181	0.388	18.284
0.1763	0.332	0.056	0.887	0.936	7.242	0.388	18.378
0.1764	0.332	0.056	0.886	0.928	7.302	0.388	18.472
0.1765	0.332	0.056	0.885	0.919	7.363	0.388	18.566
0.1766	0.332	0.056	0.884	0.911	7.423	0.388	18.660
0.1767	0.332	0.056	0.883	0.902	7.484	0.388	18.754
0.1768	0.332	0.056	0.882	0.894	7.544	0.388	18.848
0.1769	0.332	0.056	0.881	0.885	7.605	0.388	18.942
0.1770	0.332	0.056	0.880	0.877	7.665	0.388	19.036
0.1771	0.332	0.056	0.879	0.868	7.726	0.388	19.130
0.1772	0.332	0.056	0.878	0.860	7.786	0.388	19.224
0.1773	0.332	0.056	0.877	0.851	7.847	0.388	19.318
0.1774	0.332	0.056	0.876	0.843	7.907	0.388	19.412
0.1775	0.332	0.056	0.875	0.834	7.968	0.388	19.506
0.1776	0.332	0.056	0.874	0.826	8.028	0.388	19.600
0.1777	0.332	0.056	0.873	0.817	8.089	0.388	19.694
0.1778	0.332	0.056	0.872	0.809	8.149	0.388	19.788
0.1779	0.332	0.056	0.871	0.800	8.210	0.388	19.882
0.1780	0.332	0.056	0.870	0.792	8.270	0.388	19.976
0.1781	0.332	0.056	0.869	0.783	8.331	0.388	20.070
0.1782	0.332	0.056	0.868	0.775	8.391	0.388	20.164
0.1783	0.332	0.056	0.867	0.766	8.452	0.388	20.258
0.1784	0.332	0.056	0.866	0.758	8.512	0.388	20.352
0.1785	0.332	0.056	0.865	0.749	8.573	0.388	20.446
0.1786	0.332	0.056	0.864	0.741	8.633	0.388	20.540
0.1787	0.332	0.056	0.863	0.732	8.694	0.388	20.634
0.1788	0.332	0.056	0.862	0.724	8.754	0.388	20.728
0.1789	0.332	0.056	0.861	0.715	8.815	0.388	20.822
0.1790	0.332	0.056	0.860	0.707	8.875	0.388	20.916
0.1791	0.332	0.056	0.859	0.698	8.936	0.388	21.010
0.1792	0.332	0.056	0.858	0.690	9.000	0.388	21.104
0.1793	0.332	0.056	0.857	0.681	9.060	0.388	21.198
0.1794	0.332	0.056	0.856	0.673	9.121	0.388	21.292
0.1795	0.332	0.056	0.855	0.664	9.182	0.388	21.386
0.1796	0.332	0.056	0.854	0.656	9.242	0.388	21.480
0.1797	0.332	0.056	0.853	0.647	9.303	0.388	21.574
0.1798	0.332	0.056	0.852	0.639	9.363	0.388	21.668
0.1799	0.332	0.056	0.851	0.630	9.424	0.388	21.762
0.1800	0.332	0.056	0.850	0.622	9.484	0.388	21.856
0.1801	0.332	0.056	0.849	0.613	9.545	0.388	21.950
0.1802	0.332	0.056	0.848	0.605	9.605	0.388	22.044
0.1803	0.332	0.056	0.847	0.596	9.666	0.388	22.138
0.1804	0.332	0.056	0.846	0.588	9.726	0.388	22.232
0.1805	0.332	0.056	0.845	0.579	9.787	0.388	22.326
0.1806	0.332	0.056	0.844	0.571	9.847	0.388	22.420
0.1807	0.332	0.056	0.843	0.562	9.908	0.388	22.514
0.1808	0.332	0.056	0.842	0.554	9.968	0.388	22.608
0.1809	0.332	0.056	0.841	0.545	10.029	0.388	22.702
0.1810	0.332	0.056	0.840	0.537	10.089	0.388	22.796
0.1811	0.332	0.056	0.839	0.528	10.149	0.388	22.890
0.1812	0.332	0.056	0.838	0.520	10.210	0.388	22.984
0.1813	0.332	0.056	0.837	0.511	10.270	0.388	23.078
0.1814	0.332	0.056	0.836	0.503	10.331	0.388	23.172
0.1815	0.332	0.056	0.835	0.494	10.391	0.388	23.266
0.1816	0.332	0.056	0.834	0.486	10.452	0.388	23.360
0.1817	0.332	0.056	0.833	0.477	10.512	0.388	23.454
0.1818	0.332	0.056	0.832	0.469	10.573	0.388	23.548
0.1819	0.332	0.056	0.831	0.460	10.633	0.388	23.642
0.1820	0.332	0.056	0.830	0.452	10.694	0.388	23.736
0.1821	0.332	0.056	0.829	0.443	10.754	0.388	23.830
0.1822	0.332	0.056	0.828	0.435	10.815	0.388	23.924
0.1823	0.332	0.056	0.827	0.426	10.875	0.388	24.018
0.1824	0.332	0.056	0.826	0.418	10.936	0.388	24.112
0.1825	0.332	0.056	0.825	0.409	11.000	0.388	24.206
0.1826	0.332	0.056	0.824	0.401	11.060	0.388	24.300
0.1827	0.332	0.056	0.823	0.392	11.121	0.388	24.394
0.1828	0.332	0.056	0.822	0.384	11.182	0.388	24.488
0.1829	0.332	0.056	0.821	0.375	11.242	0.388	24.582
0.1830	0.332	0.056	0.820	0.367	11.303	0.388	24.676
0.1831	0.332	0.056	0.819	0.358	11.363	0.388	24.770
0.1832	0.332	0.056	0.818	0.350	11.424	0.388	24.864
0.1833	0.332	0.056	0.817	0.341	11.484	0.388	24.958
0.1834	0.332	0.056	0.816	0.333	11.545	0.388	25.052
0.1835	0.332	0.056	0.815	0.324	11.605	0.388	25.146

Times for Refractive Propagation Paths

Theta zero	t1	t2	t3	t4	t5	T1	T2
0.3400	0.168	0.027				0.195	
0.3600	0.159	0.026				0.195	
0.3800	0.151	0.025				0.175	
0.4000	0.143	0.023				0.167	
0.4500	0.128	0.021				0.149	
0.5000	0.116	0.019				0.135	
0.5500	0.107	0.017				0.124	
0.6000	0.099	0.016				0.115	
0.6500	0.092	0.015				0.107	
0.7000	0.086	0.014				0.100	
0.8000	0.078	0.013				0.090	
0.9000	0.071	0.012				0.083	
1.0000	0.066	0.011				0.077	
1.1000	0.062	0.010				0.073	
1.2000	0.060	0.010				0.069	
1.3000	0.058	0.009				0.067	
1.4000	0.056	0.009				0.066	
1.5000	0.056	0.009				0.065	
1.5708	0.000	0.000				0.000	

Table D-2 Spreading Loss Function, $G(r)$

Theta zero	Theta 1	z	R1	R2	G(R1)	G(R2)	10 log G(R1)	10 log G(R2)
------------	---------	---	----	----	-------	-------	-----------------	-----------------

Theta zero is the surface launch angle.

Theta 1 is the angle of the refractive path at the hydrophone depth (93m)

z is the maximum depth of the refractive path.

R1 is the horizontal range to the hydrophone intersected on the downward swing

R2 is the horizontal range to the hydrophone intersected on the upward swing

G(R) is the spreading loss function.

0.0835	0.002	93	2171	2284	5.2E+08	5.5E+08	87.163	87.382
0.0837	0.006	94	2068	2398	4.9E+08	5.7E+08	86.922	87.564
0.0838	0.007	94	2038	2433	4.8E+08	5.8E+08	86.844	87.614
0.0839	0.008	94	2012	2464	4.8E+08	5.8E+08	86.775	87.655
0.0840	0.009	94	1990	2492	4.7E+08	5.9E+08	86.712	87.690
0.085	0.016	96	1839	2697	4.2E+08	6.2E+08	86.239	87.901
0.086	0.021	99	1741	2848	3.9E+08	6.3E+08	85.881	88.018
0.087	0.025	101	1666	2977	3.6E+08	6.5E+08	85.575	88.097
0.088	0.028	103	1603	3094	3.4E+08	6.5E+08	85.302	88.157
0.089	0.031	106	1549	3201	3.2E+08	6.6E+08	85.051	88.203
0.090	0.034	108	1502	3302	3.0E+08	6.7E+08	84.819	88.240
0.091	0.036	111	1459	3398	2.9E+08	6.7E+08	84.600	88.271
0.092	0.039	113	1421	3491	2.8E+08	6.8E+08	84.394	88.297
0.093	0.041	116	1385	3580	2.6E+08	6.8E+08	84.197	88.320
0.094	0.043	118	1353	3666	2.5E+08	6.8E+08	84.009	88.339
0.095	0.045	121	1323	3750	2.4E+08	6.8E+08	83.829	88.356
0.096	0.047	123	1294	3832	2.3E+08	6.9E+08	83.656	88.374
0.097	0.049	126	1268	3912	2.2E+08	6.9E+08	83.489	88.387
0.098	0.051	128	1243	3991	2.2E+08	6.9E+08	83.328	88.395
0.099	0.053	131	1219	4068	2.1E+08	6.9E+08	83.171	88.406
0.100	0.055	134	1197	4145	2.0E+08	6.9E+08	83.020	88.415
0.101	0.057	136	1175	4220	1.9E+08	7.0E+08	82.872	88.424
0.102	0.059	139	1155	4294	1.9E+08	7.0E+08	82.729	88.431
0.103	0.060	142	1136	4367	1.8E+08	7.0E+08	82.589	88.438
0.104	0.062	145	1117	4439	1.8E+08	7.0E+08	82.453	88.445
0.105	0.064	147	1099	4511	1.7E+08	7.0E+08	82.320	88.451
0.106	0.065	150	1082	4581	1.7E+08	7.0E+08	82.190	88.456
0.107	0.067	153	1066	4652	1.6E+08	7.0E+08	82.063	88.461
0.108	0.069	156	1050	4721	1.6E+08	7.0E+08	81.939	88.466
0.109	0.070	159	1035	4790	1.5E+08	7.0E+08	81.817	88.470
0.110	0.072	162	1021	4858	1.5E+08	7.0E+08	81.698	88.474
0.111	0.073	165	1007	4927	1.4E+08	7.0E+08	81.581	88.478
0.112	0.075	168	993	4994	1.4E+08	7.0E+08	81.46	88.482
0.113	0.076	171	980	5061	1.4E+08	7.0E+08	81.354	88.485
0.114	0.078	174	967	5128	1.3E+08	7.0E+08	81.244	88.488
0.115	0.079	177	955	5194	1.3E+08	7.0E+08	81.135	88.491
0.116	0.081	180	943	5261	1.3E+08	7.0E+08	81.028	88.494
0.117	0.082	183	931	5326	1.2E+08	7.0E+08	80.923	88.496

Scattering Loss Function, S_{sc}

Theta zero	Theta 1	z	R1	R2	G(R1)	G(R2)	10 log G(R1)	10 log G(R2)
0.115	0.084	186	920	5391	1.2E+08	7.1E+08	80.320	88.499
0.119	0.085	190	909	5456	1.2E+08	7.1E+08	80.718	88.501
0.120	0.086	193	898	5520	1.2E+08	7.1E+08	80.618	88.503
0.121	0.088	196	888	5585	1.1E+08	7.1E+08	80.520	88.506
0.122	0.089	199	878	5649	1.1E+08	7.1E+08	80.422	88.508
0.123	0.090	203	868	5713	1.1E+08	7.1E+08	80.327	88.510
0.124	0.091	206	857	5776	1.1E+08	7.1E+08	80.230	88.511
0.125	0.093	209	849	5840	1.0E+08	7.1E+08	80.133	88.513
0.126	0.094	213	840	5905	1.0E+08	7.1E+08	80.048	88.515
0.127	0.096	216	831	5966	9.9E+07	7.1E+08	79.957	88.516
0.128	0.097	220	823	6029	9.7E+07	7.1E+08	79.868	88.518
0.129	0.098	223	814	6091	9.5E+07	7.1E+08	79.779	88.519
0.130	0.100	227	806	6154	9.3E+07	7.1E+08	79.692	88.521
0.131	0.101	230	798	6216	9.1E+07	7.1E+08	79.606	88.522
0.132	0.102	234	790	6278	9.0E+07	7.1E+08	79.521	88.524
0.133	0.104	237	782	6340	8.8E+07	7.1E+08	79.438	88.525
0.134	0.105	241	775	6402	8.6E+07	7.1E+08	79.355	88.526
0.135	0.106	244	767	6463	8.5E+07	7.1E+08	79.273	88.527
0.136	0.107	248	760	6525	8.3E+07	7.1E+08	79.192	88.528
0.137	0.109	252	753	6586	8.1E+07	7.1E+08	79.112	88.530
0.138	0.110	255	746	6647	8.0E+07	7.1E+08	79.032	88.531
0.139	0.111	259	739	6708	7.9E+07	7.1E+08	78.954	88.532
0.140	0.113	263	732	6769	7.7E+07	7.1E+08	78.875	88.533
0.141	0.114	267	726	6830	7.6E+07	7.1E+08	78.797	88.534
0.142	0.115	271	720	6891	7.5E+07	7.1E+08	78.720	88.535
0.143	0.116	274	713	6951	7.3E+07	7.1E+08	78.649	88.536
0.144	0.117	278	707	7012	7.2E+07	7.1E+08	78.578	88.537
0.145	0.119	282	701	7072	7.1E+07	7.1E+08	78.501	88.537
0.146	0.120	286	695	7132	7.0E+07	7.1E+08	78.428	88.538
0.147	0.121	290	690	7193	6.8E+07	7.1E+08	78.356	88.540
0.148	0.122	294	684	7253	6.7E+07	7.1E+08	78.285	88.541
0.149	0.124	298	678	7313	6.6E+07	7.1E+08	78.214	88.541
0.150	0.125	302	673	7373	6.5E+07	7.1E+08	78.144	88.542
0.151	0.126	306	667	7433	6.4E+07	7.1E+08	78.074	88.543
0.152	0.127	310	662	7492	6.3E+07	7.1E+08	78.006	88.544
0.153	0.128	315	657	7552	6.2E+07	7.1E+08	77.937	88.545
0.154	0.130	319	652	7612	6.1E+07	7.1E+08	77.870	88.546
0.155	0.131	323	646	7671	6.0E+07	7.1E+08	77.803	88.547
0.156	0.132	327	641	7731	5.9E+07	7.1E+08	77.737	88.548
0.157	0.133	331	637	7791	5.8E+07	7.1E+08	77.671	88.549
0.158	0.134	336	632	7851	5.7E+07	7.1E+08	77.606	88.549
0.159	0.135	340	627	7909	5.7E+07	7.1E+08	77.541	88.549
0.160	0.137	344	622	7969	5.6E+07	7.1E+08	77.477	88.550
0.161	0.137	349	617	8028	5.5E+07	7.1E+08	77.413	88.551
0.162	0.137	353	613	8088	5.5E+07	7.1E+08	77.350	88.551

Scattering Loss Function, $S(r)$

Theta zero	Theta 1	z	R1	R2	S(R1)	S(R2)	10 log S(R1)	10 log S(R2)
0.163	0.140	358	609	8146	5.4E+07	7.2E+08	77.268	88.552
0.164	0.141	362	604	8205	5.3E+07	7.2E+08	77.226	88.553
0.165	0.142	366	600	8264	5.2E+07	7.2E+08	77.184	88.554
0.166	0.144	371	596	8323	5.1E+07	7.2E+08	77.103	88.554
0.167	0.145	376	592	8382	5.1E+07	7.2E+08	77.042	88.555
0.168	0.146	380	588	8441	5.0E+07	7.2E+08	76.982	88.556
0.169	0.147	385	583	8500	4.9E+07	7.2E+08	76.922	88.556
0.170	0.148	389	579	8558	4.9E+07	7.2E+08	76.864	88.557
0.171	0.149	394	575	8617	4.8E+07	7.2E+08	76.805	88.558
0.172	0.151	399	572	8676	4.7E+07	7.2E+08	76.746	88.559
0.173	0.152	403	568	8735	4.7E+07	7.2E+08	76.689	88.559
0.174	0.153	408	564	8793	4.6E+07	7.2E+08	76.631	88.560
0.175	0.154	413	560	8852	4.5E+07	7.2E+08	76.574	88.561
0.176	0.155	418	557	8910	4.5E+07	7.2E+08	76.517	88.561
0.177	0.156	422	553	8969	4.4E+07	7.2E+08	76.461	88.562
0.178	0.157	427	549	9028	4.4E+07	7.2E+08	76.405	88.563
0.179	0.159	432	546	9086	4.3E+07	7.2E+08	76.350	88.563
0.180	0.160	437	542	9145	4.3E+07	7.2E+08	76.295	88.564
0.181	0.161	442	539	9203	4.2E+07	7.2E+08	76.240	88.565
0.182	0.162	447	535	9261	4.2E+07	7.2E+08	76.185	88.565
0.183	0.163	452	532	9320	4.1E+07	7.2E+08	76.130	88.566
0.184	0.164	457	529	9378	4.1E+07	7.2E+08	76.075	88.567
0.185	0.165	462	526	9437	4.0E+07	7.2E+08	76.020	88.567
0.186	0.166	467	522	9495	4.0E+07	7.2E+08	75.965	88.568
0.187	0.168	472	519	9553	3.9E+07	7.2E+08	75.910	88.569
0.188	0.169	477	516	9611	3.9E+07	7.2E+08	75.855	88.569
0.189	0.170	483	513	9670	3.8E+07	7.2E+08	75.800	88.570
0.190	0.171	488	510	9728	3.8E+07	7.2E+08	75.744	88.571
0.191	0.172	493	507	9786	3.7E+07	7.2E+08	75.689	88.571
0.192	0.173	498	504	9845	3.7E+07	7.2E+08	75.634	88.572
0.193	0.174	504	501	9903	3.6E+07	7.2E+08	75.579	88.573
0.194	0.175	509	498	9961	3.6E+07	7.2E+08	75.524	88.573
0.195	0.176	514	495	10019	3.6E+07	7.2E+08	75.469	88.574
0.196	0.178	520	492	10077	3.5E+07	7.2E+08	75.414	88.575
0.197	0.179	525	489	10135	3.5E+07	7.2E+08	75.359	88.575
0.198	0.180	530	487	10194	3.4E+07	7.2E+08	75.304	88.576
0.199	0.181	536	484	10252	3.4E+07	7.2E+08	75.249	88.577
0.200	0.182	541	481	10311	3.4E+07	7.2E+08	75.194	88.577
0.201	0.183	547	478	10369	3.3E+07	7.2E+08	75.139	88.578
0.202	0.184	552	476	10428	3.3E+07	7.2E+08	75.084	88.579
0.203	0.185	558	473	10486	3.2E+07	7.2E+08	75.029	88.579
0.204	0.186	564	470	10545	3.2E+07	7.2E+08	74.974	88.580
0.205	0.187	569	468	10603	3.1E+07	7.2E+08	74.919	88.581
0.206	0.188	575	465	10662	3.1E+07	7.2E+08	74.864	88.581
0.207	0.189	581	462	10720	3.0E+07	7.2E+08	74.809	88.582

Scattering Loss Function, G(r)

Theta zero	Theta 1	z	R1	R2	G(R1)	G(R2)	10 log G R1	10 log G R2
0.208	0.191	586	460	10775	3.1E+07	7.2E+08	74.384	88.553
0.209	0.192	592	458	10833	3.0E+07	7.2E+08	74.843	88.583
0.210	0.193	598	455	10891	3.0E+07	7.2E+08	74.797	88.594
0.211	0.194	604	453	10949	3.0E+07	7.2E+08	74.751	88.585
0.212	0.195	610	451	11007	3.0E+07	7.2E+08	74.736	88.585
0.213	0.196	615	448	11065	2.9E+07	7.2E+08	74.661	88.585
0.214	0.197	621	446	11123	2.9E+07	7.2E+08	74.615	88.587
0.215	0.198	627	444	11181	2.9E+07	7.2E+08	74.570	88.587
0.216	0.199	633	441	11239	2.8E+07	7.2E+08	74.527	88.588
0.217	0.201	639	439	11297	2.8E+07	7.2E+08	74.463	88.589
0.218	0.202	645	437	11355	2.8E+07	7.2E+08	74.439	88.589
0.219	0.203	651	435	11414	2.8E+07	7.2E+08	74.396	88.590
0.220	0.204	657	432	11472	2.7E+07	7.2E+08	74.352	88.591
0.221	0.205	663	430	11530	2.7E+07	7.2E+08	74.309	88.591
0.222	0.206	670	428	11588	2.7E+07	7.2E+08	74.266	88.592
0.223	0.207	676	426	11646	2.6E+07	7.2E+08	74.224	88.593
0.224	0.208	682	424	11704	2.6E+07	7.2E+08	74.181	88.594
0.225	0.209	688	422	11762	2.6E+07	7.2E+08	74.139	88.594
0.226	0.210	695	420	11820	2.6E+07	7.2E+08	74.097	88.595
0.227	0.211	701	418	11878	2.5E+07	7.2E+08	74.055	88.596
0.228	0.212	707	415	11937	2.5E+07	7.2E+08	74.013	88.596
0.229	0.213	713	413	11995	2.5E+07	7.2E+08	73.971	88.597
0.230	0.215	720	411	12053	2.5E+07	7.2E+08	73.929	88.598
0.231	0.216	726	409	12111	2.4E+07	7.2E+08	73.887	88.599
0.232	0.217	733	408	12169	2.4E+07	7.2E+08	73.846	88.599
0.233	0.218	739	406	12227	2.4E+07	7.2E+08	73.819	88.599
0.234	0.219	746	404	12285	2.4E+07	7.2E+08	73.767	88.599
0.235	0.220	752	402	12344	2.4E+07	7.2E+08	73.727	88.599
0.236	0.221	759	400	12402	2.3E+07	7.2E+08	73.687	88.599
0.237	0.222	765	398	12460	2.3E+07	7.2E+08	73.647	88.599
0.238	0.223	772	396	12518	2.3E+07	7.2E+08	73.607	88.599
0.239	0.224	779	394	12576	2.3E+07	7.2E+08	73.568	88.599
0.240	0.225	785	393	12635	2.3E+07	7.2E+08	73.529	88.599
0.241	0.226	792	391	12693	2.2E+07	7.2E+08	73.489	88.599
0.242	0.227	799	389	12751	2.2E+07	7.2E+08	73.450	88.599
0.243	0.228	806	387	12809	2.2E+07	7.2E+08	73.411	88.599
0.244	0.229	812	385	12868	2.2E+07	7.2E+08	73.372	88.599
0.245	0.230	819	384	12926	2.2E+07	7.2E+08	73.334	88.599
0.246	0.231	826	382	12984	2.2E+07	7.2E+08	73.296	88.599
0.247	0.232	833	380	13043	2.2E+07	7.2E+08	73.258	88.599
0.248	0.233	840	379	13101	2.2E+07	7.2E+08	73.220	88.599
0.249	0.234	847	377	13159	2.2E+07	7.2E+08	73.182	88.599
0.250	0.235	854	375	13217	2.2E+07	7.2E+08	73.144	88.599
0.251	0.236	861	373	13275	2.2E+07	7.2E+08	73.106	88.599

Spreading Loss Function, $G(r)$

Theta zero	Theta 1	z	R1	R2	G(R1)	G(R2)	10 log G(R1)	10 log G(R2)
0.280	0.268	1079	331	14976	1.6E+07	7.3E+08	72.183	88.617
0.290	0.278	1160	319	15567	1.5E+07	7.3E+08	71.756	88.646
0.300	0.288	1244	307	16160	1.4E+07	7.3E+08	71.440	88.555

END
DATE
FILMED

4-88

DTIC